




Vestnik of Don State Technical University

Theoretical and scientific-partical journal

Vol. **20**

no. **1**
2020

ISSN 1992-5980 
eISSN 1992-6006



Mechanics



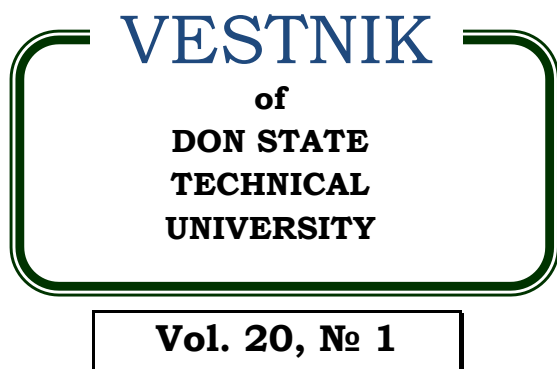
Machine Building and Machine Science



Information Technology, Computer Science, and Management

DOI 10.23947/1992-5980

vestnik.donstu.ru



**Theoretical
and scientific-practical journal**

Published since 1999

4 issues a year
January-March 2020

ISSN 1992-5980
eISSN 1992-6006
DOI: 10.23947/1992-5980

**Founder and publisher — Federal State Budgetary Educational Institution of Higher Education
Don State Technical University (DSTU)**

**Included in the list of peer-reviewed scientific editions where the basic research results of doctoral, candidate's theses
should be published (State Commission for Academic Degrees and Titles List) in the following research areas:**

01.02.01 – Analytical Mechanics (Engineering Sciences)
01.02.04 – Deformable Solid Mechanics (Engineering Sciences)
01.02.04 – Deformable Solid Mechanics (Physicomathematical Sciences)
01.02.06 – Dynamics, Strength of Machines, Gear, and Equipment (Engineering Sciences)
05.02.02 – Engineering Science, Drive Systems and Machine Parts (Engineering Sciences)
05.02.04 – Machine Friction and Wear (Engineering Sciences)
05.02.07 – Technology and Equipment of Mechanical and Physicotechnical Processing (Engineering Sciences)
05.02.08 – Engineering Technology (Engineering Sciences)
05.02.10 – Welding, Allied Processes and Technologies (Engineering Sciences)
05.02.11 – Testing Methods and Diagnosis in Machine Building (Engineering Sciences)
05.13.11 – Software and Mathematical Support of Machines, Complexes and Computer Networks (Engineering Sciences)
05.13.17 – Foundations of Information Science (Engineering Sciences)
05.13.18 – Mathematical Simulation, Numerical Methods and Program Systems (Engineering Sciences)

**The journal is indexed and archived in the Russian Science Citation Index (RSCI),
and in EBSCO International Database**

**The journal is a member of Directory of Open Access Journals (DOAJ), Association of Science Editors and Publishers
(ASEP) and Cross Ref**

*Certificate of mass media registration III № ФС 77-66004 of 06.06.2016 is issued by the Federal Service for Supervision
of Communications, Information Technology, and Mass Media*

The subscription index in Rospechat catalogue is 35578

The issue is prepared by:

Inna V. Boyko, Marina P. Smirnova (English version)

Passed for printing 26.03.2020,
imprint date 26.03.2020.

Format 60×84/8. Font «Times New Roman».

C.p.sh. 22.6. Circulation 1000 cop. Order no. 26/03 Free price.

Founder's, Publisher's and Printery Address:

Gagarin Sq. 1, Russian Federation, 344000, Russia. Phone: +7 (863) 2-738-372

E-mail: vestnik@donstu.ru <http://vestnik.donstu.ru/>



The content is available under Creative Commons Attribution 4.0 License

© Don State Technical University, 2020

Editorial Board

Editor-in-Chief — **Besarion Ch. Meskhi**, Dr.Sci. (Eng.), professor, Don State Technical University (Russian Federation);

deputy chief editor — **Valery P. Dimitrov**, Dr.Sci. (Eng.), professor, Don State Technical University (Russian Federation);

executive editor — **Manana G. Komakhidze**, Cand.Sci. (Chemistry), Don State Technical University (Russian Federation);

executive secretary — **Nadezhda A. Shevchenko**, Don State Technical University (Russian Federation);

Evgeny V. Ageev, Dr.Sci. (Eng.), professor, South-Western State University (Russian Federation);

Sergey M. Aizikov, Dr.Sci. (Phys.-Math.), professor, Don State Technical University (Russian Federation);

Kamil S. Akhverdiev, Dr.Sci. (Eng.), professor, Rostov State Transport University (Russian Federation);

Vladimir I. Andreev, member of RAACS, Dr.Sci. (Eng.), professor, National Research Moscow State University of Civil Engineering (Russian Federation);

Imad R. Antipas, Cand.Sci. (Eng.), Don State Technical University (Russian Federation);

Torsten Bertram, Dr.Sci. (Eng.), professor, TU Dortmund University (Germany);

Dmitry A. Bezuglov, Dr.Sci. (Eng.), professor, Rostov branch of Russian Customs Academy (Russian Federation);

Larisa V. Cherkesova, Dr.Sci. (Phys.-Math.), professor, Don State Technical University (Russian Federation);

Alexandr N. Chukarin, Dr.Sci. (Eng.), professor, Rostov State Transport University (Russian Federation);

Oleg V. Dvornikov, Dr.Sci. (Eng.), professor, Belarusian State University (Belarus);

Karen O. Egiazaryan, Dr.Sci. (Eng.), professor, Tampere University of Technology (Tampere, Finland);

Sergey V. Eliseev, corresponding member of Russian Academy of Natural History, Dr.Sci. (Eng.), professor, Irkutsk State Railway Transport Engineering University (Russian Federation);

Victor A. Ereemeev, Dr.Sci. (Phys.-Math.), professor, Southern Scientific Center of RAS (Russian Federation);

Mikhail B. Flek, Dr.Sci. (Eng.), professor, "Rostvertol" JSC (Russian Federation);

Nikolay E. Galushkin, Dr.Sci. (Eng.), professor, Institute of Service and Business (DSTU branch) (Russian Federation);

LaRoux K. Gillespie, Dr.Sci. (Eng.), professor, President-elect of the Society of Manufacturing Engineers (USA);

Victor M. Kureychik, Dr.Sci. (Eng.), professor, Southern Federal University (Russian Federation);

Geny V. Kuznetsov, Dr.Sci. (Phys.-Math.), professor, Tomsk Polytechnic University (Russian Federation);

Vladimir I. Marchuk, Dr.Sci. (Eng.), professor, Institute of Service and Business (DSTU branch) (Shakhty);

Igor P. Miroshnichenko, Cand.Sci. (Eng.), professor, Don State Technical University (Russian Federation);

Vladimir G. Mokrozub, Dr.Sci. (Eng.), associate professor, Rostov State Transport University (Russian Federation);

Murman A. Mukutadze, Cand.Sci. (Eng.), professor, Tambov State Technical University (Russian Federation);

Rudolf A. Neydorf, Dr.Sci. (Eng.), professor, Don State Technical University (Russian Federation);

Nguyen Dong Ahn, Dr.Sci. (Phys.-Math.), professor, Institute of Mechanics, Academy of Sciences and Technologies of Vietnam (Vietnam);

Petr M. Ogar, Dr.Sci. (Eng.), professor, Bratsk State University (Russian Federation);

Gennady A. Ougolnitsky, Dr.Sci. (Phys.-Math.), professor, Southern Federal University (Russian Federation);

Valentin L. Popov, Dr.Sci. (Phys.-Math.), professor, Institute of Mechanics, Berlin University of Technology (Germany);

Nikolay N. Prokopenko, Dr.Sci. (Eng.), professor, Don State Technical University (Russian Federation);

Anatoly A. Ryzhkin, Dr.Sci. (Eng.), professor, Don State Technical University (Russian Federation);

Igor B. Sevostianov, Cand.Sci. (Phys.-Math.), professor, New Mexico State University (USA);

Vladimir N. Sidorov, Dr.Sci. (Eng.), Russian University of Transport (Russian Federation);

Arkady N. Solovyev, Dr.Sci. (Phys.-Math.), professor, Don State Technical University (Russian Federation);

Alexandr I. Sukhinov, Dr.Sci. (Phys.-Math.), professor, Don State Technical University (Russian Federation);

Mikhail A. Tamarkin, Dr.Sci. (Eng.), professor, Don State Technical University (Russian Federation);

Valery N. Varavka, Dr.Sci. (Eng.), professor, Don State Technical University (Russian Federation);

Igor M. Verner, Cand.Sci. (Eng.), Docent, Technion (Israel);

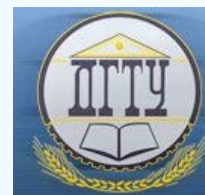
Batyr M. Yazyev, Dr.Sci. (Phys.-Math.), professor, Don State Technical University (Russian Federation);

Vilor L. Zakovorotny, Dr.Sci. (Eng.), professor, Don State Technical University (Russian Federation);

CONTENTS

ANNIVERSARY OF THE SCIENTIST	4
MECHANICS	
<i>Karnoub A., Nezhizhimov D. B., Shirinyan K. S.</i> Research and modeling of a multilayer composite material using basalt fabric	5
<i>Ivanychev D. A.</i> Two ways of organizing scalar product in the boundary state method	15
MACHINE BUILDING AND MACHINE SCIENCE	
<i>Lenivkin V. A., Rogozin D. V.</i> Study on pulsed-arc welding issues at the Machines and Welding Production Automation Department, RIAE — DSTU	25
<i>Yaitskov I. A., Kosarevskii V. V.</i> Brake rigging dynamic simulation under braking on a track section with irregularities (the case of a passenger car)	36
<i>Filyakov A. E., Sholokhov M. A.</i> On solving problems of operational forecasting of main pipeline weld joint quality	42
<i>Dolgachev Yu. V., Pustovoit V. N., Filonenko I. O., Ivankov I. V.</i> On modeling the martensite nucleation on ferromagnetic clusters	51
<i>Lazarev S. I., Lomakina O. V., Galaev V. I.</i> Determination of linear characteristics of rotor mounting groups under load	61
<i>Azimova N. N., Ladosha E. N., Kholodova S. N., Tsymbalov D. S., Yatsenko O. V.</i> Statistical analysis of sizing features of dust generated under the mechanical metal-working	68
<i>Man'shin Yu. P., Man'shina E. Yu.</i> Numerical modeling and experimental estimates of structural member fatigue characteristics	78
<i>Brover A. V.</i> Adaptation of structures of steel laser hardening zones to friction conditions	87
INFORMATION TECHNOLOGY, COMPUTER SCIENCE, AND MANAGEMENT	
<i>Poltavskii A. V., Yurushkina T. G., Yurushkin M. V.</i> Automatic license-plate recognition	93
<i>Zakharova O. A., Selikhina A. V., Vezirov T. G.</i> Modeling an analytics system for industrial safety monitoring based on expert assessments	100
<i>Kolybenko E. N.</i> Distinction between concepts of “structural-functional-parametric model” and “parametric model” of information knowledge objects	106

ANNIVERSARY OF THE SCIENTIST



Zakovorotny V. L., engineer, scientist, is 80



12 February, Vilor Lavrentievich Zakovorotny, Honoured Worker of National Science, Dr.Sci. (Engineering), professor, turned 80.

Vilor Lavrentievich Zakovorotny is a well-known international expert in the field of nonlinear dynamics of controlled systems. He has studied the dynamic monitoring and control of mechatronic systems and metalworking processes, developed the research framework of this area, and created a school of thought. His R&D results were introduced into production at 17 enterprises in Russia and neighboring countries.

For the past five years, the solutions proposed by V. L. Zakovorotny to the dynamic monitoring of machining processes on metal-cutting machines and to the dynamic diagnostics of rotor systems have been introduced into the manufacturing practice of Rostvertol, Russian Helicopters JSC, Rostselmash Combine Plant LLC, Azov Optomechanical Plant JSC, All-Russian Research Institute "Gradient" JSC, and others.

V. L. Zakovorotny has made a significant contribution to the development of engineering education in Russia, improving the educational process, training top-qualification technical and scientific manpower. He has trained more than 1,500 engineers, 7 doctors and 42 candidates of science, who work in universities and enterprises of the Rostov region.

V. L. Zakovorotny was one of the originators of training engineering personnel majoring in "Technological-Process Automation & Process Control" and "Management and IT in Engineering Systems". He carries out big job at the Academic Methodological Association on Automated Engineering.

In 1991-2007, as Pro-rector for Research, Prof. Zakovorotny made a great contribution to the reorganization of an industry-based university, Rostov Institute of Agricultural Engineering (RIAE) into a comprehensive technical university, DSTU.

V. L. Zakovorotny is the deputy chairman of the dissertation council D.212.058.02, DSTU, a member of the joint dissertation council, SFedU, a member of the editorial boards of three scientific journals included in the list of the State Commission for Academic Degrees and Titles of the Russian Federation. Prof. Zakovorotny is the author and co-author of 356 publications including seven monographs, five textbooks and teaching aids, 49 patents and copyright certificates.

For his outstanding merits, V. L. Zakovorotny is awarded with the second-class medal of the Order of Merit for the Motherland, the titles of Laureate of the State Prize of Ukraine in science and engineering, Honored Scientist of the Russian Federation, Honorary Professor and Professor of the year, DSTU. The Russian Air Force Commander awarded V. L. Zakovorotny with a Memorial Sign for his contribution to the construction and development of the Russian Air Force.

MECHANICS



UDC 631.31:681.2.083:631.421

<https://doi.org/10.23947/1992-5980-2020-20-1-5-14>

Research and modeling of a multilayer composite material using basalt fabric

A. Karnoub¹, D. B. Nezhizhimov², K. S. Shirinyan³

¹ ETH (Zurich, Switzerland)

^{2,3} Don State Technical University (Rostov-on-Don, Russian Federation)



Introduction. The range of use of composite materials (CM) is constantly expanding, finding application in many areas of mechanical engineering, agricultural technology, aircraft manufacturing, instrumentation, shipbuilding, in the manufacture of high-pressure containers, etc. Quite often, multilayer composites consisting mainly of one type of reinforcing material and a binder are used. Of particular interest is the use of various types of reinforcing materials – more durable in the places of maximum stress in the cross section – in a single composite. As an example, we can use glass and basalt fabrics and fibers using one type of binder. The work objective is to study properties of such a material and to model it using the finite element method.

Materials and Methods. The components used are commercially available. BT-11 basalt fabric, TR-0.5 fiberglass, as well as glass mat with a density of 300 g/m² were used as reinforcing materials. An epoxy resin of the ED-20 grade with a PEPA hardener was used as a binder. Two types of material were also manufactured for tensile and bending tests, respectively, the differences of which consisted in the number, type and layer sequence. For modeling, CAD COM-PASS 3D, APM-FEM module was used.

Results. Basalt fabric is used in the outer layers of the composite material, fiberglass – in the inner layers. This approach provides increasing the tensile strength of the composite during tensile and bending; however, critical failure leads to an instant loss of the bearing capacity of the material. The use of glass mat as the core of the composite material showed lower allowable stresses, both tensile and bending; but in case of bending, it turned out that when the material was delaminated, the load-bearing capacity of the material was about 10% of the maximum. Modeling of the material is possible with some assumptions, in view of the size of the final elements.

Discussion and Conclusions. The use of basalt fabrics as a reinforcing material provides obtaining products with the properties of both glass and carbon plastics. Such a CM will be slightly more expensive than fiberglass and much cheaper than carbon fiber. Products made of composite materials (equivalent to isotropic materials) can be modeled in computer-aided design systems using the finite element method. It is important to consider the type of loading on the product, since CM mainly have anisotropic properties (the load is applied taking into account the direction of fibers). In multilayer CM from structural fabrics, it is necessary to direct the loads along the fibers. In addition, it is necessary to consider the interlayer shear, different adhesion between the layers, etc. The main assumption of this method is the “constancy” of the material thickness, the number of layers and the order of their location.

Keywords: composite material, basalt fabric, fiberglass, glass mat, finite element method.

For citation: A. Karnoub, D. B. Nezhizhimov, K. S. Shirinyan. Research and modeling of a multilayer composite material using basalt fabric. Vestnik of DSTU, 2020, vol. 20, no. 1, pp. 5–14. <https://doi.org/10.23947/1992-5980-2020-20-1-5-14>

Introduction. In the work, polymer composite materials (CM) with a reinforcing composition based on basalt and glass fabrics were studied and modeled. Epoxy resin was used as a binder. The 11- and 13-layer composites were investigated.



In [1], technological and other characteristics of the CM are noted, including those determining the load distribution in the layers. Here, the principle of “simple” modeling of composite material in various computer-aided design (CAD) systems is considered, as well as the behavior of CM depending on the type of loading.

A method is described for increasing the interlayer shear resistance in polymer CM by adding finely divided solid particles (for example, glass) to the binder¹. The process of occurrence of interlayer stresses was studied [2]. It is possible that the application of this method would avoid stratification and increase the allowable stress of the samples.

In [3–5], the volume content of the binder, the methods of its application to the reinforcing material, the laying-up method, the operating procedure, etc., are determined.

It is known that the type of deformation and fracture of a composite polymer is determined by its shape, quality and binder (including its volume content)². The corresponding dependence has been derived [6, 7].

In [8–10], modeling a part from CM using the finite element method (FEM) in CAD is described.

The paper presented also uses FEM. With its help:

- reliability of determining the stresses in the places of destruction of the samples and safety factors is validated,
- specifications of using assumptions that facilitate the calculation of products from polymer CM tested previously on tensile machines, are indicated.

In [11], the influence of the shape and type of reinforcing components on the thermal and mechanical properties of a polymer composite material is described.

In [12, 13], the applicability of composites in engineering, automobile production, construction, etc., were noted.

Research Objectives:

- to justify the use of basaltic fabrics in polymer CM,
- to determine their strength properties with various reinforcing components,
- to check the possibilities of modeling CM by the finite element method.

Materials and Methods

A composite material based on basalt and glass cloth and glass mat was studied in this work. As a binder, epoxy resin ED-20 with hardener polyethylene polyamine (PEPA) was used. The reinforcing agents were fiberglass TR-0.5, basalt fabric BT-11 and fiberglass with a density of 300 g/m². A feature of the experiment was the use of several types of reinforcing material in one composite at once.

Justification for the application of basalt fabric and finite element modeling. At present, CM rarely uses basalt fabric, although it possesses characteristics important for high-quality composites: high impact strength, high specific strength, heat resistance, environmental cleanliness, high resistance to corrosion and acid, low thermal conductivity, affordable price, radio transparency, and good sound absorbing properties. It is also worth noting that basalt is a rock, and its reserves are practically unlimited. In the production of basalt fiber, the rock is melted, threads are drawn from it, which are used to make fabric, roving, etc.). In terms of strength, basalt fiber is superior to fiberglass and approaches carbon fiber. The price of basalt fiber is slightly higher than fiberglass, but significantly lower than carbon fiber. This allows fabricating products of higher quality than fiberglass, but at the same time cheaper than carbon fiber. Of particular interest is the use of several reinforcing materials in one CM: glass and basalt fabric, as well as glass mat. When modeling composites in CAD, it is required to set materials with various characteristics, which creates known difficulties. In the framework of this work, the possibility of a standard study of structures by the FEM is determined.

¹ Nezhizhimov DB. *Sposob uvelicheniya soprotivleniya mezhslainomu dvigu v mnogoslainnykh kompozitnykh materialakh* [Method for increasing interlayer shear resistance in multilayer composite materials]. In: Proc. 3rd All-Russ. Sci. Conf., Kursk, 2019. P. 84–88.

² Antibas IR, D'yachenko AG. *Issledovanie protsessy razrusheniya sloistogo kompozitnogo materiala* [Study on destruction of the layered composite material]. In: Proc. 10th Int. Sci.-Pract. Conf. within framework of the 20th Int. Agroindustrial Exhibition “Interagromash-2017”, Rostov-on-Don, 2017. P. 179–181.

For this, anisotropic material is “equated” to isotropic, and the products are designed so that loads can be applied along the direction of the fibers.

The use of structural fabrics makes it possible to model the behavior of CM with some assumption. However, it is necessary to consider the type of weaving of fabrics and the angle of rotation between the layers. Thus, it is required to obtain the results of an experiment on determining the strength properties, and to find out the tensile and bending strength. Based on this information, it is possible to simulate the composite for these types of loading since the material continues to collapse after damage to the outer layer under bending and to the defective layer under tension. If there are no defects in the composite under tension, fracture mainly occurs in a dangerous section.

Preparing for the experiment. For the experiment, samples were made from composite material (Fig. 1).

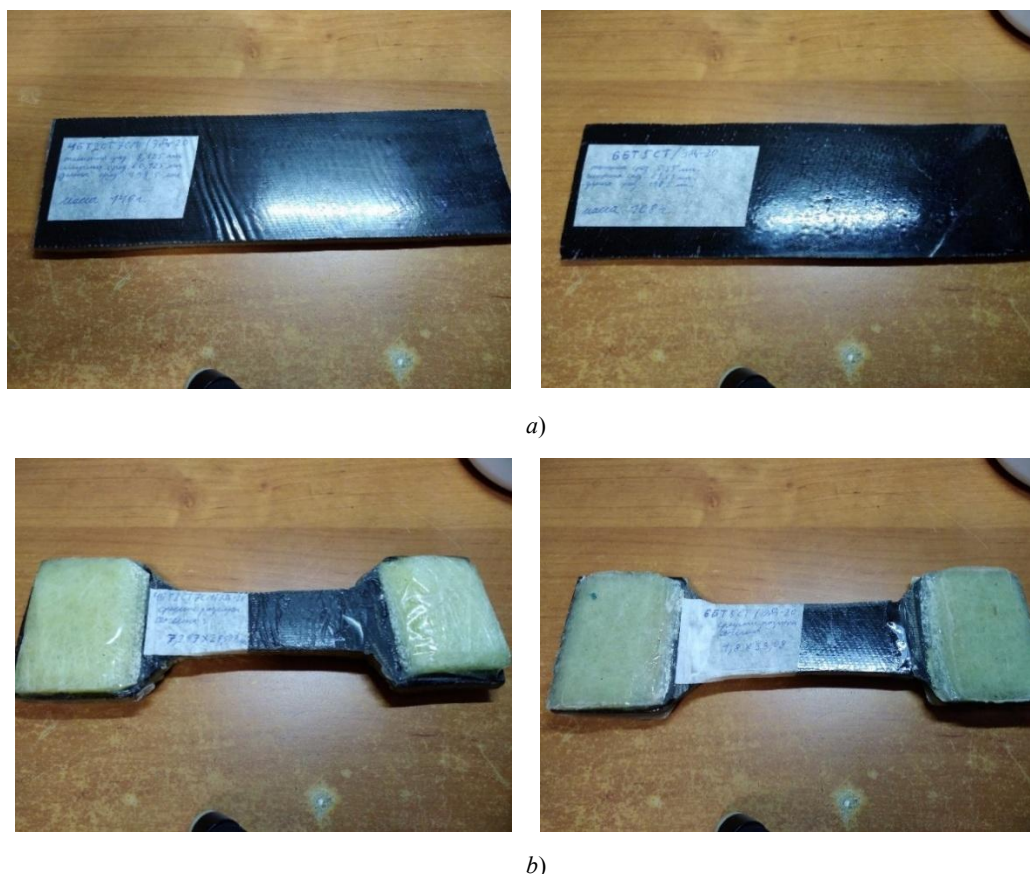


Fig. 1. Test specimens: (a) bending; (b) tensile

In the first case (see Fig. 1 a):

- the type of laying is sandwich (symmetrical arrangement of layers in all samples),
- the total number of layers per sample (first outer, then middle, then inner) are indicated,
- 4 layers of basalt fabric (BF),
- 2 layers of fiberglass (FG),
- 7 layers of glass mat (GM).

In the second case (see Fig. 1 b):

- 6 layers of basalt fabric (BF),
- 5 layers of fiberglass (FG).

In both cases, the binder is ED-20 resin, the hardener is PEPA.

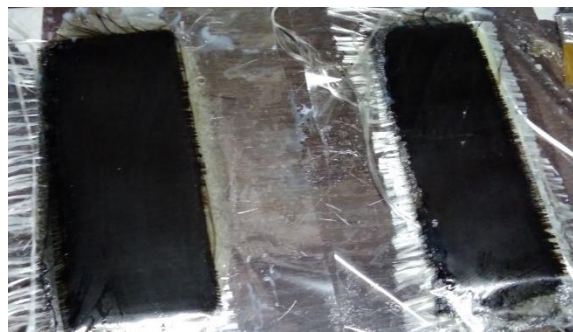
Thus, two types of material are obtained. Their differences allow you to check:

- if using fabrics with mats is worthwhile,
- what effects a combination of different types of materials will give.

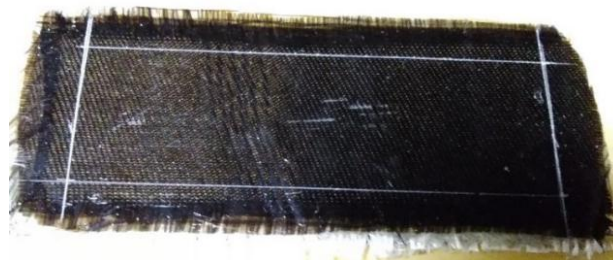
Sampling. Samples were made through sequential placing of fabric layers (Fig. 2 *a*) on a base covered with a film, since there is no adhesion between the resin and the films.



a)



b)



c)

Fig. 2. Sampling: (*a*) material cutting; (*b*) removal of excess resin; (*c*) machine processing

After placing all the layers, they were heated and smoothed at the same time with a spatula through the film (see Fig. 2 *b*); in this case, a smooth surface without excess resin was obtained. Sampling scheme:

- 1) cutting samples with a margin for machining,
- 2) preparation of the foundation,
- 3) resin activation,
- 4) placing layers,
- 5) smoothing,
- 6) fixation,
- 7) curing,
- 8) machining (see Fig. 2 *c*).

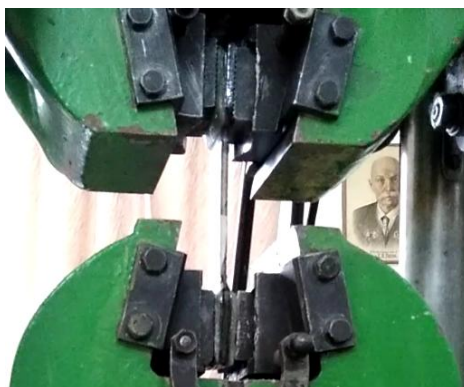
Tensile and bending tests. Tensile and bending tests were carried out on a breaking machine (Fig. 3-5).



Fig. 3. Breaking machine



a)



b)

Fig. 4. Testing: (a) bending; (b) breaking



a)



b)

Fig. 5. Results of destruction of samples: (a) tensile; (b) bending

Research Results

Test Conclusions. Based on the test results, the following conclusion can be drawn: when combining fabrics and mats, a characteristic feature of fracture is delamination at the border of various types of material (see Fig. 5). When in comes only to tissue layers, such an obvious feature is not observed. Tissues used as reinforcing agents are torn at the place of maximum stress and then are sharply destroyed. Initially, individual fibers are destroyed, which is accompanied by a characteristic sound. Then the fibers are pulled out of the matrix — and the matrix itself is destroyed. This is shown by decoloration — the place of destruction “turns white” and looks more matt. The test results are presented in Table 1.

Table 1

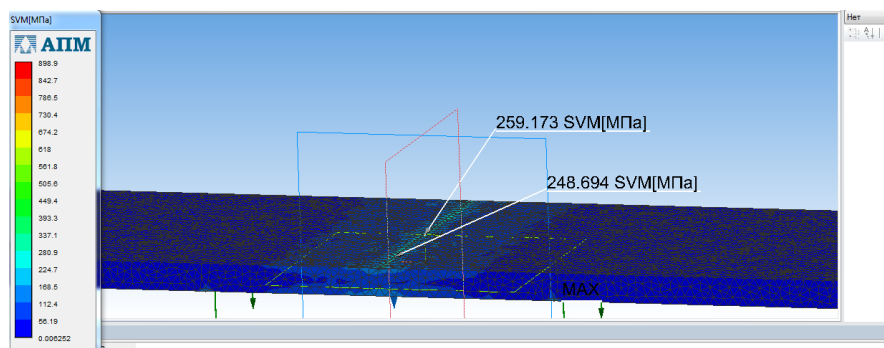
Characteristics of CM tested for bending and breaking

	6BT5ST/ED-20	4BT2ST7SM/ED-20
Max. bending force, kg	500	965
Max. breaking force, kg	3560	2600
Max. bending stress, MPa	265.1	239.5
Max. tensile strength, MPa	191.8	120
Sample parameters and distance between supports under bending, mm*	$b = 64.2; h = 5.5; L = 70$	$b = 61.7; h = 8.2; L = 70$
Section dimensions at break, mm	$b = 35; h = 5.2$	$b = 29.5; h = 7.2$
Density, kg/m ³	650	700
*Here, b is sample average width, h is sample average thickness, L is distance between supports.		

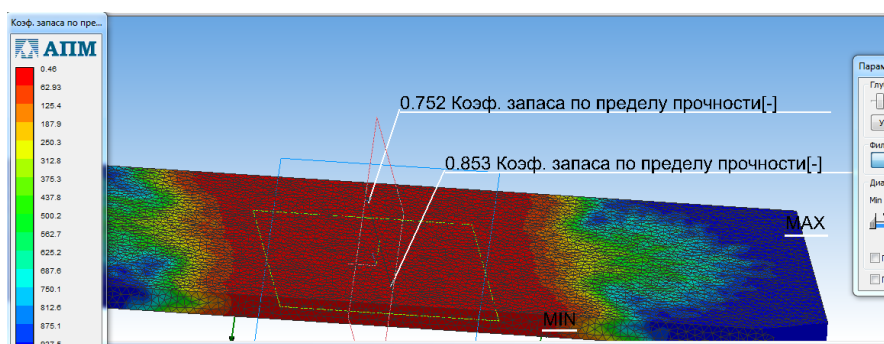
Composite material modeling and test validation. For modeling, the material 6BT5ST was selected. Its characteristics are included in the Compass 3D library, and solid models are created. Using the APM FEM module for

Compass 3D, finite element calculations were performed. In this case, difficulties arose due to the selection of the optimal sizes of the finite elements. The following assumptions were used for calculations: the fixing and load points were performed by slight stretching of the “strips” of 0.1–0.2 mm wide. In these areas, the results of stresses and safety factors should not be considered since they are incorrect. Such simplifications enable to apply loads and install fixation in any place on the models. The optimal mesh size is from 2 to 3 mm.

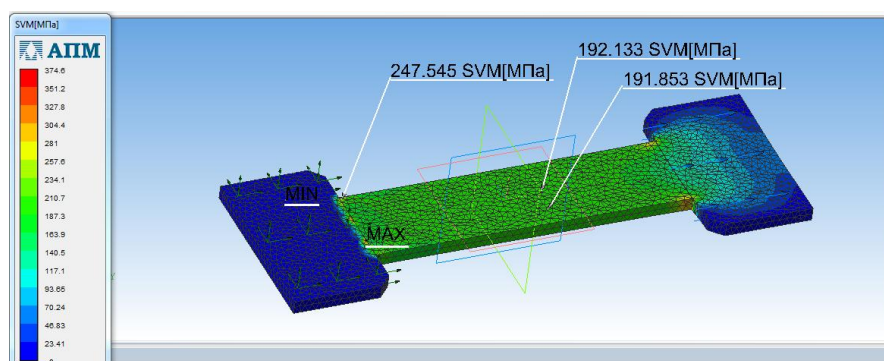
The calculation results charts of stresses and safety factor of the ultimate strength are presented in Fig. 6.



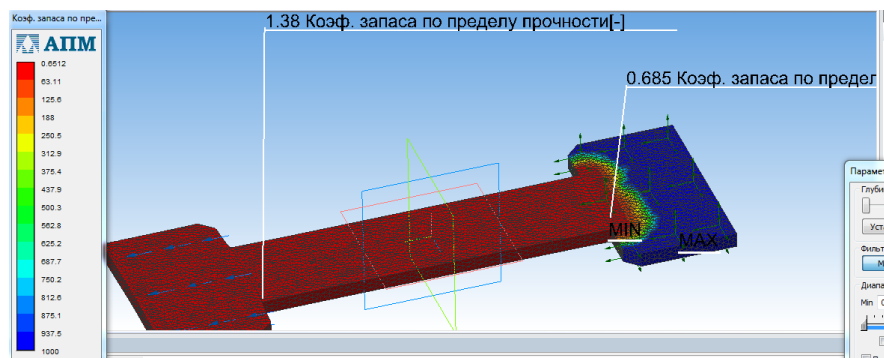
a)



b)



c)



d)

Fig. 6. Results charts: (a), (c) by stress; (b), (d) by safety factor

The simulation results suggest that these samples are destroyed in places subjected to maximum stress. Due to the modeling error, the safety factor is other than unity, and the reduction in the size of the finite elements solves this problem. It is also worth saying that this method will be normally implemented when modeling structures operating in tension or compression, since these processes are accompanied mainly by normal stresses. However, during the tests, it has been found that at different elongation factors for the reinforcing materials, delamination occurs along the loading line at the layer boundary due to insufficient interlayer adhesion and high shear stresses.

Discussion and Conclusions. The use of basalt fabrics as a reinforcing substance provides obtaining products with the properties of both glass and carbon plastics. Moreover, such a CM will be slightly more expensive than fiberglass and much cheaper than carbon fiber. Good indicators of the specific strength of basalt, its absolute incombustibility, high impact strength, and resistance to UV radiation should be mentioned. Basalt is a dielectric; therefore, it can be used in the manufacture of cases for radio equipment.

The experiments have shown higher strength characteristics of those CM in which there are more layers of basalt fabric, and glass mat is not used. The use of glass mat as a core causes high interlayer shear stresses, which stimulates interlayer fracture both in tension and in bending. The maximum bending stresses for a sample with a large number of layers of basalt fabric amounted to 261.5 MPa (versus 239 MPa with a smaller number of layers of basalt fabric). In addition, there was a clear superiority in maximum tensile stresses — 190 MPa versus 120 MPa.

The calculation results allow us to state that products made of composite materials (equated to isotropic materials) can be modeled in CAD using the finite element method. It is very important to consider the type of loading on the product, since CM largely have anisotropic properties (the load is applied allowing for the direction of the fibers). So, in multilayer CM from structural fabrics, it is required to direct the loads along the fibers. In addition, it is necessary to consider the interlayer shear, different adhesion between the layers, etc. The main assumption of this method is the “constancy” of the thickness of the material, the number of layers and the order of their location.

The data and method obtained need further research, which will allow us to create a range of composite materials with known characteristics, to simulate them, and to perform the corresponding calculations.

References

1. Nezhizhimov DB. Osobennosti izdelii iz kompozitnykh materialo [Features of products from composite materials]. In: Actual problems of science and technology. Rostov-on-Don: Izd-vo DGTU; 2019. 376–377 p. (In Russ.)
2. Antypas IR, Partko SA, Sirotenko AN. Vliyanie formy gofirovannogo kartona na amortiziruyushchie svoystva upakovki [Effect of corrugated cardboard shape on the packing damping properties]. Vestnik of DSTU. 2016;16,1(84):36–42. (In Russ.)
3. Antypas IR, D'yachenko AG. Vliyanie soderzhaniya drevesnogo dispersnogo napolnitelya na dolgovechnost' kompozitsionnykh materialov [Effect of wood particulate filler content on durability of composite materials]. Vestnik of DSTU. 2017;17,1(88):67–74. (In Russ.)
4. Antypas IR, D'yachenko AG. Opredelenie kharakteristik komponentov kompozitnykh materialov, prednaznachennykh dlya proizvodstva detalei sel'skokhozyaistvennoi tekhniki [Studies on characterization of composite materials components for part production in agricultural industry]. Vestnik of DSTU. 2017;17,3(90):60–69. (In Russ.)
5. Antypas IR, D'yachenko AG. Izgotovlenie teploizolyatsionnogo materiala i izuchenie ego teplofizicheskikh i mekhanicheskikh svoystv [Production of heat-insulating material and study on its thermophysical and mechanical properties]. In: Proc. 10th Int. Sci.-Pract. Conf. within framework of the 20th Int. Agroindustrial Exhibition “Interagromash-2017”. Rostov-on-Don: Izd-vo DGTU; 2017. 182–183 p. (In Russ.)
6. Antypas IR, D'yachenko AG. Ehfekt vlazhnogo travleniya kompozitnogo materiala iz steklovolokna i poli-amida na ego svoystva pri izgibe i udare [The effect of wet etching of a fiberglass and polyamide composite material on

its properties under bending and impact]. In: Proc. V Int. Sci.-Pract. Conf. (ITNO-2017). Rostov-on-Don: DGTU-Print; 2017. 26–30 p. (In Russ.)

7. Kharmanda G, Antypas IR. Integration of reliability and optimization concepts into composite yarns. In: Proc. 10th Int. Sci.-Pract. Conf. within framework of the 20th Int. Agroindustrial Exhibition «Interagromash-2017». Rostov-on-Don: Izd-vo DGTU; 2017. 174–176 p.

8. Antypas IR, Partko SA. Sravnenie amortiziruyushchikh svoystv gofrirovannoi kartonnoi upakovki raznoi struktury pri deistvii vertikal'noi nagruzki [Comparison of the cushioning properties of corrugated cardboard packaging of different structures under vertical load action]. In: Proc. 8th Int. Sci.-Pract. Conf. within framework of the 18th Int. Agroindustrial Exhibition «Interagromash-2015». Rostov-on-Don: Izd-vo DGTU; 2015. 232–235 p. (In Russ.)

9. Antypas IR, D'yachenko AG, Savostina TP. Issledovanie vliyaniya dobavok armiruyushchikh volokon na nekotorye mekhanicheskie svoystva perspektivnykh kompozitnykh materialov [Investigation of the effect of reinforcing fiber additives on some mechanical properties of advanced composite materials]. In: Proc. XII Int. Sci.-Pract. Conf. within framework of XXII Agroindustrial Forum of the South of Russia and Exhibition “Interagromash”. Rostov-on-Don: Izd-vo DGTU; 2019. 240–244 p. (In Russ.)

10. Antypas IR, D'yachenko AG. Modelirovanie, izuchenie i izgotovlenie stoiki kul'tivatora iz kompozitnykh materialov [Modeling, studying and manufacturing a cultivator rack from composite materials] Mordovian University Bulletin. 2018;28 (3):366–378. (In Russ.)

11. Al-Jeebory AA, Al-Mosawi AI, Abdul Allah SA. Effect of Percentage of Fibers Reinforcement on Thermal and Mechanical Properties for Polymeric Composite Material. The Iraqi Journal for Mechanical and Materials Engineering. 2009 17–18 May, Special Issue:70–82.

12. Vincenzini P, Singh M. Advanced Inorganic Fibrous Composites V. Advances in Science and Technology. 2006;50:97–106.

13. Dixit A, Mali HS. Modeling techniques for predicting the mechanical properties of woven-fabric textile composites: a Review. Mechanics of Composite Materials. 2013;49(1):1–20.

Submitted 19.12.2019

Scheduled in the issue 03.02.2020

About the authors

Amer Karnoub, Guest Researcher at the Physics and Technology Laboratory, Department of Materials, ETH Zurich (Rämistrasse 101, 8092 Zurich, Switzerland), Cand.Sci. (Eng). ORCID: <http://orcid.org/0000-0002-9824-7364>
amerkarnoub@gmail.com

Nezhizhimov, Danil B., graduate student of the Machine Design Principles Department, Don State Technical University (1, Gagarin sq., Rostov-on-Don, 344000, RF). ORCID: <https://orcid.org/0000-0002-1036-5746>
nezhizhimov96@mail.ru

Shirinyan, Karen S., graduate student of the Machine Design Principles Department, Don State Technical University (1, Gagarin sq., Rostov-on-Don, 344000, RF). ORCID: <https://orcid.org/0000-0001-7697-6411>
shirinyan.karen@yandex.ru

Claimed contributorship

A. Karnoub: academic advising, research objectives and tasks correction, analysis of the test results, analysis of the calculation results, the text revision, correction of the conclusions. D. B. Nezhizhimov: basic concept formulation, research objectives and tasks setting, procurement of materials, prototyping, testing, text preparation, analysis of tests and calculations, formulation of conclusions. K.S. Shirinyan: consultations in the formulation of the basic concept, consultations in setting the goals and objectives of the study, testing, consultation in the calculation.

All authors have read and approved the final manuscript.

MECHANICS



UDC 539.3

<https://doi.org/10.23947/1992-5980-2020-20-1-15-24>

Two ways of organizing scalar product in the boundary state method

D. A. Ivanychev

Lipetsk State Technical University (Lipetsk, Russian Federation)



Introduction. The influence of two ways of organizing scalar product on the convergence rate of the solution in the energy method of boundary states is considered. The method is based on the spaces of internal and boundary states which are conjugated through isomorphism. Both spaces are orthonormalized using one scalar product or another. The desired state is expanded in the Fourier series according to the elements of the orthonormalized basis; and the coefficients of this linear combination are determined. The two methods differ in the assignment of scalar products and the calculation of the Fourier coefficients.

Materials and Methods. In relation to the method of boundary states, a new theory of organizing a scalar product in the spaces of internal and boundary states is proposed. Computational algorithms are constructed for its practical implementation. In the traditional (first) approach, the internal energy of elastic deformation is used as an orthogonalizer in the space of internal states. Here, the Fourier coefficients are the work of given forces on the basis vectors of displacement of the boundary points. In the studied (second) approach, scalar products are integrals of the cross products of the basis force vectors at the boundary. Accordingly, the Fourier coefficients are calculated as integrals of the product of the given forces at the body boundary by the basic force vectors.

Results. A numerical study of the first primal axisymmetric problem of the elasticity theory for a transversely isotropic cylinder in the absence and presence of mass forces is conducted. In the absence of mass forces, an analysis of the elastic fields obtained for the same number of used basic elements has shown that the second method has the greatest accuracy of the results. Under solving the problem with the presence of mass forces, the second method did not show efficiency in terms of the uniqueness of the solution; however, it is quite suitable for constructing a multitude of elastic fields used to solve more complex problems.

Discussion and Conclusions. The results obtained can be used to solve boundary-value problems of mechanics of not only an anisotropic body, but also an isotropic one. When solving more complex problems, such as contact and mixed ones, the issue of the rate of convergence requires a separate study.

Keywords: boundary state method, scalar product, internal energy, state spaces, the first main task, mass forces.

For citation: D. A. Ivanychev. Two ways of organizing scalar product in the boundary state method. Vestnik of DSTU, 2020, vol. 20, no. 1, pp. 15–24. <https://doi.org/10.23947/1992-5980-2020-20-1-15-24>

Funding information: The study was carried out with the financial support of RFBR and the Lipetsk Region as part of the research project No. 19-41-480003 "p_a".



Introduction. The boundary-value problems of the elasticity theory in mechanics are sufficiently studied; therefore, in recent years, case studies have been carried out. For example, the first primal axisymmetric problem for a half-strip [1] is considered, the solution of which is constructed in the form of expansions in systems of Fadl-Papkovich functions and has an explicit form. A general method for solving the first primal problem of the elasticity theory for a rectilinear anisotropic body in the case of plane deformation is proposed [2]. Closed systems of boundary value problems similar to Hilbert's problems are used, which makes it possible to achieve a more general method. Plane isotropic problems are solved using the finite element method based on the Castigliano variational principle [3]. This has provid-

ed for obtaining stress fields on grids of a sufficiently low dimension including those for incompressible materials. Contact problems on the implementation of elliptical stamps in a transversely isotropic elastic half-space are solved [4].

The method of boundary states under solving boundary value problems for anisotropic bodies also found its application. For example, the elastic equilibrium of a transversely isotropic cylinder under the action of axisymmetric surface forces is considered [5]. The problems of torsion of extended cylinders of a material with general anisotropy are studied [6]. A mathematical model is shown for obtaining explicit parametric solutions for isotropic and anisotropic bodies [7, 8], where the medium constants are included as parameters in the elastic fields. A technique has been developed for solving problems of the elasticity theory using computer algebra [9]. In solving problems of a stress-strain unbounded elastic medium containing spherical cavities or inclusions, the boundary-state method was used under different conditions [10].

In this paper, we study two approaches to the assignment of a scalar product in the “body” of the boundary state method. In this case, each state is tested using the example of solving the first primal problem of the elasticity theory. In each task, the same number of used elements is held and the error level is estimated.

Materials and Methods. The boundary state method (BSM) [11] is an energy one; it uses the fundamental theory of series to solve the basic problems of mechanics. The concepts of internal and boundary states are used as supporting ones.

The internal state ξ is due to a set of displacement vector u , strain tensor ε , and stress tensor T :

$$\xi = \{u, \varepsilon, T\}. \quad (1)$$

The boundary state is determined by a set of displacement vector of the boundary points u^v and forces p on the body boundary:

$$\gamma = \{u^v, p\}.$$

The totality of such states forms the basis of the spaces of internal $\Xi = \{\xi_1, \xi_2, \xi_3, \dots, \xi_k, \dots\}$ and boundary $\Gamma = \{\gamma_1, \gamma_2, \gamma_3, \dots, \gamma_k, \dots\}$ states. Next, orthogonalization of state bases is carried out, where the following expression is used as an orthogonalizer in the basis of boundary states:

$$(\xi_i, \xi_j) = \int_V \varepsilon_i T_j dV,$$

in the basis of boundary states – the expression:

$$(\gamma_i, \gamma_j) = \int_S u_i^v p_j dS. \quad (2)$$

A single element $\xi_k \in \Xi$ corresponds to each element $\gamma_k \in \Gamma$, besides, this correspondence is one-to-one: $\xi_k \leftrightarrow \gamma_k$. This enables to reduce finding the internal state to the construction of a boundary state isomorphic to it. In the case of the first primal problem, the desired internal and boundary states are the Fourier series:

$$\xi = \sum_{k=1}^{\infty} c_k \xi_k; \quad \gamma = \sum_{k=1}^{\infty} c_k \gamma_k, \quad (3)$$

here, c_k are the Fourier coefficients:

$$c_k = \int_S p u_k dS, \quad (4)$$

where p is the vector of given surface forces; u_k is the displacement vector in the k -th basic element of the basis of internal states. In this case, basic sets are formed on the ground of a general or fundamental solution to the problem.

The first general solutions to the Lamé equation of the linear elasticity theory were built back in the 30s of the last century. The Lamé equation is the Euler equation of motion (in this case, equilibrium):

$$\nabla T + f = 0,$$

where T is stress tensor; ∇ is Hamilton operator acting as a divergence; f is mass forces.

In the Lamé equation, the stress tensor T in accordance with Hooke's law is represented through the strain tensor ε . In turn, the strain tensor in accordance with the Cauchy relation is represented through the displacement vector u . In general solutions to the Lamé equation, the displacement vector is determined: through the harmonic vector B and the harmonic scalar in the theory of isotropic elasticity, and through the stress function F — in the theory of anisotropic elasticity.

Vector B (function F) can be represented as a series of basic vectors $B_k = B_k(\alpha^i)$ — coordinate functions α^i . As a result, the following basic elements will be associated with each harmonic basis vector B_k (function F_k):

- displacement vector u_k ;
- strain tensor ε_k ;
- stress tensor T_k ;
- mass forces vector f_k (from equilibrium equations);
- surface forces vector (from Cauchy fundamental relationship):

$$p_k = n \cdot T_k,$$

where n is the external unit normal to the surface of the body.

According to the listed basic elements, the corresponding vectors or tensors are expanded in Fourier series with the same coefficients c_k , which are determined from the conditions of orthogonality of the basic functions. For example, for the first primal problem in the absence of mass forces, when external forces p are given on the entire surface of the body S and orthogonalization of the basis vectors

p_k ($\int_S p_i p_j dS = \delta_{ij}$ is Kronecker delta) is implemented, the coefficients c_k are determined from the expression:

$$c_k = \int_S p p_k dS. \quad (5)$$

This expression follows from the representation:

$$p = \sum_{k=1}^{\infty} c_k p_k.$$

Thus, we study the solution generation method using the expression for scalar products in the basis of boundary states:

$$(\gamma_i, \gamma_j) = \int_S p_i p_j dS \quad (6)$$

and the expression for Fourier coefficients (5).

In the case of the second primal problem, there are the dependencies:

$$(\gamma_i, \gamma_j) = \int_S u_i^v u_j^v dS;$$

$$c_k = \int_S u u_k^v dS,$$

where u is the given displacement vector of points of the body boundary; u_k^v is the displacement vector in the k -th base element of the boundary states basis.

Research Results. Parameters of the convergence rate of series and the result accuracy are considered using the example of solving the problem of the elastic equilibrium of a transversely isotropic cylinder of dark-gray siltstone [12] in a dimensionless form (Fig. 1).

The boundary conditions are:

$$\begin{aligned} p &= 0, S_1 | \quad z = -2, 0 \leq r \leq 1; \\ p &= 0, S_2 | \quad z = 2, 0 \leq r \leq 1; \\ p_r &= 4 - z^2, p_z = 0, S_3 | \quad r = 1, -2 \leq z \leq 2. \\ &<...> \end{aligned}$$

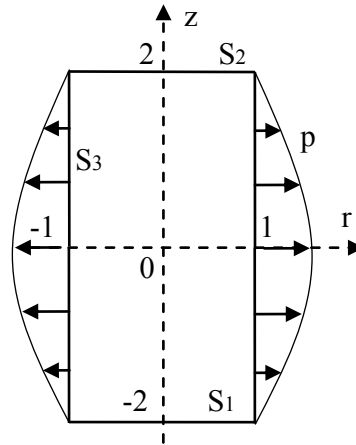


Fig. 1. Boundary conditions for the transtropic cylinder

The methodology for solving the first primal problem in the traditional way using the scalar product (2) is described in detail in [6]. The basis of internal states (1) is constructed as follows:

- using a general solution to the plane deformation problem [13], basis sets of plane auxiliary states are constructed;
- basis sets of spatial axisymmetric states are determined from the transition formulas;
- orthonormalization of the internal states basis is carried out according to the Gram-Schmidt matrix algorithm using the scalar product (2);
- the orthonormal basis of boundary states is reduced from the orthonormal basis of internal states;
- Fourier coefficients (4) are calculated, and series (3) are constructed in an expanded form (index k is placed on top):

$$u_i = \sum_{k=1}^{\infty} c_k u_i^k; \quad p_i = \sum_{k=1}^{\infty} c_k p_i^k; \quad \sigma_{ij} = \sum_{k=1}^{\infty} c_k \sigma_{ij}^k; \quad \varepsilon_{ij} = \sum_{k=1}^{\infty} c_k \varepsilon_{ij}^k.$$

We omit the information on the fields of the stress-strain state characteristics obtained with one and the other method of assigning the scalar product, and we give only the main results. In addition, we call the traditional approach used in [11] as the first method for solving the problem, and the approach using the scalar product (6) and Fourier coefficients (5) as the second method. The solution accuracy while keeping the same number of basic elements is higher in the second method. In Fig. 2, a comparison of the obtained boundary conditions (BC) with the specified ones when using the 8 values of the Fourier coefficient is given for each method. The efforts are shown to scale, for example, the true value p_r in the first graph of Fig. 2 is equal to the value on the graph multiplied by the coefficient κ .

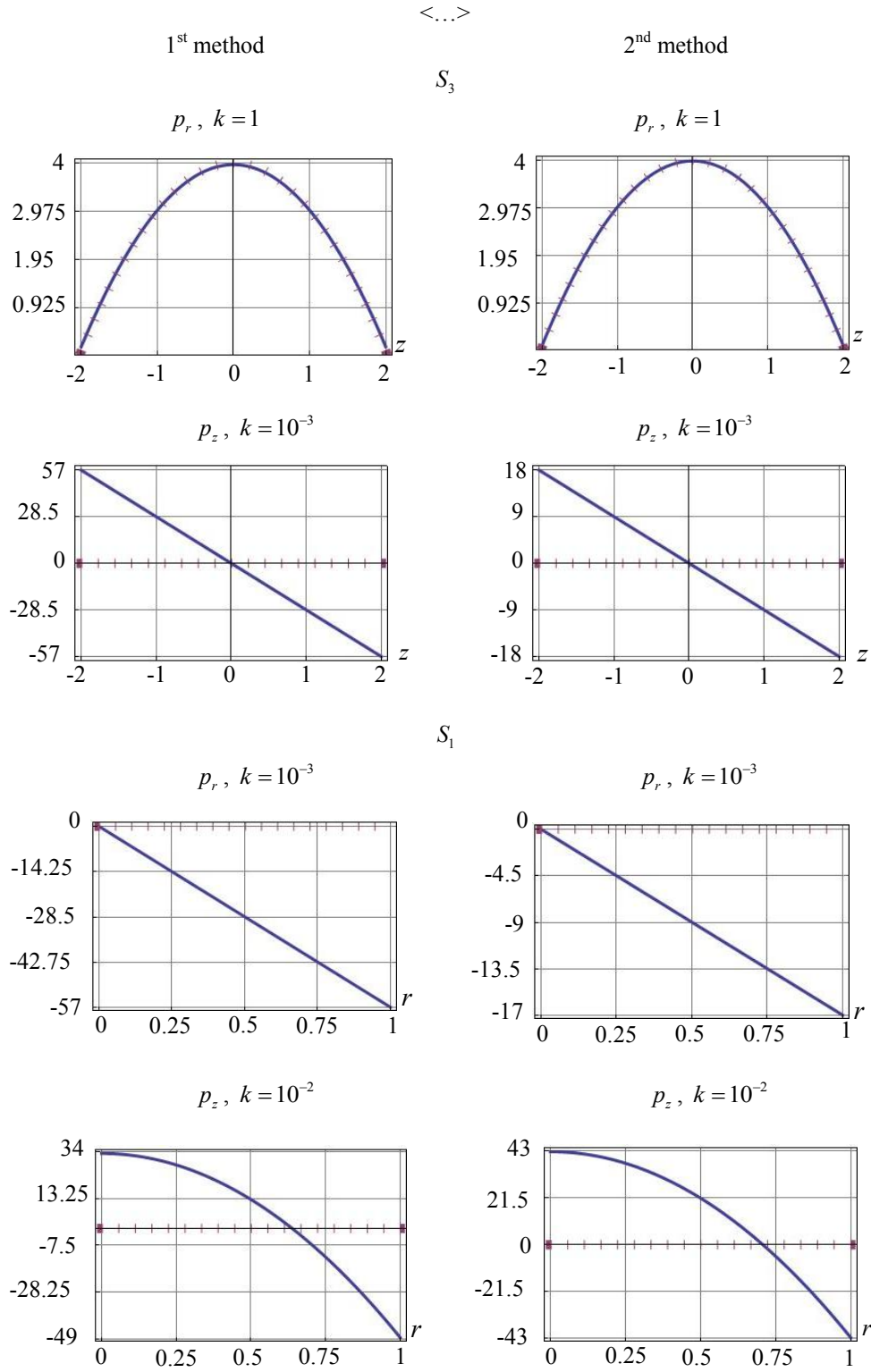


Fig. 2. Verification of BC for cylinder with 8 basis elements

This trend is preserved with an increase in the number of basis elements used. For the 61st element, verification of the boundary conditions is presented in Fig. 3 (comparison of the force p_z on the border section S_3 is given). If we evaluate an error as the maximum deviation of the obtained value from the given value, then in the second method the error is less.

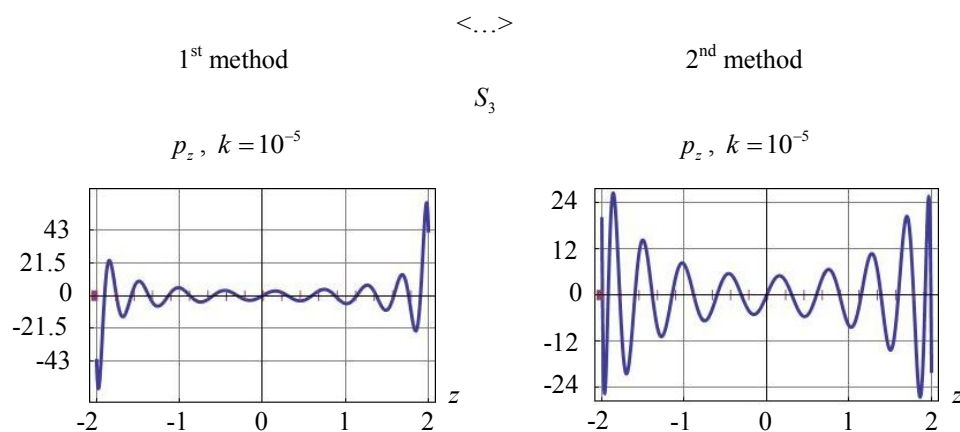


Fig. 3. Verification of BC for cylinder with 61-st basis element

Next, we examine the solution accuracy for a transversely isotropic axisymmetric body of noncanonical shape (Fig. 4). Border conditions are:

$$\begin{aligned}
 p &= 0, S_1 \cup S_2; \\
 p_r &= 0, p_z = 0, 25, S_3 \mid z = 1, 0 \leq r \leq 1; \\
 p_r &= 0, p_z = -1, S_4 \mid z = -1, 0 \leq r \leq 0,5.
 \end{aligned}$$

<...>

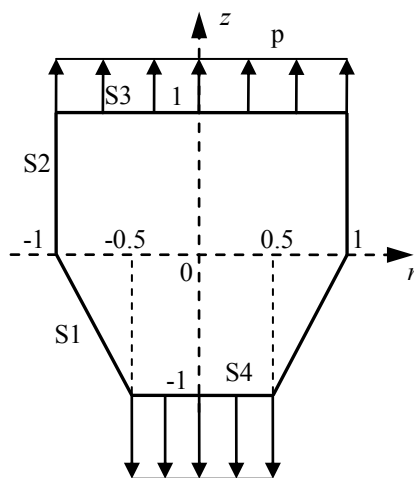


Fig. 4. Boundary conditions for axisymmetric body

15 elements of the basis are kept. Fig. 5 presents a comparison of the boundary conditions for each method (not all boundary sections and components of the force vector are shown).

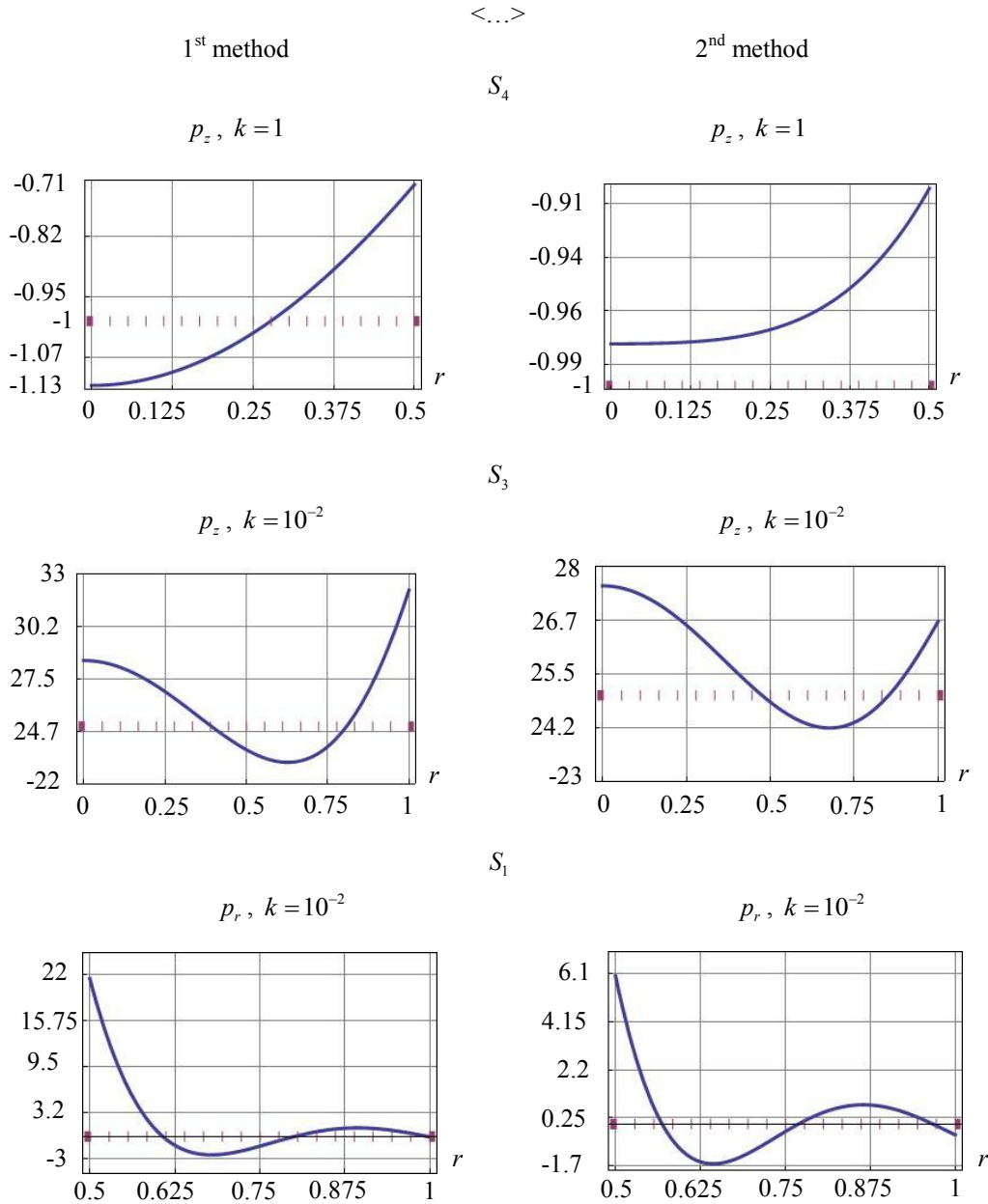


Fig. 5. Verification of BC for axisymmetric body

As can be seen from the graphs, for a body of a more complex shape, a difference in the convergence rate is observed in favor of the second method. Consider tasks involving mass forces. The sequence of the solution generation is as follows:

1. The dependence of the displacement vector of the planar auxiliary state on the coordinates $y^\alpha z^\beta$ is specified and, on its basis, the displacement vector of the spatial axisymmetric state is determined.
2. For such a vector, the following parameters are determined:
 - strain tensor according to the Cauchy relation;
 - stress tensor from Hooke's law;
 - efforts on the body surface from the fundamental Cauchy relation;
 - mass forces from the equilibrium equation.
3. An exact particular solution to the problem corresponding to the displacement function specified at each point of the body is constructed.
4. Sorting $\alpha + \beta \leq n$ ($n = 1, 2, 3 \dots$), a set of exact particular solutions of the problem of the linear theory of elasticity for the parameters is constructed:

- displacement vectors;
- strain tensors;
- stress tensors;
- vectors of surface forces;
- vectors of mass forces.

5. The bases of internal $\Xi = \{\xi_1, \xi_2, \xi_3, \dots, \xi_k, \dots\}$ and boundary $\Gamma = \{\gamma_1, \gamma_2, \gamma_3, \dots, \gamma_k, \dots\}$ states in which the equalities are respected, are generated:

$$\xi_k = \{u_k, \varepsilon_k, T_k\},$$

$$\gamma_k = \{u_k^v, p_k, X_k\}.$$

6. We leave only linearly independent among these solutions and carry out their orthogonalization in accordance with scalar products in the bases of internal and boundary states:

$$(\xi_i, \xi_j) = \int_V \varepsilon_{ij}^{(i)} \sigma_{ij}^{(j)} dV,$$

$$(\gamma_i, \gamma_j) = \int_S p_i^{(i)} u_{vi}^{(j)} dS + \int_V X_i^{(i)} u_i^{(j)} dV$$

(indices i and j , responsible for the numbers of elements, are placed on top and are enclosed in brackets).

7. As a result, we obtain a basis through which the corresponding vectors or tensors are expanded to series (3) with equal coefficients:

$$c_k = \int_V X u_k dV + \int_S p u_k^v dS,$$

where X is the vector of given mass forces.

We study the possibility of constructing an elastic field in the presence of mass forces using relations (6) and (5). Consider the first primal problem with unbalanced forces for a transversely isotropic cylinder (Fig. 6). Border conditions are:

$$p = 0, S_1 \cup S_3;$$

$$p_r = 0, p_z = r^2, S_3 | z = 2, 0 \leq r \leq 1.$$

<...>

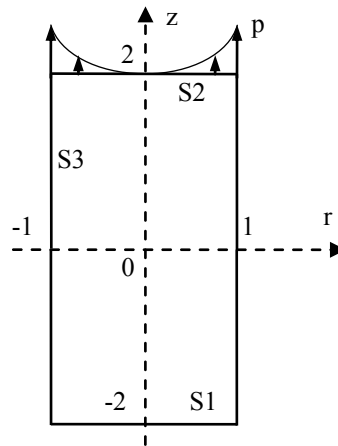


Fig. 6. Boundary conditions for cylinder

The expressions for the orthonormal basis set of the displacement vector components $u = \{u, w\}$ are given in Table 1.

Table 1

Orthonormal basis set of displacement vector components

	u	w
ξ_1	0	$0.1213z$
ξ_2	$0.0788r$	$-0.1126z$
ξ_3	0	$0.0331z^2$
ξ_4	$0.0592rz$	$-0.0268z^2$
ξ_5	$-0.02rz$	$0.0975r^2 + 0.009z^2$
ξ_6	$0.1535r$	$-0.9163z + 0.0691z^3$
ξ_7	$-0.2896r + 0.0724rz^2$	$1.2067z - 0.1005z^3$
ξ_8	$1.8629r - 0.4824rz^2$	$-8.2447z + 0.4824r^2z + 0.6701z^3$
ξ_9	$0.0908rz$	$-0.0454r^2 - 0.4347z^2 - 0.0511z^4$
ξ_{10}	$-0.1757rz + 0.0439rz^3$	$-0.0195r^2 + 0.3661z^2 - 0.0457z^4$
ξ_{11}	$0.2881rz - 0.0804rz^3$	$-0.144r^2 - 0.7209z^2 + 0.1206r^2z^2 + 0.0837z^4$

<...>

To obtain a rigorous solution, it took 11 Fourier coefficients, non-zero values: $c_1 = 0.2178$; $c_2 = -0.1226$; $c_3 = 0.2377$; $c_4 = -0.0732$; $c_5 = 0.0247$; $c_8 = 0.1443$; $c_{11} = 0.1443$. We give the expressions for displacements and mass forces (4 decimal places are kept):

$$u = 0.2592r + 0.0367rz - 0.0696rz^2 - 0.0116rz^3;$$

$$w = -0.0183r^2 - 1.1497z + 0.0696r^2z - 0.094z^2 +$$

$$+ 0.0174r^2z^2 + 0.0967z^3 + 0.0121z^4;$$

$$R = -0.2814r - 0.1407rz; \quad Z = 1.2012 - 0.25r^2 - 3.6038z - 0.9z^2.$$

If we construct a basis of internal states through planar auxiliary states formed using monomial $z^\alpha y^\beta$, then the orthonormal basis and the Fourier coefficients change. In this case, the decision will also be rigorous and will be accepted in:

$$u = 0.0363r - 0.0913rz + 0.0309r^3z - 0.0287rz^2;$$

$$w = 0.0456r^2 - 0.0077r^4 - 0.4148z + 0.0287r^2z + 0.0257z^2 + 0.0399z^3;$$

$$R = -2.0145r - 1.6178rz; \quad Z = -0.25r^2 - 1.4893z.$$

Similarly, other particular solutions to the problem can be obtained using different types of polynomials, for example, $z^\alpha y^\beta + z^\alpha$, etc. to form the basis.

The approach under study provides for lots of solutions of one boundary value problem of the elasticity theory in the presence of mass forces. Displacements and mass forces whose combinations give the distribution of stresses satisfying the given forces at the boundary are also subject. The first method is devoid of this feature because mass forces in it are part of the given conditions, and the task is only to find the field of displacements.

Discussion and Conclusions. The second method to solve the problem has the best convergence. In addition, unlike the first method, when calculating scalar products in the process of orthogonalization and in determining the Fourier coefficients, the second method does not use deformations and displacements. Here, a basic set of stresses is generated, and its trace at the boundary is a basis set of surface forces with which orthogonalization and series construction are performed. This means that when calculating scalar products, there is no error associated with the components responsible for the rigid displacement that may occur during the formation of the basis [11].

If problems with mass forces are considered, then the second method may be useful in the formation of many particular solutions whose stresses satisfy certain conditions at the boundary. These solutions can be used as the basis ones for a more complex problem, and also be useful under determining the elastic fields realized from fictitious loads resulting from the application of the Poincare method [7, 8].

The accuracy of solving problems of the elasticity theory by the boundary-state method is analyzed using different approaches to the construction of scalar products. The solution to the problem of the linear elasticity theory using

the representation of a general solution to the Lamé equation in the form of a Fourier series on basis functions and expression (6) as the orthogonalizer of these functions had the best convergence.

References

1. Gogoleva OS. Primery resheniya pervoi osnovnoi kraevoi zadachi teorii uprugosti v polupolose (simmetrichnaya zadacha) [Examples of solving the first basic boundary value problem of the elasticity theory in a half-string (symmetric problem)]. Vestnik of OSU. 2012;9(145):138–142. (In Russ.)
2. Volodchenkov AM, Yudenkov AM. Ob odnom metode resheniya pervoi osnovnoi zadachi teorii uprugosti dlya odnorodnogo anizotropnogo tela [About the solution method of the first major task of the elasticity theory for homogeneous anisotropic theory]. Universum: Technical Sciences. 2015;(18):1–9. Available from: <http://7universum.com/ru/tech/archive> (accessed: 07.12. 2019). (In Russ.)
3. Sukhodolova YuS, Trufanov NA. O konechnom ehlemente na osnove variatsionnogo printsipa Kastil'iano dlya ploskikh zadach teorii uprugosti [About a finite element based on the Castigliano variational principle for plane elasticity problems]. PNPRU Mechanics Bulletin. 2012;1:168–178. (In Russ.)
4. Pozharskii DA, Davtyan DB. Sravnenie tochnykh reshenii kontaktnykh zadach dlya transversal'no izotropnogo poluprostranstva [Comparison of contact problem exact solutions for transversely isotropic half-space]. Vestnik of DSTU. 2015;15(1):23–28. DOI : 10.12737/10371. (In Russ.)
5. Ivanychev DA. Metod granichnykh sostoyanii v prilozhenii k ose-simmetrichnym zadacham dlya anizotropnykh tel. [The boundary state method as applied to axisymmetric problems for anisotropic bodies]. News of Higher Educational Institutions of the Chernozem Region. 2014;1:19–26. (In Russ.)
6. Ivanychev DA, et al. The method of boundary states in problems of torsion of anisotropic cylinders of finite length. International Transaction Journal of Engineering, Management, & Applied Sciences & Technologies. 2019;10(2):183–191. DOI : 10.14456/ITJEMAST.2019.18.
7. Penkov VB, et al. An algorithm for full parametric solution of problems on the statics of orthotropic plates by the method of boundary states with perturbations. Journal of Physics: Conf. Series. 2018;973(012015):10. DOI : 10.1088/1742-6596/973/1/012015.
8. Penkov VB, et al. An algorithm for analytical solution of basic problems featuring elastostatic bodies with cavities and surface flaws. Journal of Physics: Conf. Series. 2018;973(012016):11. DOI : 10.1088/1742-6596/973/1/012016.
9. Penkov VB, et al. Using computer algebra to construct analytical solutions for elastostatic problems. Journal of Physics: Conf. Series. 2019;1203(012020):12. DOI : 10.1088/1742-6596/1203/1/012020.
10. Penkov VB, Satalkina LV, Shulmin AS. The use of the method of boundary states to analyse an elastic medium with cavities and inclusions. Journal of Applied Mathematics and Mechanics. 2014;78(4):384–394. DOI : 10.1016/j.jappmathmech.2014.12.010.
11. Pen'kov VB, Pen'kov VV. Metod granichnykh sostoyanii dlya resheniya zadach lineinoi mekhaniki [Boundary conditions method for solving linear mechanics problems]. Far Eastern Mathematical Journal. 2001;2(2):115–137. (In Russ.)
12. Lekhnitskii SG. Teoriya uprugosti anizotropnogo tela [Elasticity theory of an anisotropic body]. Moscow: Nauka; 1977. 416 p. (In Russ.)
13. Aleksandrov AY, Solov'ev YuI. Prostranstvennye zadachi teorii uprugosti [Spatial problems of the elasticity theory]. Moscow: Nauka; 1978. 464 p. (In Russ.)

Submitted 13.01.2020

Scheduled in the issue 09.03.2020

About the author

Ivanychev, Dmitrii A., associate professor of the General Mechanics Department, Lipetsk State Technical University (30, st. Moskovskaya, Lipetsk, 398055, RF), Cand.Sci. (Phys.-Math.), ORCID: <http://orcid.org/0000-0002-7736-9311>, Lsivdmal@mail.ru

The author has read and approved the final manuscript.

MACHINE BUILDING AND MACHINE SCIENCE



UDC 621.791.754

<https://doi.org/10.23947/1992-5980-2020-20-1-25-35>

Study on pulsed-arc welding issues at the Machines and Welding Production Automation Department, RIAE — DSTU

V. A. Lenivkin, D. V. Rogozin

Don State Technical University (Rostov-on-Don, Russian Federation)



Introduction. The history of solving the problem of welding structures made of stainless and heat-resistant metals and alloys goes back several decades. Researchers were particularly interested in working with deformed aluminum alloys 2–6 mm thick. As a rule, such thin-walled structures are welded in an argon shielding gas at relatively small currents; therefore, metal transfer is large-droplet (the weld is shaped in the form of separate large droplets with a narrow penetration of the welding components). At the same time, the weld is very convex, which does not meet the operational requirements of the structures. Thus, it was important to solve the following problems: to obtain a controlled fine-drop transfer of electrode metal at currents corresponding to a large-drop transfer; to determine a condition for the controlled transfer; to develop a power supply system for the welding arc.

Materials and Methods. The behavior and parameters of the arc were recorded through the high-speed film and video shooting with synchronous oscillography of the electrical process parameters – current and voltage. They were recorded by light-beam oscilloscopes and two-screen oscilloscopes. The data were processed using a computer complex and *Diadem* 10.1 software.

Results. The basic condition for the controlled metal transfer is determined through applying current pulses to the welding arc from special pulse sources with and without energy storage devices. Transients in the electrical circuits of the main welding source during the current pulse action and pause are considered. The factors providing stability of rigid and flexible pulsed-arc welding (PAW) are indicated.

Discussion and Conclusions. The results of studying the possibility to control the welding arc processing behavior and the proposed methods for calculating the parameters of the PAW mode became the basis for the development of technology and equipment for the mechanized GMAWP of aluminum alloy assemblies. They are introduced at the enterprises of the aviation industry, shipbuilding. Solutions for stainless and heat-resistant steels and alloys are used at the motor industry enterprises. As a result of studies on the mechanized CO₂ activated electrode wire welding, a mechanized PAW technology was developed for units of stainless steel electric furnace bodies, structures of road-building, agricultural machinery and ships.

Keywords: welding in shielding gases, consumable electrode, current pulse parameters, controlled metal transfer.

For citation: V. A. Lenivkin, D.V. Rogozin. Study on pulsed-arc welding issues at the Machines and Welding Production Automation Department, RIAE — DSTU. Vestnik of DSTU, 2020, vol. 20, no. 1, pp. 25–35. <https://doi.org/10.23947/1992-5980-2020-20-1-25-35>



Introduction. Since early sixties of the XX century, gas-shielded consumable-electrode welding of metal structures has been studied [1]. One of the basic problems of this process is the manufacture of welded structures from stainless and heat-resistant metals and alloys. Of particular difficulty was the creation of deformed aluminum alloys 2–6 mm thick. These materials are used in aviation, motor and shipbuilding, in light, food, and chemical industries. Welding of thin-walled structures of these metals was performed, as a rule, by a non-consumable electrode in the argon shielding gas medium with relatively low process productivity. Mechanized consumable-electrode welding at relatively small currents

was also used, which means with large-drop metal transfer. In this case, the weld at small currents is formed in the form of separate fused large droplets with a narrow, small penetration of the welded elements, which does not always meet the technical requirements for the structure design.

It is known that there is a critical current under welding in argon. In a narrow range of its changes, the character of metal transfer sharply changes. At currents below the critical level, the metal transfer is globular, and above the critical one, it is spray transfer. In case of the globular metal transfer, a weld of improper shape is obtained – with a narrow, shallow penetration and a large convexity. If the current is higher than critical, during spray transfer, the weld has finger-shaped penetration, which reduces the durability of the weld joint.

During the mechanized welding of a melting electrode wire, the current value periodically changed for a short time. The purpose of this operation is to obtain controlled fine-droplet transfer of electrode metal at currents corresponding to globular metal transfer. In this case, the geometric shape of the weld should meet the technical requirements for welded structures.

Materials and Methods

The arc power system for pulsed arc welding (PAW). To achieve this goal, an arc power system from two electric energy sources has been developed. The system includes:

- the normal power supply is the PSG-500 welding transducer with a flat-dipping volt-ampere characteristic (VAC) since at that time there were no welding rectifiers for the mechanized welding in shielding gases;
- a special switching power supply (SPS) is a pulse energy storage generator.

The normal and pulsed sources were connected in parallel to the arc gap.

In the first arc SPS developed, 150 A current ignitrons were used as power controlled rectifiers. Then, when the VK-200 and VT-150 power semiconductor rectifiers became available, they began to manufacture and introduce switching power supplies for semiconductor valves at enterprises. Switched energy storage power supplies are protected by copyright^{1, 2}.

When the normal and SPS of the arc are connected in parallel [2], an increased voltage is applied to the arc under the current pulse pile-up. It is directed opposite to the normal source and “locks” it due to the presence of an uncontrolled rectifier $V2$ in its circuit (Fig. 1). A decrease in current in the normal source circuit under the action of a current pulse is meant by “locking”.

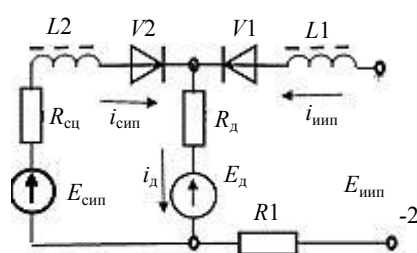


Fig. 1. Equivalent circuit of arc supply from normal and switched power sources: $E_{сип}$, $E_{нп}$, $E_{д}$ are voltage of welding, switched power sources and arc; $i_{сип}$, $i_{нп}$, $i_{д}$ are current of welding, pulsed sources and arc; $R_{сц}$, $R1$, $R_{д}$ are active resistance of the welding circuit, pulse source and arc; $L2$, $L1$ are inductance of the circuit of the welding and pulse sources; $V2$, $V1$ are rectifiers in the circuit of the welding and pulse sources

However, despite the presence of the $V2$ rectifier, the “locking” of the normal source does not occur instantly. Due to the inductive resistance $L2$, a transient process occurs in the circuit (during the pulse pile-up and after its action).

Consider the transition process of current variation in the normal source circuit when a current pulse is applied. To do this, we solve a linear differential equation compiled for the normal power supply circuit (see Fig. 1):

¹ Budnik NM, Dyurgerov NG, Sagirov KhN, et al. *Ustroistvo dlya impul'sno-dugovoi svarki: A.S. 226752 SSSR* [Device for pulsed-arc welding: author's cert. no. 226752] USSR, 1968.

² Budnik NM, Sagirov KhN, Dyurgerov NG, et al. *Ustroistvo dlya impul'sno-dugovoi svarki: A.S. 299111 SSSR* [Device for pulsed-arc welding: author's cert. no. 226752] USSR, 1971.

$$E_c = L_2 \frac{dI_6}{dt} + R_2 I_6 + R_d i_{\text{инп}}. \quad (1)$$

Here, $E_c = E_{\text{сип}} - E_d$, $R_2 = R_d + R_{\text{сип}}$; I_6 is current of the normal power source; $i_{\text{инп}}$ is free current in the pulse (for example, for sinusoidal pulses with a damping amplitude):

$$i_{\text{инп}} = \frac{E_{\text{инп}} - E_d}{\omega_0 L_1} \exp\left(-\frac{R_{\text{инп}}}{2L_1} t\right) \sin \omega_0 t,$$

where $R_{\text{инп}} = R_1 + R_d$, $\omega_0 = \sqrt{\frac{1}{L_1 C} - \frac{R_{\text{инп}}^2}{4L_1^2}}$.

After the pulse end, the current in the normal source circuit increases exponentially, it is determined by the time constant of the normal power source circuit $\tau_{\text{сип}} = R_{\text{сип}}/L_2$.

$$I_6(t)_{t_{\text{н}} \rightarrow t_{\text{к}}} = [I_{d0} - I_6(t)_{t=t_6}] \left(1 - \exp - \frac{t}{\tau_{\text{сип}}}\right) + I_6(t)_{t=t_6}. \quad (2)$$

Based on the equations (1 and 2), the law of the current variation in the circuit of the normal source was obtained during the current pulse pile-up and after its end [3, 4].

Research methodology. The arc behavior and its parameters under welding at various spatial positions of non-ferrous and ferrous metal samples were recorded by high-speed film shooting up to 5000 frames/s and video shooting 2000 frames/s. At the same time, synchronous oscillographic testing of the process electrical parameters was performed: the arc current and voltage were recorded by the light-beam and electronic oscilloscopes. The data obtained by means of a two-screen electronic oscilloscope was processed using a computer complex and *Diadem 10.1* software.

We studied the nature of metal transfer, the weld formation, and determined the PAW physical and process parameters in the protective gases of these metals.

Research Results

Welding in argon protective environment. An analysis of the obtained patterns provides evaluating of the effect of the PAW mode parameters on the joint operation of the arc feeding system, in which the welding process becomes unstable. Oscillograms of the PAW process at various inductances of the welding power supply circuits are shown in Fig. 2.

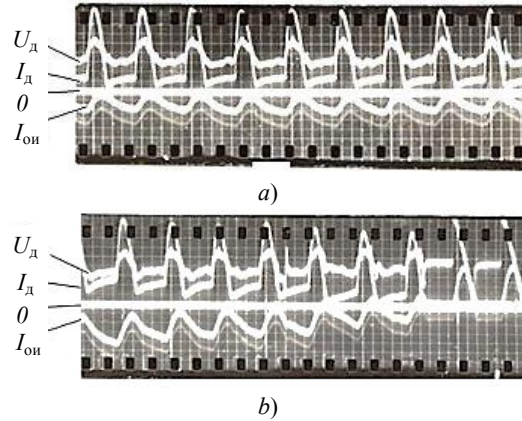


Fig. 2. Oscillogram of current (I_d), voltage (U_d) of the arc and current in the circuit of the welding power source ($I_{\text{сип}}$) ($t_{\text{н}} = 4.6 \cdot 10^{-3}$ s, $I_{\text{н}} = 690$ A, $f = 100$ cps): continuous arcing $I_{\text{ср}} = 70$ A, $L = (1.0 \div 1.1) \cdot 10^{-3}$ H (a); intermittent arc burning $I_{\text{ср}} = 150$ A, $L = 0.3 \cdot 10^{-3}$ H (b)

The natural (non-pulsed) and pulsed welding processes are considered. It is established that for identical values of the effective current, the velocity of droplet movement in the arc gap is always higher under PAW. Moreover, a larger current in the pulse at the moment of its detachment from the electrode always corresponds to a larger drop velocity. Separation of the droplet from the electrode can occur in various phases. It depends on the welding mode and current pulse parameters.

When the droplet is detached at the end of the pulses, the current is close to the base current of the welding process, and the droplet flying speed reaches 1.2–2.0 m/s. In this case, a controlled directional metal transfer is provided under welding in all spatial positions with minimal metal loss through splatter (Fig. 3 a).

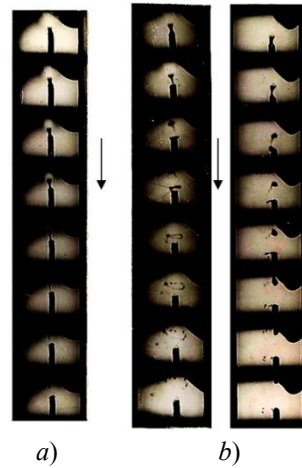


Fig. 3. PAW records of aluminum alloy AMg6 in the overhead position under various modes (shooting speed is 4000 frames/s, welding wire is AMg61 1.6 mm in diameter): effective current is $I_{\text{эф}} = 100$ A, $t_{\text{и}} = 2.5 \cdot 10^{-3}$ s, $I_{\text{и}} = 310$ A, $f = 50$ cps (a); $I_{\text{эф}} = 180$ A, $t_{\text{и}} = 4.5 \cdot 10^{-3}$ s, $I_{\text{и}} = 500$ A, $f = 50$ cps (b)

It is established that the minimum amplitude of the current pulse $I_{\text{и min}}$, which provides a transition from uncontrolled transfer to controlled transfer, depends on:

- surface tension of the electrode metal $\sigma_{\text{и}}$,
- electrode diameter $d_{\text{э}}$,
- welding mode parameters, $I_{\text{эф}}$, $\nu_{\text{и}}$:

$$I_{\text{и min}}^2 t_{\text{и}} = A_1 \sigma_{\text{и}} d_{\text{э}}^2 f^{0.5} / I_{\text{с}}. \quad (3)$$

In the case of droplet detachment from the electrode at an amplitude value of the pulse current, its flying speed in the arc gap can exceed 8 m/s. This causes the appearance of:

- near-weld splashes (due to spattering of molten metal from the weld pool),
- a weld-affected zone of fine droplet spraying formed when a neck of a molted metal breaks between an electrode and a droplet (see Fig.3 b).

To reduce the metal loss due to spatter, the amplitude of the current pulse should not exceed $1.1 I_{\text{и min}}$.

The increase in $I_{\text{и}}$ is limited by the condition of continuous arc burning: if the effective current is constant, then with an increase in the amplitude, frequency, and pulsewidth, the base current decreases.

When the base current decreases below the minimum steady-state current of the arc, its breaks occur (the welding current is interrupted), the stability of the welding process is violated (see Fig. 2 b). This condition was used to determine the maximum values of the pulse parameters. For example, the maximum amplitude of a pulse from a source with energy storage for unipolar current pulses (damped sinusoid):

$$I_{\text{и max}} < \frac{2I_{\text{с}}}{\pi t_{\text{и}} f^{0.5}} \sqrt{(\pi^2 t_{\text{и}}^2 + t_{\text{и}})} / \sqrt{t_{\text{и}} \left(1 - \exp\left(\frac{2t_{\text{и}}}{RC}\right)\right)}. \quad (4)$$

Fig. 4 shows the dependences of the minimum required amplitude of the pulse current (curves 1, 1') and the maximum allowable amplitude (curves 2, 2') on their repetition rate for different pulsewidth. Curves 1, 1' (with increasing current) are the boundary of the transition from uncontrolled transfer of metal droplets to the controlled transfer. Curves 2, 2' are the boundary of the transition from controlled droplet transfer to arc burning cessation. These curves limit the range of the PAW modes by a consumable electrode.

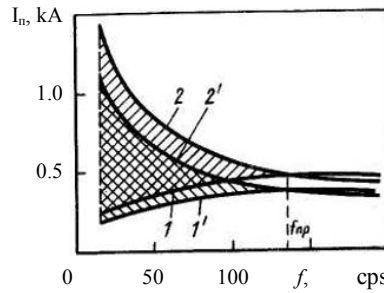


Fig. 4. Areas of permissible amplitude values of current pulses: argon, alloy AMg6, $I_{\Phi} = 140$ A; 1, 2 — $t_n = 1.4$ ms; 1', 2' — $t_n = 2.2$ ms

From the equations (3) and (4), it follows that with an increase in the pulse repetition rate, the minimum required amplitude of the current increases, and the maximum allowable amplitude decreases. The area of controlled drop transfer narrows.

Under the limiting current pulse rate (f_{np}), the frequency is adopted at which the minimum required amplitude of the current pulse is the maximum allowed. This frequency was determined through solving equations describing $I_{\text{n min}}$ (3) and $I_{\text{n max}}$ (4).

Welding in active shielding gases. Welding in active shielding gases (CO_2 , N_2 and mixtures of $\text{Ar} < 80\% + \text{CO}_2 > 20\%$) and He on the current of direct and reverse polarity is considered. It was established that in this case, the current pulse pile-up with the parameters used for welding in argon does not provide the controlled metal transfer [4, 5]. The current pulse pile-up under the activated electrode wire welding (alkali salts) by the current of direct polarity provides stabilization of the arc – it takes the shape corresponding to the current higher than critical. However, in the pulse spacing, when the arc current is less than critical, it wanders intensively. If a drop passes from the electrode at the end of the pulse, when the current decreases to below a critical value, then the detachment and transfer of the drop takes place in an erratic arc. In the pulse spacing, the electrode wire melts, and at its end, there is always a certain amount of molten metal. Due to the wandering of the arc, the drop moves relative to the axis of the electrode wire. When a pulse pile-up, the drop detaches and may not fall into the weld pool. The pulse pile-up with duration of 1.2–1.8 ms causes the detachment of droplets from the electrode wire with each current pulse; however, it does not provide directional transfer of metal into the weld pool and is characterized by increased spatter.

It was found that non-coaxial droplets, under current pulse pile-up, deviate to a greater extent from the electrode wire axis than coaxial ones. The largest number of misaligned droplets detaches from the electrode at an angle of 20–30° and does not fall into the weld pool. Coaxial drops detach at an angle not exceeding 10°.

When the pulsewidth is 4.0–5.0 ms, the base current of the welding process decreases due to the integral self-regulation of electrode melting [6, 7]. At the end of the electrode wire, despite the wandering of the arc during cessation, a small volume of molten metal is formed. As a rule, under the current pulse action, several coaxial droplets are formed, which are transferred to the weld pool, and this causes small spatter.

To reduce the metal loss due to spatter under the activated electrode welding in active shielding gases and their mixtures, it is required to combine the processes of melting and droplet transfer into the weld pool. The electrode wire should melt at a current above critical, when the arc is spatially stable and does not cause deviation of the flight trajectory of droplets from the electrode axis in the interelectrode gap [8, 9]. This is achieved as follows: current pulses of the same polarity are superimposed on a continuously burning arc with the minimum possible amplitude $I_n = (1.5\text{--}2.0) I_{\text{kp}}$ and the maximum possible duration $t_n = 4.0\text{--}10$ ms at a pulse repetition rate of 100–50 cps. The base current is selected to be minimal (so that during cessation, the electrode wire does not practically melt). In this case, during the period of the pulse action, short-term spray transfer (ST), called intermittent spray transfer (IST), occurs. When the pulse amplitude decreases below $1.5 I_{\text{kp}}$, metal spray transfer is impossible.

A nonstorage switched power supply has been developed and manufactured for the practical implementation of the described process.

For the first time, the features of the weld formation under PAW were determined. The nature of the molten metal displacement in the weld pool was studied with and without current pulse pile-up on the arc. This provided determining factors that improve the weld formation and the retention of the metal of the weld pool under PAW in various spatial positions.

Using high-speed filming (up to 5000 frames per second), it was found that under PAW, molten metal is displaced from the head end of the weld pool under the action of arc pressure and pressure created by drops of a transferred electrode metal [3]. It turned out that the speeds of molten metal movement caused by the arc pressure under the action of the current pulse and the kinetic energy of the droplets were commensurate. Therefore, in case of PAW, in one cycle, the molten metal is twice displaced from the head end of the pool to its tail end.

The move frequency of molten metal in the pool increases with an increase in the pulse frequency, *ceteris paribus* (constant welding current and arc voltage). This cuts cycle time and reduces the amount of transported metal, which crystallizes in a thinner layer, which helps to improve the primary crystallization of the weld metal.

PAW when feeding an arc from two sources (see Fig. 1), as a rule, is performed according to a rigid program with a fixed pulse repetition rate. The shape of the current pulses is similar to the curve of the applied increased voltage (see Fig. 2).

Since 1989, research has been carried out to create welding rectifiers with inverter converters for various consumable and non-consumable electrode welding methods^{1,2}.

PAW by pulses of a rectangular shape. Welding rectifiers with an inverter converter are created on the basis of high-frequency inverters with a current conversion frequency of 16 kHz. In this case, power sources of the welding arc are low-inertia — high-speed ones. This provides a curve of the welding current of various shapes with a change in magnitude over a wide range. The rectifiers with combined volt-ampere static characteristics with three prominent sections are most used when performing welding operations. The steep-dipping section at currents less than 30A provides reliable arc striking and the establishment of the welding process. The flat-dipping section and the bayonet section in the range of operating modes provide stabilization of the welding current in a wide range of its regulation, in a wide range of changes in the voltage drop across the arc.

The digital control system for the arc power source provides a fast shape change of the welding current curve and maintaining the bayonet section of the volt-ampere characteristics in the range of the current control limit. The source is equipped with a control system for the consumable and non-consumable electrode welding.

PAW by rectangular pulses from a single arc power source can be obtained for the mechanized consumable-electrode wire welding with a constant feed rate. For this, it is required to use a discrete two-level switching of the volt-ampere characteristic of the power supply (PS VAC) with a bayonet section in the range of operating currents of the welding rectifier.

Let us consider how the welding electrical parameters change at a constant feed rate of the electrode wire and discrete switching of the VAC of a welding rectifier with an inverter converter (Fig.5).

¹Lenivkin VA, Petrov PI, Oleinikov AG. *Sposob dugovoi svarki plavleniem: A. S. 1776517 SSSR*: [Fusion arc welding method: author's cert. no. 1776517] USSR, 1991.

²Oleinikov AG, Lenivkin VA, Petrov PI, Zhmailov BB. *Istochnik pitaniya dlya dugovoi svarki: RF patent 2063850* [Arc welding power source] RF Patent no. 2063850, 1994.

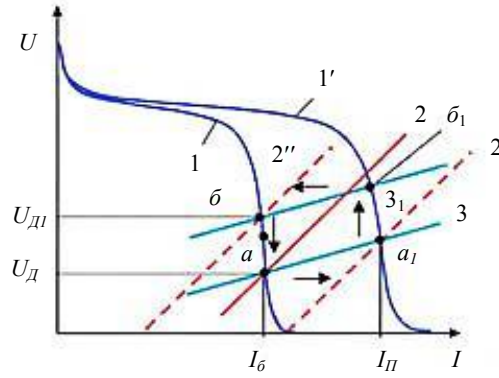


Fig. 5. Variation of mode energy parameters under PAW according to flexible program: 1 and 1' are PS VAC providing base current I_{δ} and pulse current I_{Π} , respectively; 2 is the given curve of self-regulation characteristics of electrode wire melting; 2' and 2'' are dummy curves of the self-regulating melting behavior of the electrode wire; 3 and 3₁ are static arc VAC before and after the current pulse action

The electrical parameters (voltage U_{Δ} and arc current I_{δ}) of a stable mechanized consumable-electrode wire welding are determined by the point a (here, PS VAC I and the characteristic line of self-regulating melting of the electrode wire 2 meet at a constant feed rate).

It is known that at any point of stable welding operation, the electrode wire feed speed (v_n) is equal to its melting rate (v_s), and the arc gap length (ℓ_a) depends on the voltage drop across the arc and remains unchanged. Therefore, the static volt-ampere characteristic of the arc (A VAC) 3 with its constant length ℓ_a passes through quiescent point a (Fig. 5).

The current value at point a (see Fig. 5) is selected less than the critical current value, that is, the process of arc welding with a globular droplet metal transfer for a specific diameter and type of electrode wire corresponds to the base current of the welding process I_{δ} , which is determined approximately through the dependence:

$$I_{\delta} = v_n / k_{CT}. \quad (5)$$

Here, v_n is the electrode feed rate; k_{CT} is the coefficient of arc current self-regulation; $k_{CT} = \frac{1}{28.3\gamma} \frac{\alpha_{n\Delta}}{d_s^2}$ ($\alpha_{n\Delta}$ is the electrode wire fusion coefficient, g/A h); γ is the electrode wire density, g/cm³.

The voltage drop across the arc (U_{Δ}) at point a is selected so that PS VAC I can provide stable arc burning without short circuits of the arc gap.

Under a discrete switching of PS VAC from position 1 to position 1' and a constant arc length, the welding mode parameters of point a move to the position of point a_1 . (In Fig. 5, the arrows indicate the direction of change in the magnitude of I_{Δ} and U_{Δ}). The arc current value at the point a_1 corresponds to the given amplitude value of the pulse current (I_{Π}), which is selected from the condition for providing the ST under its operation:

$$I_{\Pi} \geq (1.5 \pm 2.0) I_{kp},$$

where I_{kp} is the critical current, which is determined by the welding current magnitude, the diameter and grade of the electrode wire, the length of the arc gap.

A stable welding process with continuous arc burning at point a_1 and an unchanged arc length ℓ_a and I_{Π} can be established at the intersection of PS VAC 1' with the self-regulating melting line of the electrode wire 2' if the voltage drop is slightly greater than at point a ($v_n = v_s$). This is due to the fact that under real conditions of welding, when measuring the voltage drop across the arc, the voltage drop at the electrode wire extension is simultaneously taken into account. Therefore, an increase in the voltage drop at point a_1 is caused by an increase in the voltage drop at the electrode extension and the arc resistance at a higher current I_{Π} .

When PS VAC are switched from position 1 to 1', the welding mode parameters (arc current and voltage) are determined through the intersection of PS VAC 1' and A VAC 3. In this case, the welding process is unstable since the melting rate of the electrode wire at point a_1 remains unchanged and is determined by the self-regulating melting curve of electrode 2, and v_s at I_{Π} will be more than v_n by the value Δv_s :

$$\Delta v_3 = k_{cm}(I_n - I_\delta). \quad (6)$$

At that, the arc length will start to increase. The static characteristic of arc 3 will start to shift equidistantly up from point a_1 in the direction of point δ_1 .

It is established that with an increase in the arc length at a constant value of the welding current and a constant feed rate of the electrode wire, its stick out decreases, and the thermal power spent on melting the electrode decreases. The frequency of metal spray transfer decreases and the size of the transferred droplets increases. Spray transfer transforms monotonously into globular one.

When combining point a_1 with the intersection point of PS VAC 1' and the self-regulating melting line of electrode wire 2, a new point of stable operation with metal transfer is established, as at point a , at which $v_n = v_s$, but with a different arc length.

For PAW with ST, it is required to switch the PS VAC from position 1' to position 1 with a shorter arc length ℓ_{a3} than at point δ_1 , at which the ST is not violated yet.

During the arc burning on a current I_n A VAC moves equidistantly from point a_1 to point δ_1 . In this case, the arc length increases by $\Delta\ell_{a1}$, and the arc static characteristic will occupy position 3₁ (Fig. 5). The voltage drop across the arc will increase by

$$\Delta U_a = k_a \Delta\ell_{a1} + k_{ar}(I_n - I_\delta), \quad (7)$$

where k_a is the arc core voltage gradient, V/mm; k_{ar} is the coefficient characterizing the slope (A VAC).

Under a discrete switching of PS VAC from position 1' to position 1, the mode parameters and the welding process go from point δ_1 corresponding to the pulse current I_n , to point δ corresponding to the base current I_δ . Welding at point δ would be stable if PS VAC intersected by the line of the self-regulation characteristic of the electrode wire melting 2, which corresponds to lower v_n than the specified curve speed of the self-regulation characteristic of electrode wire melting 2.

Therefore, the melting rate of the electrode wire v_s at point δ slows down sharply at almost constant base current I_δ . The arc gap starts to contract since $v_n > v_s$. The arc static characteristic is shifted equidistantly from point δ to quiescent point a . During the arc burning at the base current, the arc length decreases by $\Delta\ell_{a2}$.

When combining the static A VAC 3₁ with characteristic 3 $\Delta\ell_{a1} = |\Delta\ell_{a2}|$, the voltage on the arc becomes equal to the specified lower level of operation of the two-level sensor. At this moment, PS VAC switches from position 1 to position 1', and the process is periodically repeated.

The pause time t_n is determined by the burning time of the arc between points δ and a at current I_δ , and the pulse length t_n — between the points a_1 and δ_1 at current I_n .

PS VAC from position 1 to position 1' and back, switches automatically depending on the specified voltage drop of the arc burning at the base and pulse current. The voltage drop is set for the base current a and pulse current δ_1 . The power supply control system receives data on the base and pulse voltages using a two-level voltage sensor. In this case, the control system of the welding power source operates according to a flexible program. The switching frequency «pulse – pause» depends on the set difference in the voltage drop between the values of the base and pulse currents.

In some cases, for example, when welding in the vertical and overhead positions, a higher flight speed of droplets is required than under the natural metal transfer. Therefore, the pulsed process should also be carried out in case when the welding current corresponds to the fine-droplet metal transfer and the following condition should be satisfied:

$$k_{hp} = f_k / f \geq 1, \quad (8)$$

where k_{hp} is the coefficient of droplet transfer irregularity, f_k is the droplet transition frequency under the impact of current pulses, f is the droplet transition frequency of a natural process.

The optimal parameters of the pulse process, depending on the spatial position of the weld, should meet the conditions described by the equations (3) and (8).

The minimum pulse length providing intermittent spray transfer is $(4.5-5.0) \cdot 10^{-3}$ s at $I_n = (1.5-0) I_{kp}$. In this case, the pulse repetition rate is maximum (110–100 cps). The maximum pulse length is determined from the condition

for providing ST at a constant value of I_n and the maximum allowable ℓ_d . The pulse repetition rate is selected from the condition of uniformity in the formation of the weld width along its length and should not be less than 10 cps.

Fig. 6 shows fragments of the PAW current and voltage oscillographs with intermittent spray transfer¹.

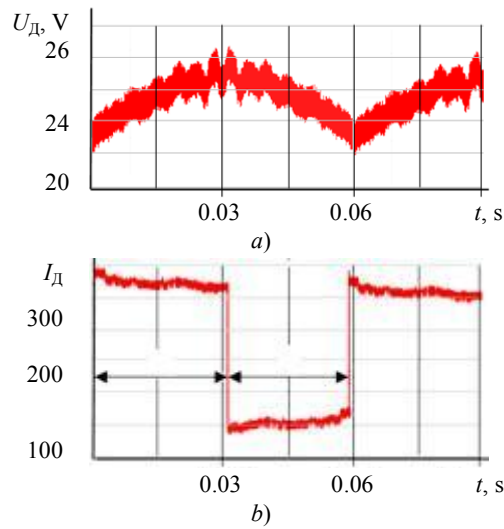


Fig. 6. Section fragment of synchronous oscillograms of PAW by rectangular current pulses with IST:
(a) voltage, (b) arc current

On the oscillograms, the moment of transition of arc burning from the base current of 160A (point 1) to the pulse current ($I_n = 375$ A, point 2) is recorded. The current of 160A is less than the critical current for an electrode wire of 1.2 mm (I_{kp} is 190÷200A). In this case, the current in the pulse is $(1.97 \div 1.87) I_{kp}$. The voltage drop across the arc at the time of switching from I_0 to I_n is 22.8V. When the arc burns during the current pulse action, the voltage across it increases to 25.8V.

Therefore, during the action of the current pulse t_n with a duration of $31 \cdot 10^{-3}$ s, the arc length increases by $\Delta \ell_d \leq 2$ mm, and during the arc burning by I_0 in a pause t_n with a duration of $29 \cdot 10^{-3}$ s, the arc length decreases by the same amount. The pulse repetition rate is 16,6 cps.

PS VAC switches automatically from position 1, corresponding to welding at a pause current (I_0), to position 1₁ (corresponds to the pulse current) and back. The switching depends on the set voltage drop

$$\Delta U_d = k_d \Delta \ell_d,$$

where k_d is the voltage gradient of the arc core under welding in argon at a current above critical 1.4 V/mm) between points a and b_1 (corresponds to the arc length at these points, see Fig. 5).

Using a two-level voltage sensor, the power supply control system receives information on the variation in the voltage between the base and pulse currents.

Discussion and Conclusions. Two main varieties of PAW are known. The first one is a “pulse-drop” operation: at t_n , equal to $(1.5-2.5) \cdot 10^{-3}$ s, each pulse at the end of its action transfers one drop of electrode metal from the electrode wire to the weld pool. In this case, the processes of melting and transfer of the electrode metal are largely separated in time.

In the second type of PAW, the pulse acts much longer ($t_n \geq 4.0 \cdot 10^{-3}$ s and more), and the intermittent spray metal transfer occurs. In this case, the processes of melting and metal transfer are combined.

The control system of the pulse-arc welding process provides a smooth adjustment of the repetition rate of current pulses, which depends on the specified increment of the arc gap length, i.e., on the operating voltage of the two-level sensor and the amplitude of the pulse current. The repetition rate of current pulses, the duration of pulses and pauses change smoothly and are determined by incrementing the arc gap length under the action of the pulse current depending on the values of the specified current in the pause and pulse.

¹ Lenivkin VA, Kiselev DM, Dyurgerov NG. *Sposob impul'sno-dugovoi svarki*: RF patent 2570145 [Pulse arc welding method]. RF Patent no. 2570145, 2015.

The flexibility of the IST program is achieved through the use of a two-level voltage sensor. The lower level of the sensor response voltage is determined by the parameters of the welding mode, which provide a stable process in a pause at a current below the critical level. The upper level depends on the elongation of the arc by 0.5–2.0 mm under the arc burning at a current that provides ST.

The developed PAW system with rectangular pulses through switching the integrated VAC-rectifier with an inverter converter is used for the mechanized welding in argon and a gas mixture (argon > 80% and CO₂ < 20%) according to the rigid “pulse-drop” program and the flexible “intermittent spray transfer” program.

The study results of the capability of controlling the processing behavior of the welding arc and the proposed methods for calculating the PAW mode parameters laid the groundwork for the development of technology and equipment for the mechanized consumable-electrode PAW of aluminum alloys AMts, AMtsM, AD1, AMg6, AMg61, 01915. These developments were introduced at the enterprises of the aviation industry, shipbuilding. Solutions for stainless and heat-resistant steels and alloys are used at the motor industry enterprises.

As a result of the studies on the features of the mechanized activated electrode wire welding in carbon dioxide, the mechanized activated electrode wire Sv-08G2S PAW technology was developed for the electric furnace body units made of stainless steel X18H10T, the structural components of road-building, agricultural machines and ships. According to the scientific research results in 1985, the monograph “Equipment for pulsed arc consumable electrode welding” was published in Energoatomizdat.

The developments are protected by 17 copyright certificates and patents for inventions. Based on the research results, 31 papers were published in journals included in the list of the State Commission for Academic Degrees and Titles of the Russian Federation.

References

1. Potap'evskii AG. Svarka v zashchitnykh gazakh plavyashchimsya ehlektrodom. Chast' 1. Svarka v aktivnykh gazakh [Gas-shielded consumable-electrode welding. Part 1. Welding in active gases]. Kiev: Ekhkotehnologiya; 2007. 192 p. (In Russ.)
2. Dyurgerov NG, Sagiroy KhN, Lenivkin VN. Oborudovanie dlya impul'sno-dugovoi svarki plavyashchimsya ehlektrodom [Equipment for pulse-arc consumable-electrode welding]. Moscow: Ehnergoatomizdat; 1985. 80 p. (In Russ.)
3. Lenivkin VA, Dyurgerov NG, Sagiroy KhN. Tekhnologicheskie svoystva svarочноi dugi v zashchitnykh gazakh [Processing properties of a welding arc in shielding gases]. 3rd ed. Moscow: Mashinostroenie; 2011. 368 p. (In Russ.)
4. Krampit AG. Vliyanie parametrov impul'sov svarочноgo toka na formirovanie svarного shva [The influence of parameters of welding current pulses on the weld formation]. Welding and Diagnostics. 2013;2:11–13. (In Russ.)
5. Krampit AG. Vliyanie velichiny zhidkoi prosloiki na formirovanie zapolnyayushchikh sloev pri impul'sno-dugovoi svarke v shchelevuyu razdelku [The effect of the liquid interlayer size on the formation of filling layers during pulse-arc welding in slotted preparation]. Welding and Diagnostics. 2014;2:13–16. (In Russ.)
6. Paton BE, Sidoruk VS, Maksimov SYu, Saraev YuN. K voprosu samoregulirovaniya dugi pri svarke plavyashchimsya ehlektrodom [On the issue of arc self-regulation during consumable-electrode welding]. Svarочноe Proizvodstvo. 2014;12:3–11. (In Russ.)
7. Dyurgerov NG, Sagiroy KhN. Ustoichivost' sistemy samoregulirovaniya pri mekhanizirovannoi i avtomaticheskoi svarke [Stability of the self-regulation system in mechanized and automatic welding]. Svarочноe Proizvodstvo. 2009;2:13–14. (In Russ.)
8. Dyurgerov NG, Sagiroy KhN. Opredelenie svoystv dugi pri impul'snykh protsessakh [Determination of arc properties in impact acceleration processes] Svarочноe Proizvodstvo. 2004;4:14–18. (In Russ.)

9. Aleshin NP, Gladkov EhA, Brodyagin VN, et al. Impul'snye tekhnologii upravleniya kapleperenosom pri MIG/MAG svarke [Pulse droplet control technology for MIG/MAG welding]. Welding and Diagnostics. 2014;3:43–47. (In Russ.)

Submitted 27.12.2019

Scheduled in the issue 03.02.2020

About the authors

Lenivkin, Vyacheslav A., Leading Research Scholar, Centre of Scientific Competence, Don State Technical University (1, Gagarin sq., Rostov-on-Don, 344000, RF), Dr.Sci. (Eng.), ORCID: <https://orcid.org/0000-0002-3325-5515>, weld-dstu@ya.ru

Rogozin, Dmitrii V., Head of the Machines and Welding Fabrication Automation Department, Don State Technical University (1, Gagarin sq., Rostov-on-Don, 344000, RF), Cand.Sci. (Eng.), ORCID: <https://orcid.org/0000-0003-33110524>, dmrogozin@ya.ru

Claimed contributorship

V.A. Lenivkin: basic concept formulation, research objectives and tasks setting, development of the theoretical foundations for pulse-arc consumable-electrode welding, academic advising. V.D. Rogozin: study on the gas-shielded pulse-arc welding self-regulation, calculation and report.

All authors have read and approved the final manuscript.

MACHINE BUILDING AND MACHINE SCIENCE



UDC 629.4.02+06

<https://doi.org/10.23947/1992-5980-2020-20-1-36-41>

Brake rigging dynamic simulation under braking on a track section with irregularities (the case of a passenger car)

I. A. Yaitskov, V. V. Kosarevskii

Rostov State Transport University (Rostov-on-Don, Russian Federation)



Introduction. The paper considers simulation of the dynamic processes of the brake rigging of a passenger car under braking on a track section with irregularities. The work objectives include the development of a “rigging brakeblock - wheel working surface” contact module in a full-scale computer model of a passenger car in the “Universal Mechanism” software package; and a computer simulation of the braking operating mode from 50 to 32 km/h considering vertical and horizontal track rail irregularities for determining the mechanism of variation of the longitudinal acceleration of the brakeblock and its angular acceleration. The subject of the study is the force interaction of the elements and dynamic processes in the brake system of passenger cars.

Materials and Methods. A new “rigging brakeblock - wheel working surface” contact module, which provides the determination of the longitudinal and angular accelerations of the brake rigging of a passenger car, is proposed to the “Universal Mechanism” software package. The simulated modeling of the brake rigging system of a passenger car with KVZ-TsNII type II trolleys equipped with shoe brakes is carried out.

Results. A full-scale computer model of a passenger car, which includes the designed contact module “linkage brake pad - wheel working surface”, has been developed in the “Universal Mechanism” software package. The car is presented as a system of solids connected by elastic and dissipative elements. Using computer simulation, the operating mode of braking was reproduced under reducing the speed of a passenger car from 50 to 32 km/h considering vertical and horizontal irregularities of a railway track. The simulation result was the laws of change in the longitudinal acceleration of the brakeblock and its angular acceleration under braking in the above speed range. Their spectra of longitudinal angular acceleration of the brakeblock were constructed. It was determined that the presence of track irregularities affects the spectral composition of the accelerations. In addition, under the superposition of the bogie-frame pitching and bouncing oscillations, when moving along an uneven track, the rigging block can move up and down the wheel-working surface within a range of up to 50 mm. The simulation functionality of the dynamic processes of the brake system of a passenger car was expanded in the “UM-Loko” software package.

Discussion and Conclusions. The results obtained can be used in the design of new rigging brake systems of passenger cars and modernization of existing ones at the engineering enterprises and railway-car repair works. This, in turn, should ensure uniform distribution of efforts across all brake rigging brakeblocks of a passenger car.

Keywords: rigging, brake system, wagon, block, dynamics, simulation, braking, track with irregularities.

For citation: I. A. Yaitskov, V. V. Kosarevskii. Brake rigging dynamic simulation under braking on a track section with irregularities (the case of a passenger car). Vestnik of DSTU, 2020, vol. 20, no. 1, pp. 36–41. <https://doi.org/10.23947/1992-5980-2020-20-1-36-41>



Introduction. The problem of efficient and reliable operation of the brake systems of passenger cars becomes even more urgent when high-speed traffic is introduced on the Russian railways. The main part of modern brake systems is the lever transmission system of a passenger car, whose efficiency and reliability depend directly on the quality of design, operation, maintenance and repair of the brake equipment. The mechanical part of the brake system combines a rigging brake transmission, an automatic rigging transmission regulator and friction brake components (brakeblocks

and pads). One of the key requirements for the brake rigging system is to provide uniform force distribution across all brakeblocks. However, under the operating conditions, there is some variation in the efforts of pressing the brakeblocks on the wheelsets both within the wagon and within each bogie. The nonuniformity of pressing brakeblocks may be one of the basic reasons for their uneven wear. The subject of the study is the force interaction of elements and dynamic processes in the brake rigging system of passenger cars. The level of theoretical studies on dynamic processes of structural elements of the traction rolling stock is quite high [1–12].

Materials and Methods. To clarify and confirm the results of theoretical studies, it is required to carry out computer simulation of the dynamic processes of the brake rigging system of a passenger car, which occurs under braking on a flat section of the track. Major causes of the dynamic processes in the contact “rigging brakeblock – wheel working surface” may be fluctuations of the car underframe when moving along a track with irregularities. This is because the brakeblocks and the brake rigging system components are structurally connected with the bogie frame, which, due to deformation of the axlebox suspension, moves with respect to the wheel pairs rolling along the rails. It is required to consider the simulation of the braking process in the presence of uneven tracks.

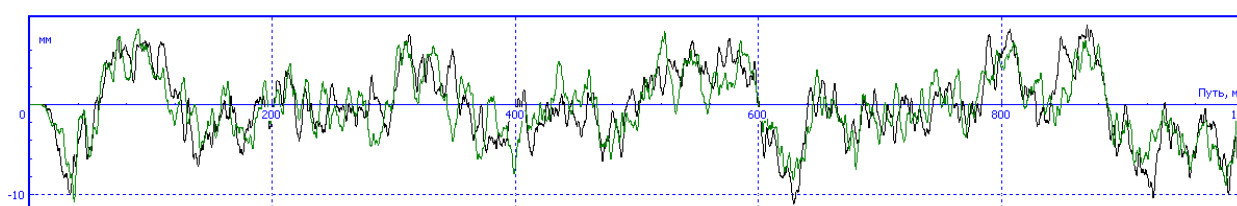


Fig. 1. An example of the vertical track rail irregularities

Files of vertical and horizontal irregularities of track rails, which are a generalization of the measurement results, are available in the UM-Loko software package. Fig. 1 shows vertical irregularities on a track of 1000 m long as an example.

Research Results. The simulation results of the dynamic processes of the lever transmission of the brake system on a flat track are presented in Fig. 2. The picture of the “wheel – rail” contact patches for all four wheelsets of the car, in the presence of track irregularities, is shown in Fig. 3. Comparison of simulation results with Fig. 2 provides the conclusion that the presence of irregularities causes the emergence of vertical oscillations of the car underframe and, as a result, a significant change in the forces within the “wheel – rail” contact patch.

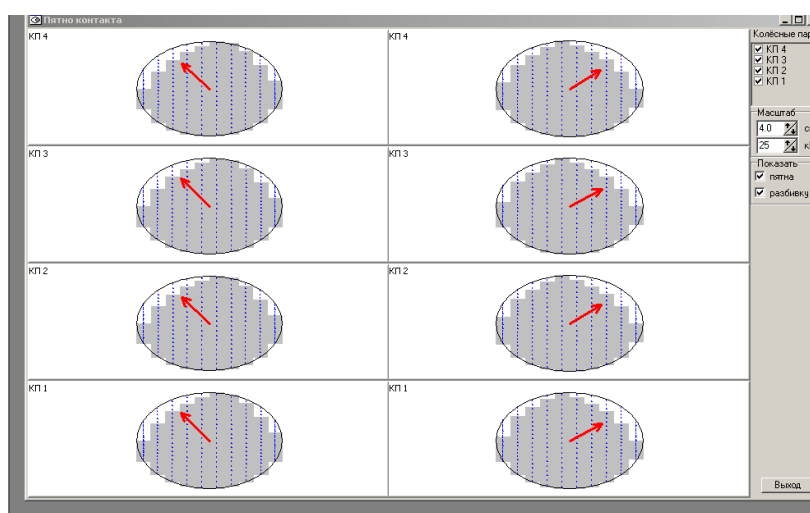


Fig. 2. “Wheel – rail” contact patches and force distribution (on level)

When moving along a track with irregularities, the oscillations of the truck-frame bouncing have an amplitude reaching 18 mm; frequencies of 0.8 are visible in the spectrum of vibrations; 0.95 and 1.07 Hz. The last frequency is close to the natural frequency of the car-body pitching.

Pitching oscillations of the bogie frame have amplitude up to 0.0025 rad. In the spectrum, there are frequencies of 0.25; 0.8; 0.95; 3.7 and 3.9 Hz.

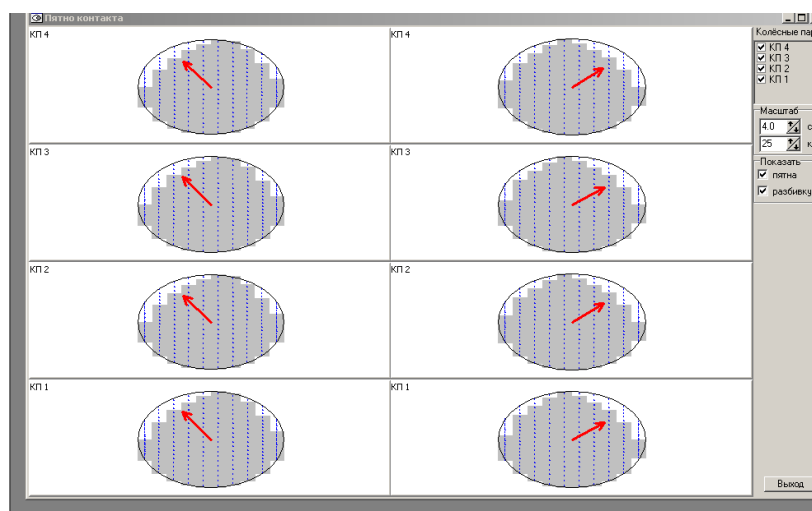


Fig. 3. “Wheel – rail” contact patches and force distribution (uneven track)

Fig. 4 and 5 show a graph of the longitudinal acceleration of the rigging brakeblock under braking in the presence of track irregularities and its spectral composition.

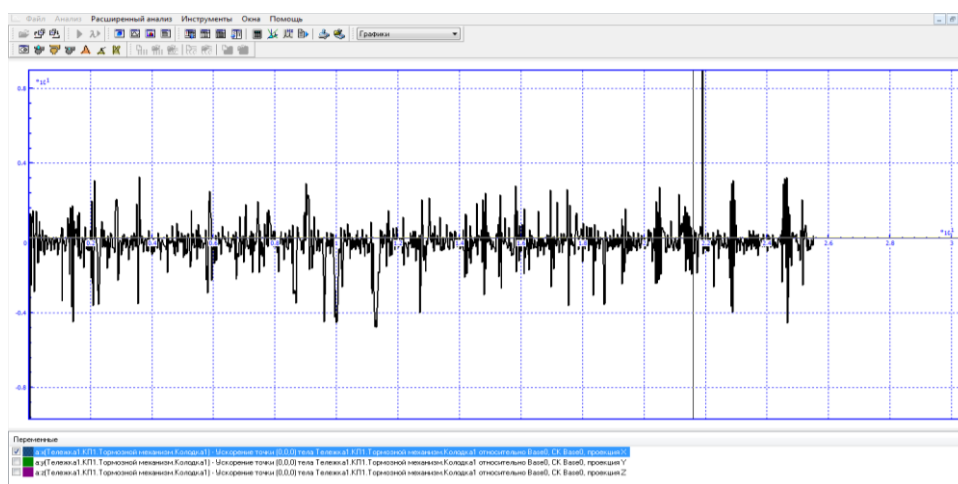


Fig. 4. Longitudinal acceleration of the rigging brakeblock under braking (track irregularities)

Fig. 6 and 7 show a graph of the angular acceleration of the rigging brakeblock under braking in the presence of track irregularities and its spectral composition.

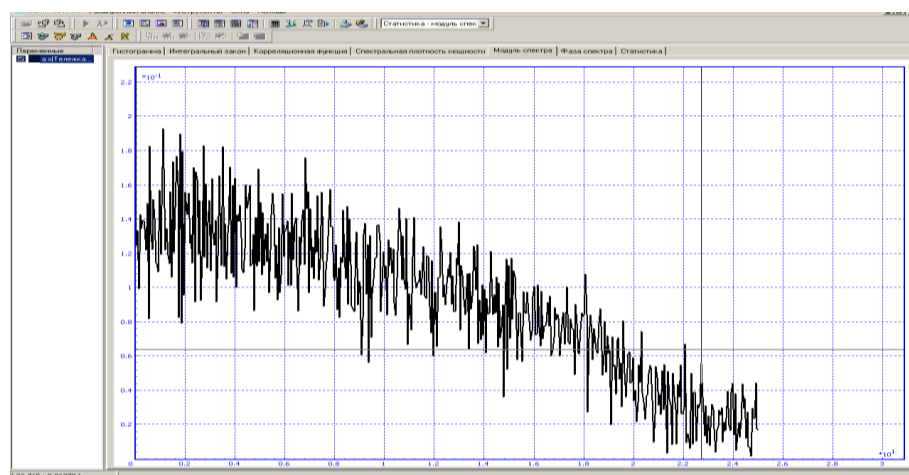


Fig. 5. Spectral composition of longitudinal acceleration of rigging brakeblock (track irregularities)

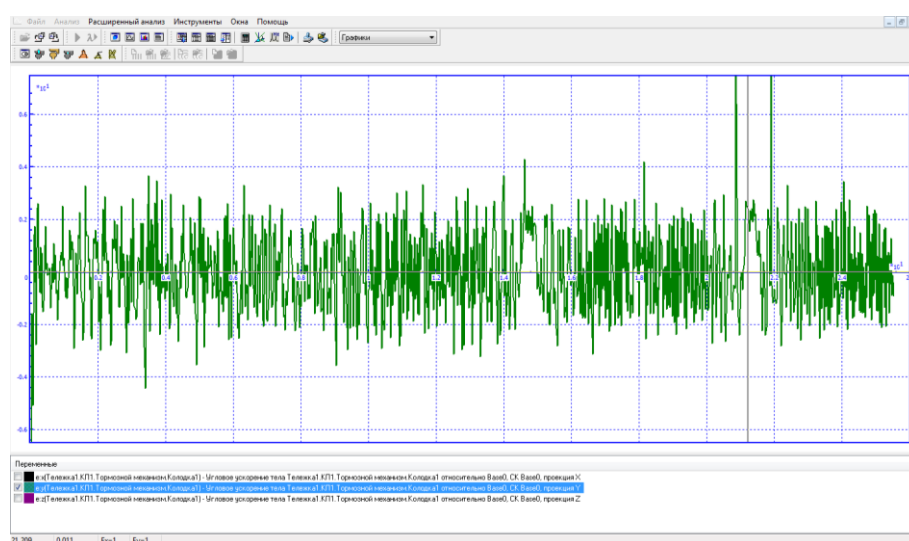


Fig. 6. Angular acceleration of rigging brakeblock (track irregularities)

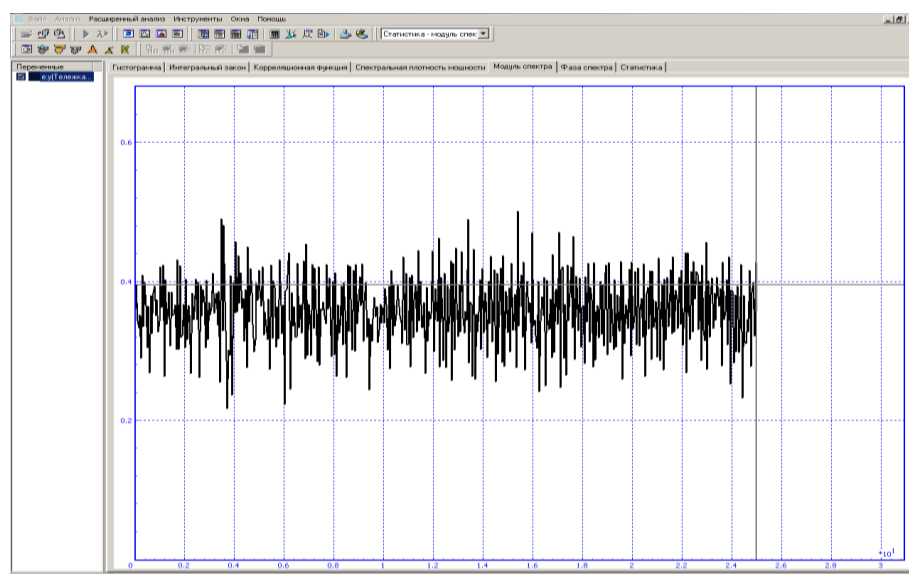


Fig. 7. Spectral composition of angular acceleration (track irregularities)

The simulation results show that in the presence of track irregularities, the longitudinal and angular vibrations of the brakeblocks occur in the frequency range up to 25 Hz, and their spectral composition is somewhat different from the case when braking occurs on level.

Discussion and Conclusions. A full-size computer model of a passenger car is developed in the “Universal Mechanism” software package. A car is presented as a system of solids connected by elastic and dissipative elements. The structure of the model includes the developed “rigging brakeblock – wheel working surface” contact. Using the computer model, the operating mode of braking from 50 to 32 km/h is reproduced. The option when the track has vertical and horizontal irregularities of lengths of rails is considered. Because of the simulation, the variation pattern of the longitudinal acceleration of the brakeblock and its angular acceleration under braking from 50 to 32 km/h were obtained, and their spectra were constructed. The track irregularities affect the spectral composition of accelerations. In addition, under the superposition of bouncing and pitching oscillations of the bogie frame when moving along the uneven track, the rigging brakeblock can move up and down along the wheel working surface with a swing up to 50 mm. The results obtained can be used under the design of new and modernization of existing brake rigging systems of passenger cars at machine-building enterprises and car repair enterprises to provide an even force distribution across all brakeblocks.

References

1. Lilov LK. Modelirovanie sistem svyazannykh tverdykh tel [Modeling systems of connected solids]. Moscow: Nauka; 1993. 272 p. (In Russ.)
2. Shilen V. Dinamika sistem tverdykh tel. V sb.: Dinamika vysokoskorostnogo transporta; pod red. T. A. Tibilova [Dynamics of solids systems]. In: Dynamics of high-speed transport, T.A. Tibilov, ed. Moscow: Transport; 1988. P. 32–39. (In Russ.)
3. Schiehlen W. (ed.) Multibody systems handbook. Berlin: Springer; 1991.
4. Kreuzer E. Generation of symbolic equations of motion of multibody systems In: Computerized symbolic manipulations in mechanics. Springer-Verlag; 1994. P. 1–67.
5. Efimov GB, Pogorelov DYU. Nekotorye algoritmy avtomatizirovannogo sinteza uravnenii dvizheniya sistemy tverdykh tel [Some algorithms for the automated synthesis of motion equations of a rigid body system]. Moscow: Inst. prikl. matem. im. M.V. Keldysha RAN; 1993. 30 p. (In Russ.)
6. Pogorelov DYU. Modelirovanie mekhanicheskikh sistem s bol'shim chis-lom stepenei svobody. Chislennyye metody i algoritmy. avtoreferat dis. ... d-ra fiz.-mat. nauk [Modeling of mechanical systems with a large number of degrees of freedom. Numerical methods and algorithms: Dr.Sci. (Phys.-Math.), diss., author's abstract]. Bryansk; 1994. 18 p. (In Russ.)
7. Pogorelov DYU. Vvedenie v modelirovanie dinamiki sistem tel [Introduction to modeling the dynamics of body systems]. Bryansk: Izd-vo BGTU; 1997. 155 p. (In Russ.)
8. Fiset P, Lipinski K, Samin JC. Dynamic behavior comparison between bogies: rigid or articulated frame, wheelset or independent wheels. In: The Dynamics of Vehicles on Roads and on Tracks: Vehicle System Dynamics Supplement. 1996;25:152–174.
9. Bakhvalov YuA, et al. Dinamicheskie protsessy v asinkhronnom tyagovom privode magistral'nykh ehlektrovozov [Dynamic processes in an asynchronous traction drive of main electric locomotives]. Moscow: Marshrut; 2006. 374 p. (In Russ.)
10. Balon LV, Koropets PA, Kosarevskii VV. Nestatsionarnyye dinamicheskie protsessy v sisteme «tormoznaya kolodka-koleso» [Non-stationary dynamic processes in the “breaking shoe – wheel” system]. Vestnik RGUPS. 2008;3:33–42. (In Russ.)
11. Kosarevskii VV, Balon LV, Koropets PA. Matematicheskaya model' i metodika issledovaniya dinamiki rychnozhnoi tormoznoi sistemy v ustanovivshikhsya rezhimakh [Mathematical model and research technique for the dynamics of the lever break system in the steady state modes]. Vestnik RGUPS. 2009;3:15–22. (In Russ.)
12. Kosarevskii VV, Balon LV, Koropets PA. Dinamicheskie kharakteristiki rychnozhnoi tormoznoi sistemy v ustanovivshikhsya rezhimakh [Dynamic characteristics of break lever transmission under the established modes]. Vestnik RGUPS. 2009;4:33–42. (In Russ.)

Submitted 29.01.2020

Scheduled in the issue 02.03.2020

About the authors:

Yaitskov, Ivan A., Dean of the Electromechanical Faculty, associate professor of the Wagons and Rolling Stock Department, Rostov State Transport University (2, Rostovskogo Strelkovogo Polka Narodnogo Opolcheniya sq., Rostov-on-Don, 344038, RF), Cand.Sci. (Eng.), associate professor, ORCID: <http://orcid.org/0000-0001-8937-8875>
via3@rgups.ru

Kosarevskii, Valerii V., associate professor of the Wagons and Rolling Stock Department, Rostov State Transport University (2, Rostovskogo Strelkovogo Polka Narodnogo Opolcheniya sq., Rostov-on-Don, 344038, RF), ORCID: <http://orcid.org/0000-0001-5040-5098>, kosarevskij@yandex.ru

Claimed contributorship

I. A. Yaitskov: academic advising; analysis of the research results; exploratory study on the practical implementation of the methodology involved. V.V. Kosarevskii: setting the research objective and task; collecting and processing of material; computational analysis; text layout; drawing conclusions.

All authors have read and approved the final manuscript.

MACHINE BUILDING AND MACHINE SCIENCE



UDC 621.791.01:621.643.053

<https://doi.org/10.23947/1992-5980-2020-20-1-42-50>

On solving problems of operational forecasting of main pipeline weld joint quality

A. E. Filyakov¹, M. A. Sholokhov²

¹ Bauman Moscow State Technical University (Moscow, Russian Federation)

² Yeltsin UrFU, (Ekaterinburg, Russian Federation)



Introduction. Since welding is the only means to connect pipe lengths into a continuous line when constructing main pipelines, modern quality management systems for the welding industry products are based on minimizing the occurrence of specific defects. This is achieved through monitoring and documenting welding procedures.

Materials and Methods. The analysis of monitoring systems customized for manual, mechanized and automatic orbital welding has shown that the industry urgently needs systems that not only control and document the welding process, but also predict the quality of weld joints. This actualizes the need to develop an intelligent module that could, basing on real-time monitoring results, predict the quality of welded joints on the fly.

Results. Since the theoretical connection between the forecasting results and weld quality attributes is characterized by the interaction of a significant number of physical phenomena continuous in time, the results of welding can be described only by a sufficiently complete nonstationary physicomathematical model of the welding process. However, in order to be able to predict the results of welding directly during the monitoring of the process, a simplified forecasting model is proposed whose key feature is the ability to perform calculations synchronously with the real process, which is implemented in a real-time mode with a given interval.

Discussion and Conclusions. The major obstacle to the successful functioning of the operational forecasting module, apart from the length of the numerical solution of equations, is an estimation error. To ensure the minimum error of virtual display during simplification, it is necessary to conduct comprehensive studies of the significance and influence of individual factors and phenomena on quality attributes. These observations determined the content and sequence of work on the creation and implementation of an intelligent module for the operational forecasting of welding quality. Undoubtedly, the information on the forecasting of the weld joint quality should enter a higher-level pipeline quality management system, as well as be analyzed by construction organizations in order to develop preventive measures to improve the organization and performance of welding work.

Introduction. Since welding is the only means to connect pipe lengths into a continuous line when constructing main pipelines, modern quality management systems for the welding industry products are based on minimizing the occurrence of specific defects. This is achieved through monitoring and documenting welding procedures.

Materials and Methods. The analysis of monitoring systems customized for manual, mechanized and automatic orbital welding has shown that the industry urgently needs systems that not only control and document the welding process, but also predict the quality of weld joints. This actualizes the need to develop an intelligent module that could, basing on real-time monitoring results, predict the quality of welded joints on the fly.

Results. Since the theoretical connection between the forecasting results and weld quality attributes is characterized by the interaction of a significant number of physical phenomena continuous in time, the results of welding can be described only by a sufficiently complete nonstationary physicomathematical model of the welding process. However, in order to be able to predict the results of welding directly during the monitoring of the process, a simplified forecasting model is proposed whose key feature is the ability to perform calculations synchronously with the real process, which is implemented in a real-time mode with a given interval.

Discussion and Conclusions. The major obstacle to the successful functioning of the operational forecasting module, apart from the length of the numerical solution of equations, is an estimation error. To ensure the minimum error of virtual display during simplification, it is necessary to conduct comprehensive studies of the significance and influence of individual factors and phenomena on quality attributes. These observations determined the content and sequence of work on the creation and implementation of an intelligent module for the operational forecasting of welding quality. Undoubtedly, the information on the forecasting of the weld joint quality should enter a higher-level pipeline quality management system, as well as be analyzed by construction organizations in order to develop preventive measures to improve the organization and performance of welding work.



Keywords: welding, quality forecasting, welding procedures, weld joint, main pipeline, physical and mathematical model

For citation: A. E. Filyakov, M. A. Sholokhov. On solving problems of operational forecasting of main pipeline weld joint quality. Vestnik of DSTU, 2020, vol. 20, no. 1, pp. 42–50. <https://doi.org/10.23947/1992-5980-2020-20-1-42-50>

Introduction. The consistent development of the oil and gas industry infrastructure requires continuous improvement of pipeline systems since pipeline transport is currently most preferred for transportation of hydrocarbon raw materials and products of its processing. It is known that at the present stage of technological development of the construction of main pipeline systems, welding is the only way to connect individual pipes into a continuous line on site.

Given the consequences of accidents and failures in operation, trunk pipelines are classified as hazardous production facilities. Since, according to Rostekhnodzor, over 85% of accidents and catastrophes at facilities occur due to depressurization or failure of welded joints, the quality maintenance of welded joints is quite a challenge. Therefore, the quality of welding is the basis for the safe operation of any pipeline transport system [1].

The quality of the weld is assessed by the dimensions of its cross section, the mechanical properties of the weld metal and the heat-affected zone (HAZ), the distribution of stresses and residual deformations, probability of cold and hot cracks, the presence of pores, non-fusion and other defects. Modern quality management systems for welding products are based on minimizing the probability of specific defects. For this, accident-preventive measures are taken to prepare and implement welding processes. This approach contributes not only to improving the quality of welded joints, but also to improving welding technologies, rational selecting welding materials, and developing methods for monitoring welding processes. In this regard, we consider in more detail the basic welding technologies used in the construction of pipelines.

Materials and Methods. Currently, the most commonly used method of joining pipes of main pipelines into a string is fusion arc welding. In the construction of pipelines, manual, mechanized and automatic welding is used. Manual arc welding is characterized by simplicity of implementation, equipment mobility, but it is quite laborious and requires a large number of qualified personnel. In addition, under manual arc welding, a significant number of defects can occur. Mechanized (semi-automatic) pipe welding, in comparison to manual arc welding, is more productive. However, it is not free from shortcomings, the major of which are increased spatter of electrode metal, problems of gas protection, aerosol emission, especially under FCAW wire welding. It should be noted that the methods of manual and mechanized welding are characterized by a high degree of subjective influence of performers. The “human factor” is less significant for automatic welding methods. However, orbital welding, in comparison to manual and mechanized welding, is less mobile. Currently, among installations for orbital welding, it is required to single out equipment for consumable electrode welding with controlled droplet transfer of electrode metal [2]. To reduce the impact of characteristic disturbances, it is very promising to use adaptive technologies that promptly correct the welding process [3].

Among consumables widely used for automatic and mechanized welding, gas-proof flux-cored wires can be distinguished. FCAW wires, despite a number of advantages, are used in much smaller volumes.

In recent years, attempts have been intensified to introduce more efficient automatic welding technologies under construction, for example, plasma, laser, butt-resistance welding, and also welding with a combination of various heat sources [4]. However, all these welding methods are not yet industrially usable or are used on a very limited basis. The introduction of automatic welding processes reduces the human impact on the quality of weld joints. However, close attention is paid to issues related to the fulfillment of the prescribed requirements and instructions on the work execution by a welder or operator of welding equipment.

Currently, welding monitoring procedures have become an integral part of scientific and technical support for the construction of trunk pipelines. Monitoring procedures provide observation of energy parameters of welding processes, prevention of causes for non-compliance of welded joints with the requirements of standards and technical documentation (STD), and control of their elimination. At the same time, monitoring procedures provide the implementation of a number of requirements for documenting the work performed. This is achieved by connecting special recorders with appropriate software to the modern welding equipment [5].

A typical operation scheme of such systems is shown in Fig. 1.

A number of domestic high-tech science-based enterprises are involved in the development of such systems of monitoring, registration and documentation of the parameters of the welding process. Systems can be integrated into modern digital sources of welding current or manufactured as separate units.

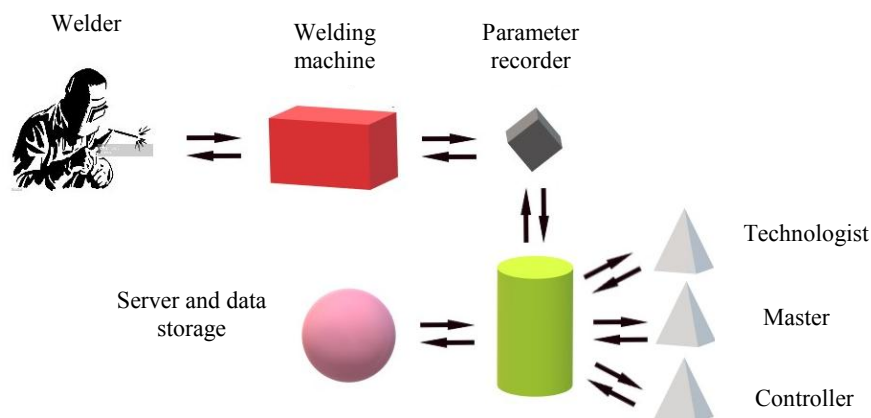


Fig. 1. Information flows of welding process monitoring

When monitoring the process of arc welding for recording parameters, the authors of [6] developed a polyweld (up to 64 welding points) recording system for measuring, displaying and saving data on the welding current, arc voltage and temperature of the weldable workpieces being welded. The registers of such a system can be located at a distance of up to 300m from the installation site of a personal computer with dedicated software.

Similar solutions are used by other developers of welding process documentation systems, for example, “Storm” enterprises, NPF ITS, “Telma”, “Alloy”, and others. The “Weld Telecom” monitoring and control system developed by “Alloy” provides data both from a single point and from a whole stock of welding equipment through a remote server using a wired or wireless Wi-Fi network. Such capabilities of the Weld Telecom system provide monitoring of the operations performed by the welders, and monitoring of the technical condition of the welding equipment. Moreover, the system allows both monitoring the process and transmitting commands for adjusting welding modes, which should be considered a significant step in implementing the Industry 4.0 concept using sensors and networks. In addition, the system provides documentation of welding processes with the automation of the collection, systematization and data storage for the formation of the weldable product certificates and their application in managing product quality. The Weld Telecom system capabilities for processing and visualizing the welding mode parameters are shown in Fig. 2.

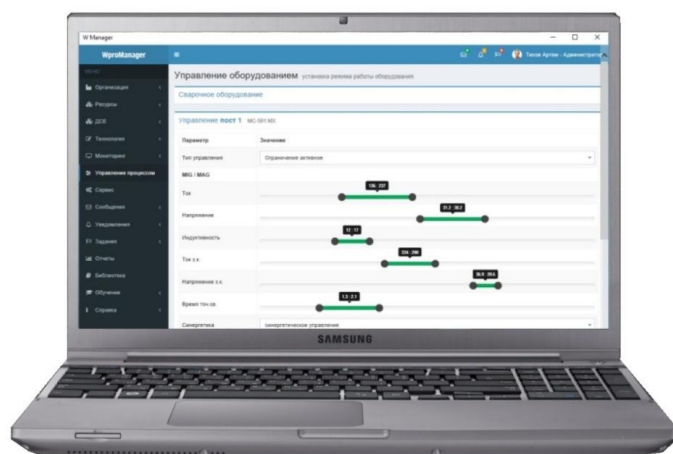


Fig. 2. Weld Telecom system visualization options

Foreign developers and manufacturers of welding equipment are actively involved in the development of systems for registering and documenting welding processes. Fronius (Austria), Kemppi (Finland), Miller Electric (USA) and a number of other foreign companies demonstrate solutions similar to Russian companies for registering welding process parameters.

It should be noted that Production Monitoring systems from Lincoln Electric (USA) and Merkle Quality Control from Merkle Group Inc (USA) have somewhat greater capabilities. These systems not only monitor and record the welding process parameters, but also identify and record data on their deviations [7]. The on-line Production Monitoring system compares the voltage, current, electrode wire feed speed, time interval of the welding process predefined by the user to the actual values. Merkle Quality Control system provides documentation and control of up to 8 parameters of the mechanized welding process with the possibility of archiving. Such capabilities of the deviation fixation system are provided by independent sensors of current, voltage, wire and gas. However, such systems work stably only with the proprietary equipment.

Therefore, it can be stated that the most popular systems for monitoring welding processes are used to document their parameters, as well as to analyze the consumption of materials, use uptime, register the out-of-tolerance condition, and discipline welders. However, none of the systems answers the key question – what consequences will the identified deviations lead to. Given the entry, we need systems that not only control and document the welding process, but also predict its results. Based on the foregoing, we need systems that could not only control and document the welding process, but also predict its results. Despite the attempts to predict the weld joints operational quality according to the monitoring results of the welding process parameters undertaken both earlier this century [8] and later [9], no forecasting systems on site exist to this date. All this actualizes the need to develop an intelligent module that can quickly predict the quality of weld joints. However, such a module can only be created through linking the quality indicators of welded joints with the actual parameters of the welding mode recorded in the on-line mode.

Discussion and Conclusions. Unfortunately, the theoretical relationship between the forecasting results and weld quality indicators is characterized by the interaction of a significant number of physical phenomena that are continuous in time since they determine the heat supply, the conditions for the formation and crystallization of the weld pool, the dimensions of the weld and the HAZ microstructure [10]. However, the representation of welding processes in the form of complex, multifactor systems provides using mathematical modeling under their study. It is easier to collect the data required for forecasting under stationary shop-floor conditions [11]. However, under the conditions of the route, it is difficult to measure a number of the manual and mechanized welding parameters. For example, movements of a welder's hand and parameters of the electrode oscillations in cutting under manual or mechanized welding are uncontrollable values. They can be judged only by indirect signs.

The impact of the joint assembly on the quality of the weld formation should be considered, since even the assembled joints accepted by the Quality Control Dept (QCD) will have deviations within tolerance. If under orbital welding, scanning laser-television systems can be used to determine the real profile of welded edges [12], then it is rather difficult to use them for manual and mechanized welding. Therefore, predicting the quality of manual and mechanized welding only by the results of processing the actual values of the process energy parameters can only be approximate, just a matter of judgment. To increase the reliability of such a forecast, real data on the distribution of grooving sizes along the pipe joint are required. In cases where it is impossible to use laser-television scanning, other approaches should be used. Thus, if we neglect the change in the gap under welding due to thermal expansion and deformation of the metal, then monitoring the joint assembly under welding can be replaced by measuring its dimensions before welding starts. Since the gap size varies relatively slowly along the joint, it is sufficient to measure at several points, and determine the remaining dimensions of the joint through interpolating the available results. There is another possibility of increasing the reliability of the forecast when it is difficult to consider welding parameters. Their possible spread (for example, wire diameter tolerance, possible variations in welding and wire feed speeds, joint clearance, etc.) can be taken into account. However, in this case, it is rather difficult to impose deviations from the instability of those parameters that are not measured on the simulation result.

It should be noted that due to fluctuations in the welding process parameters, the quality indicators of welds are unevenly distributed both along the length and thickness of the welded joint. Therefore, the final task of the module for predicting the quality of joints is to identify precisely those sections of the weld where the deterioration probability of quality indicators is critically high. Obviously, such a complex relationship of quality indicators and the results obtained requires using modern forecasting tools.

With this in mind, the predicted results can only be described by a dynamic (non-stationary) physicomathematical model. Considering the problems of fixing an extended set of parameters, surrogate optimization techniques should be used in the model [13]. Given these considerations, Fig. 3 shows the structure of the dynamic physical and mathematical model used as part of the operational forecasting module for the quality of weld joints by the minimum number of analyzed parameters.

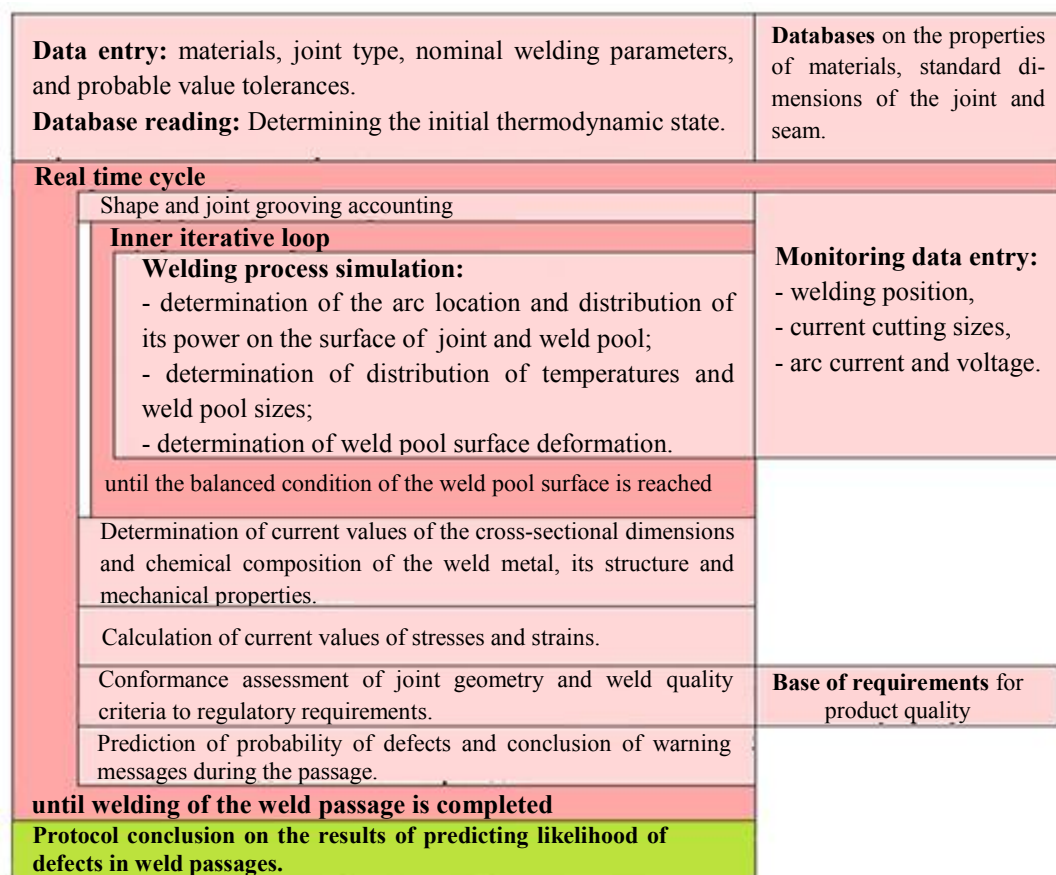


Fig. 3. Structure of physicomathematical model for predicting welding process results as part of intelligent module

Before welding, information on the process is input into the program: the type of connection and the form of cutting, the thickness of the weldable parts, the grade of steel, the grade and diameter of the electrode wire, shielding gas, and the recommended welding modes. Then, this information is given in the certificates for welded joints, which also contains data on the joint number, the serial number of the welding equipment, the name of the welder, the start and end times of the joint welding process.

A unique feature of the model for performing a quality forecast under welding is the need for synchronization with the real process of calculations, which is implemented in a real-time cycle with a given step determined by the weld pool response time. Therefore, it should be less than the length of the change in the depth of the crater on the surface of the bath when the arc current changes. The modeling of the thermodynamic state of the joint should be carried out at each step of the real time cycle since a major feature of arc welding, in addition to the possibility of the arc penetration into the crater of the weld pool, is its volume variation. With this in mind, the energy and mass balance should be achieved in a time not exceeding the selected step. The thermodynamic state of the metal makes it easy to determine the size of the weld pool, the thermal welding cycle, and the chemical composition of the weld, which enables to calculate the number of structural components and evaluate the mechanical properties of the weld metal and HAZ. In addition, using the known methods [14], stresses and strains in the vicinity of the weld pool can be calculated.

Such solutions provide to evaluate not only the possibility of hot cracking, but also the tendency of the weld metal and HAZ to cold cracking according to the results of calculating the amount of martensite.

Embedding a physicomathematical model in the computer program of the operational forecasting module allows you to evaluate the probability of defects directly under welding (Fig. 4).

For reliability of the results, it is required for the speed of virtual reproduction of the process to be greater than its real course. Therefore, the major obstacle to the successful functioning of the operational forecasting module is the duration of the numerical solution to the equations of the physicomathematical model. This circumstance forces us to simplify both the model itself and its numerical implementation. The model simplification can be achieved through limiting the scope of its application (specialization), as well as through reducing the number of measured parameters and determined quality indicators. However, to reduce the error of virtual reproduction under such simplification, it is necessary to conduct comprehensive studies to assess impact of individual factors and phenomena on the quality indicators of welded joints.

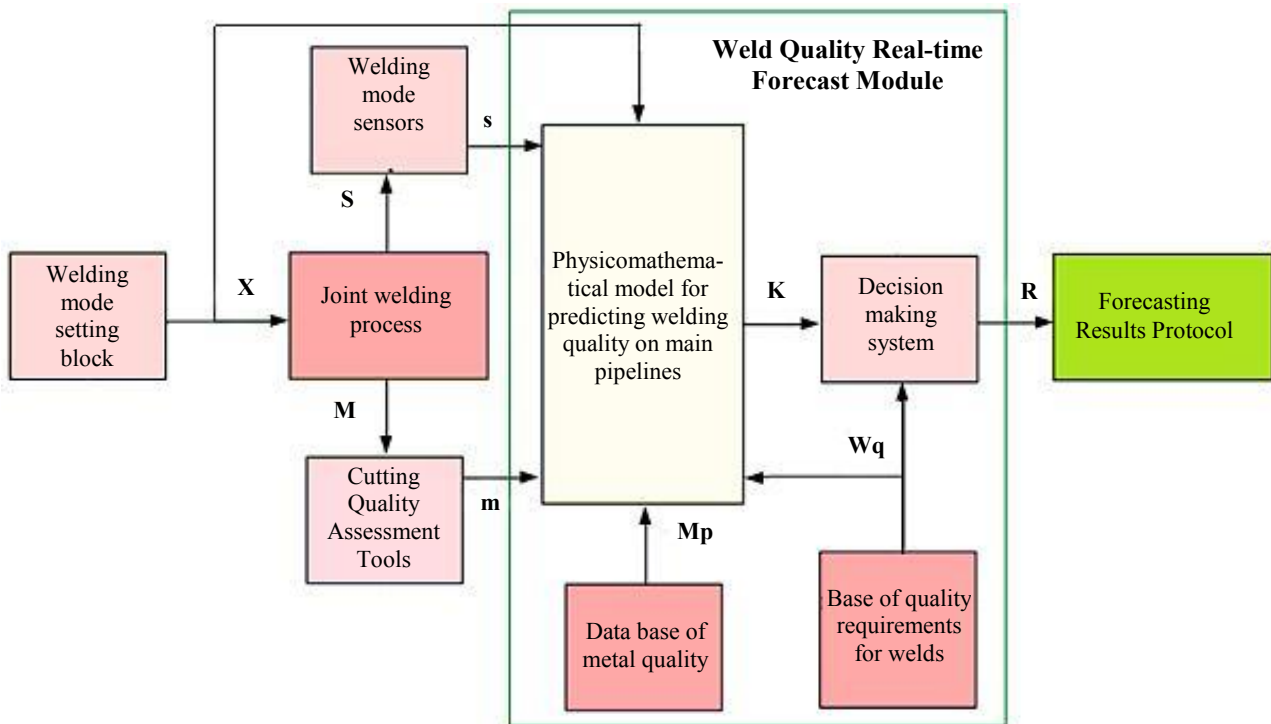


Fig. 4. Structure of system for predicting welding results:

X are set parameters of welding process; S are controlled parameters of welding process; s are measurement results of welding parameters; M is data on joint geometry, cutting quality and spatial position; m are measurement results;

Mp is data on physical properties of welded metal; Wq is regulatory data on quality requirements for weld;

Sp is comparison base of mode parameters; K is information flow;

R is signal of results of comparison of weld quality to regulatory requirements

It stands to reason that the structure of the intelligent module for predicting the welding process results, its software will be specified and revised according to the results of pilot industrial use under the real-time forecasting of the quality of welded joints directly during welding work.

The desired sequence of work on the creation and implementation of an intelligent module for real-time forecasting of welding quality and the sequence of their implementation are presented in Fig. 5.

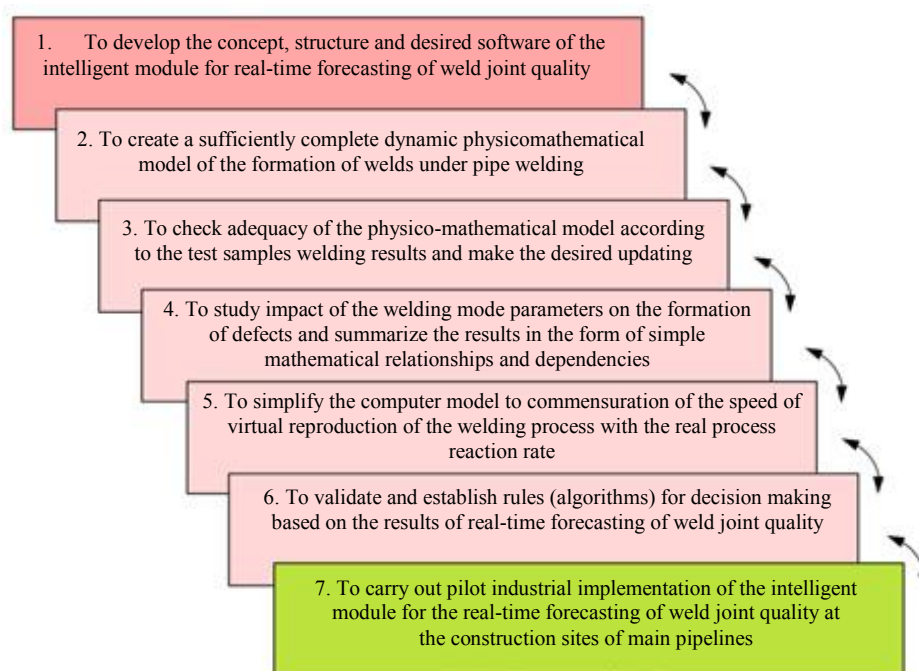


Fig. 5. Content and operating sequence on creation and implementation of an intelligent module for real-time forecasting of welding quality

To diagnose the technical condition of the main pipelines, it is required to collect all available information about the facility. To do this, information on predicting the quality of welded joints should go to a higher-level pipeline quality management system, for example, to an integrated diagnostic monitoring system for the linear part of main gas pipelines [15], or to a system for information analysis on the state of oil pipeline components [16, 17]. Construction organizations need information not only about defects in welded joints, but also about the causes of their occurrence. Therefore, data on the real-time forecasting of the quality of welded joints should be analyzed by construction organizations to develop preventive measures to improve the organization and performance of welding operations. It is advisable to carry out such an analysis under stationary conditions, with the inclusion of a more complete computer model of the welding process and an information storage device with appropriate filters in the structure of the forecasting module. However, this approach also requires additional study on the significance of individual factors and phenomena by quality indicators. Only then will the information on real-time forecasting the quality of welded joints become a truly efficient tool for taking preventive measures and removing the causes of defects.

Conclusions

1. A method is proposed for processing data for monitoring the welding process using a deterministic physicomathematical model that provides a sufficiently accurate prediction of the welded joints quality directly during welding, based on the relationships between the mode parameters and specified quality indicators of the joints.
2. Real-time forecasting is provided by a special intelligent module whose software includes a computer program for the implementation of a physicomathematical model of online forecasting of the quality of welded joints.
3. Since the major obstacle to the application of the proposed method of online data processing is high requirements for the speed of solving the model equations, then, to provide a high speed of virtual reproduction of the welding process, it is proposed to conduct comprehensive studies of the significance of individual factors and phenomena on quality indicators. These considerations determined the content and sequence of work on the creation and implementation of an intelligent module for the online forecasting of welding quality.

References

1. Mustafin FM, Blekherova NG, Bykov LI. *Sovremennyye tekhnologii svarki truboprovodov: uchebnoe posobie* [Modern technology for welding pipelines]. Saint Petersburg: Nedra; 2010. 560 p. (In Russ.)
2. Getskin OB, et al. *Opyt razrabotki i primeneniya sovremennykh otechestvennykh tekhnologii i oborudo-*

vaniya dlya avtomaticheskoi orbital'noi svarki magistral'nykh gazoprovodov [Experience in development and application of modern domestic technologies and equipment for automatic orbital welding of gas mains]. *Welding and Diagnostics*. 2010;6:51–57. (In Russ.)

3. Aleshin NP, et al. Realizatsiya adaptivnykh tekhnologii svarki kol'tsevykh stykov magistral'nykh truboprovodov [Implementation of adaptive technologies for welding ring joints of trunk pipelines]. *Welding and Diagnostics*. 2011;5:49–53. (In Russ.)

4. Aleshin NP, Lysak VI, Luk'yanov VF. *Sovremennye sposoby svarki: uchebnoe posobie* [Modern welding methods]. Moscow: MGTU im. N.Eh. Bauman = Bauman MSTU; 2011. 58 p. (In Russ.)

5. Gladkov EhA. Registrator parametrov svarki [Welder Recorder]. *Svarochnoe Proizvodstvo*. 2000;3:46–47. (In Russ.)

6. Gavrilov AI, Gladkov EhA, Perkovskii RA. Videokomp'yuternye tekhnologii postroeniya kompaktnykh modelei protyazhennykh svarnykh shvov v sistemakh avtomatizirovannogo monitoringa kachestva pri stroitel'stve magistral'nykh truboprovodov [Video-computer technologies for constructing compact models of extended welds in automated quality monitoring systems in construction of trunk pipelines]. *Welding and Diagnostics*. 2014;1:57–61. (In Russ.)

7. Kuvin BF, Kren LA. Captured: Real-Time welding data to optimize quality, efficiency. *MetalForming magazine*. 2016;50(3):40–43.

8. Adolfsson S, et al. On-line quality monitoring in short-circuit gas metal arc welding. *Welding Journal*. 1999;78(2):59s–73s.

9. Li XR, et al. Monitoring and control of penetration in GTAW and pipe welding. *Welding Journal*. 2013;92(6):190s–196s.

10. Choi JH, Lee JY, Yoo CD. Simulation of dynamic behavior in a GMAW system. *Welding Journal*. 2001;80(10):239s–245s.

11. Park M-H, et al. Control of the weld quality using welding parameters in a robotic welding process. *Journal of Achievements in Materials and Manufacturing Engineering*. 2018;87(1):32–40.

12. Bulychev VV. *Sposoby i sredstva monitoringa i avtomatizatsii svarochnykh protsessov: uchebnoe posobie* [Methods and means of monitoring and automation of welding processes]. Kaluga: Manuscript; 2018. 44 p. (In Russ.)

13. Leifsson L, Koziel S. Surrogate modelling and optimization using shape-preserving response prediction: a review. *Journal Engineering Optimization*. 2015;48(3):476–496.

14. Soy U, et al. Determination of welding parameters for shielded metal arc welding. *Scientific Research and Essays*. 2011;6(15):3153–3160.

15. Kharionovskii OV. Monitoring ob"ektov lineinoi chasti magistral'nykh gazoprovodov [Monitoring of linear part of gas pipeline facilities]. *Oil and Gas Territory*. 2009;4:22–25. (In Russ.)

16. Lisin AA, Aleksandrov YuV. Monitoring magistral'nykh nefteprovodov v slozhnykh geologicheskikh usloviyakh [Monitoring of trunk oil pipelines in difficult geological conditions]. *Science & Technologies: Oil and Oil Products Pipeline Transportation*. 2013;2:22–27. (In Russ.)

17. Surikov VI, et al. Sozdanie, vnedrenie i soprovozhdenie arkhiva ehlektronnykh kopii i otsifrovannykh dannykh trassy magistral'nogo nefteprovoda [Creation, introduction and support of archive for electronic copies and digitized data of trunk oil pipeline route]. *Science & Technologies: Oil and Oil Products Pipeline Transportation*. 2015;4:52–60. (In Russ.)

Submitted 14.01.2020

Scheduled in the issue 05.03.2020

About the authors:

Filyakov, Aleksei E., postgraduate student, Bauman Moscow State Technical University, (5/1, ul. Baumanskaya 2-ya, Moscow, 105005, RF), ORCID: <https://orcid.org/0000-0001-9051-7078>
filyakov.92@mail.ru

Sholokhov, Mikhail A., Head of the Welding Production Automation and Robotization Department, Yeltsin Ural Federal University (19, Mira Str., Ekaterinburg, 620002, RF), ORCID: <https://orcid.org/0000-0002-7666-5645>
uni@shtorm-its.ru

Claimed contributorship

A. E. Filyakov: setting the research objective and tasks; literature analysis; text preparation; formulation of conclusions. M. A. Sholokhov: academic advising; the text revision; correction of the conclusions.

All authors have read and approved the final manuscript.

MACHINE BUILDING AND MACHINE SCIENCE



UDC 669

<https://doi.org/10.23947/1992-5980-2020-20-1-51-60>

On modeling the martensite nucleation on ferromagnetic clusters

Yu. V. Dolgachev, V. N. Pustovoit, I. O. Filonenko, I. V. Ivankov

Don State Technical University (Rostov-on-Don, Russian Federation)



Introduction. The study of the austenite magnetic state in steels has provided the mechanism of the external magnetic field impact on steel under the hardening process. Previous studies have established a positive practical effect of heat treatment in a magnetic field. The work objectives were to create a computer model of the magnetic state of carbon steel austenite; to conduct computational experiments with a system of spins at various values of temperature and external magnetic field.

Materials and Methods. The positions of the Ising model were used. The canonical ensemble of spins was modeled by the Monte Carlo method using the Metropolis algorithm.

Results. The algorithm was implemented with the initial parameters selected through experimental data on the magnetic state of austenite. The inhomogeneity of this state without exposure to a magnetic field was studied. Data on the sizes of ferromagnetic clusters in austenite at various temperatures were obtained. It has been noted that the presence of an external magnetic field counteracts the temperature disordering of spins. Data on an increase in the size of ferromagnetic clusters under growing magnetic field strength were obtained.

Discussion and Conclusions. A two-dimensional computer model of the spin state of austenite of carbon steel has been developed. The computational experiments with various parameters of the model have shown that there is a short-range order in the arrangement of spins above the Curie temperature. With a rise of the temperature of the system, the sizes of ordered regions decrease; but when an external magnetic field is applied, they increase.

Keywords: quenching, steel, magnetic field, martensite, martensitic transformation, austenite.

For citation: Yu.V. Dolgachev, V.N. Pustovoit, I.O. Filonenko, I. V. Ivankov. On modeling the martensite nucleation on ferromagnetic clusters. Vestnik of DSTU, 2020, vol. 20, no. 1, pp. 51-60. <https://doi.org/10.23947/1992-5980-2020-20-1-51-60>



Introduction. The magnetic state of austenite in steels and the effect that an external constant magnetic field can exert on it is considered. Previous studies have shown that heat treatment in a magnetic field has positive practical value [1–4]; therefore, it appears important to study the mechanisms of such an effect. C. Zener [5] pointed out the need to take into account the role of magnetic transformations when considering martensitic transitions in iron-based alloys. In calculating the thermodynamic characteristics of the martensitic transformation, he used two parameters – the magnetic and non-magnetic components of the change in the free energy of pure iron.

A number of researchers [6–8] found a deviation of the temperature dependence of the inverse magnetic susceptibility from the linear Curie – Weiss law in the paramagnetic region of some steels. In this case, the curve was satisfactorily described by the Langevin function for superparamagnetics. This change in the magnetic properties of austenite in steels is associated with spontaneous fluctuations of the long-range ferromagnetic order.

The experiments [9, 10] proved the existence of short-range order of spins (the so-called “swarms”) above the Curie temperature using magnetic neutron diffraction.

A constant magnetic field during quenching cooling affects regions with an ordered arrangement of spins in austenite and their interaction. As a result, the nucleation of martensitic crystals on ferromagnetic clusters is initiated.

Materials and Methods. At the moment, there is only one accurate and detailed method for experimental studies of “swarms” of spins – magnetic neutron diffraction. In this paper, the magnetic state of austenite of carbon steel is studied through a computational experiment. The positions of the Ising model [11–13] are applied. Using the Monte Carlo method [14–16], a canonical ensemble¹ of spins was modeled, the use of which provides simulating the behavior of the spin system at a constant temperature. To obtain an arbitrary non-uniform probability distribution, the Metropolis algorithm is used [17] – a special case of the sampling procedure by significance when some possible samples are dropped.

The Ising model is used to simulate phase transitions in magnetic substances or binary alloys. This lattice model takes into account interactions between the nearest nodes. Spins are represented by the magnetic moments of atoms in the lattice sites, which interact with each other and with an external magnetic field (if any).

The Ising model is based on the following simplifications:

- kinetic energy of lattice sites is not considered;
- when calculating the energy of interaction of spins, only the nearest neighbors are taken into account;
- only two possible spin states are provided (positive \uparrow or negative \downarrow direction along z axis).

As shown in [18], the study of the classical two-dimensional Ising model reveals common behavior patterns of magnetic systems near the phase transition temperature, even despite the simplifications.

Using the Ising model, such macroscopic system characteristics as the average energy $\langle E \rangle$, average magnetization $\langle M \rangle$, specific heat C and magnetic susceptibility χ were studied. When calculating the average values for all system configurations, the period until the system reached a relaxation state, which was excluded from the calculations, was taken into account².

Research Results. Let us describe the total energy of the system of two-dimensional spins in the Ising model taking into account the possible magnetic field h :

$$E = -J \sum_{\langle i,j \rangle} s_i s_j - h \sum_{i=1}^N s_i.$$

Here, J is the exchange coupling constant, which characterizes the strength of interaction of neighboring spins; N is the number of all spins; $\langle i, j \rangle$ means summation over all the nearest pairs of spins. The number s_i is associated with each i -th lattice site. It characterizes the direction of the magnetic moment and can take the values either +1 (if the spin is oriented in the positive direction of the z axis), or –1 (if the spin is oriented in the negative direction of the z axis).

If the value of the exchange interaction constant is greater than zero, then the unidirectional state of two neighboring spins is energetically more favorable, i.e., the state with the lowest total energy is ferromagnetic. Otherwise, it will be more preferable that the neighboring spins are antiparallel with each other (antiferromagnetic state).

The application of an external magnetic field along the z axis adds or subtracts additional internal energy of the spins according to their direction along the z axis.

In further discussions on the thermodynamic characteristics of the system, the energies J and h will be measured in temperature units. This is convenient when considering the interaction between spins, because when heated, the communication system between them weakens.

We find the relation between the specific heat C and the system energy fluctuation in the canonical ensemble:

$$C = \frac{1}{T^2} (\langle E \rangle^2 - \langle E^2 \rangle).$$

¹ The canonical ensemble is a statistical ensemble corresponding to a special physical system. It exchanges energy with the environment (thermostat) being in thermal balance with it, but does not exchange matter since it is separated from the thermostat by a membrane that is impermeable to particles. For a brief description of such a system, two parameters are used: number of particles N and average energy E [13].

² Further in the text, when it comes to system configurations, the configurations after the system reaches relaxation state are implied.

The magnetization M of the system was calculated by adding all the values of s_{ij} in this configuration. Then, the average magnetization $\langle M \rangle$ over all system configurations was calculated

Magnetic susceptibility χ at a given temperature:

$$\chi = \frac{1}{T} (\langle M^2 \rangle - \langle M \rangle^2).$$

Possible configurations of the spin system will be determined by the values of 2^N spin numbers s . Using the Metropolis algorithm, spin configurations S with probability $w(S)$ can be generated, and then the sought quantities over all configurations can be averaged. The configurations that differ among themselves by one spin flip were considered. The decision on the flip of one or another spin (i.e., on the adoption of a trial configuration S_p) depended on the ratio of weight functions:

$$r = \frac{w(S_p)}{w(S)} = e^{-\frac{E_{S_p}}{T}} \cdot e^{\frac{E_S}{T}},$$

where E_s and E_{S_p} are energies of the systems with spin configurations S and S_p , respectively.

Spin s_{ij} flipped over and a new configuration was adopted if $r > 1$ or $r < 1$, but greater than a random number generated due to the uniform distribution over the interval from 0 to 1. Otherwise, the spin remained unchanged. At one Monte Carlo step, a number of flip attempts equal to the number of spins of the system N is made.

For the two-dimensional case, toroidal boundary conditions were chosen: the lattice is represented by a ring in which spins located on the right boundary of the original square lattice interact with spins located on the left boundary. A similar ring interaction is provided for the upper and lower boundaries. This provides the same number of interactions for all spins. The interaction of any spin with neighbors can be considered as the interaction with one spin whose value is equal to the sum of the values of four neighboring spins (it can be 0, ± 2 , or ± 4). In the two-dimensional case, the minimum possible value of the energy change when the considered (central) spin is overturned is $4J$.

Algorithm and initial parameters for the implementation of the model of the magnetic state of austenite.

The algorithm structure and the basic functions developed under its implementation are performed in a mathematical package taking into account the recommendations [19].

The model was implemented through sequential performing the following operations.

1. Setting the initial conditions: the number of spins of the system N , the exchange interaction constant J , the intensity of the external magnetic field h , temperature T , the number of steps of the Monte Carlo method N_t (analogue of time).

2. Performing the function that creates the initial configuration of the system considering the given N , J , h .

3. Calculation of the instantaneous system configurations for each step N_t considering N , J , h and the initial state of the system.

4. Visualization of:

- instantaneous system configurations at points of interest,
- the dependence of the instantaneous energy of the system on time,
- the dependence of the instantaneous magnetization of the system on time.

Through observing spin configurations, the current magnetic state of the system can be evaluated. A study of these time dependences provides estimating the required relaxation time of the system τ for considering it in subsequent calculations.

5. Calculation of the average energy of the system $\langle E \rangle$, the specific heat C , the magnetic susceptibility χ and the average magnetization $\langle M \rangle$.

6. Calculation of parameters characterizing the sizes of ferromagnetically ordered regions: average size, maximum size, minimum size, root-mean-square size deviation. (The calculation is based on a set of spin configurations.)

The algorithm was implemented at the initial parameters selected due to experimental data on the magnetic state of austenite [8, 20]. The temperature of the Curie point of iron-carbon austenite of U8 steel is ~ 180 K, i.e., if it

were possible to keep the austenite lattice to this temperature, then below the Curie point, austenite would obtain ferromagnetic properties. The exchange interaction constant of the two-dimensional model was selected so that the system experienced a magnetic phase transition at a given temperature. The value of the exchange interaction constant for the two-dimensional case does not coincide with the real value of this constant for the iron-carbon alloy. However, in the framework of the two-dimensional model, the following parameters were selected: $N = 625$, $J = 0.78$, $h = 0$, $N_i = 2500$. Due to this, under modeling in the temperature range including the region of the Curie point of austenite, effects have been observed that are completely analogous to the effects of a real system experiencing a phase magnetic transition from the paramagnetic state to the ferromagnetic state, namely:

- maxima of the specific heat and magnetic susceptibility at the Curie point,
- sharp decrease in the average magnetization during the phase transition,
- discrepancy between the magnetization curve and the specific heat and magnetic susceptibility curves upon transition to the ferromagnetic state (Fig. 1).

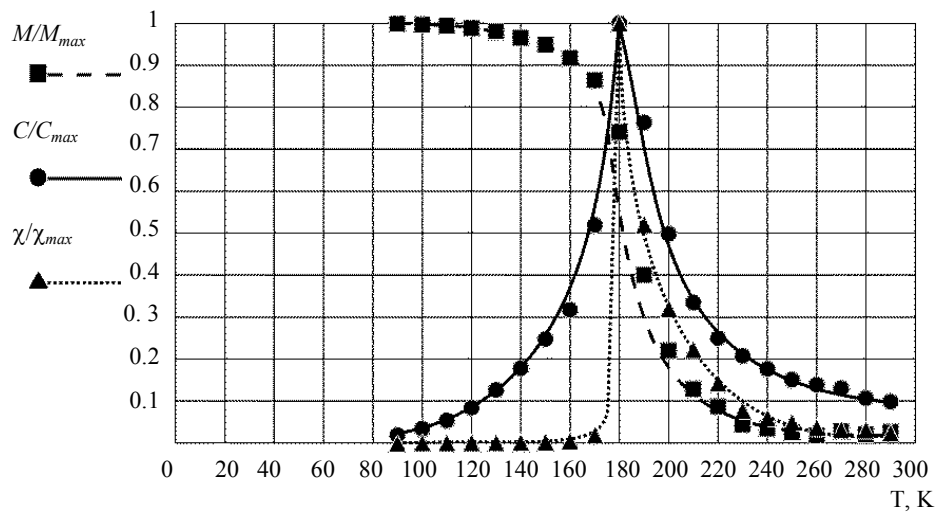


Fig. 1. Behavior of steel U8 properties near the ferromagnetic Curie point of austenite according to the results of computational experiments

Fig. 1 shows that the magnetization does not drop to zero at the Curie point. The remains of the “anomalies” above the Curie point were repeatedly observed experimentally [6–10, 19]. L. D. Landau [12] and other researchers [6, 8, 9, 19] attributed this to fluctuations of order at $T > \Theta$. Fluctuations of spontaneous magnetization should be most pronounced near the Curie point, because they tend to infinity at the Curie point itself.

Fig. 2 schematically shows the temperature dependence of the short-range order parameter σ from [19].

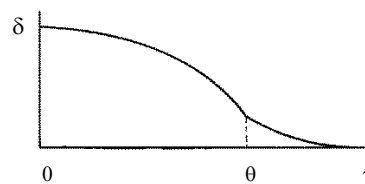


Fig. 2. Temperature dependence of the short-range magnetic order parameter [19]

Near the Curie temperature, σ decreases sharply, and at $T > \Theta$, it asymptotically tends to zero. From the point of view of short-range order, this “unsharpness” of the Curie temperature predetermines the following phenomenon: all anomalies of ferromagnetics have a steep maximum at the Curie point, however, at $T > \Theta$ they should not immediately go to zero, but only gradually decrease in accordance with the gradual destruction of order at close distances.

As shown in [19], the exchange interaction energy often determines the forces that are noticeably acting precisely at close distances. Therefore, the thermodynamically-equilibrium state of a ferromagnetic should be determined by the short-range order between spins. This is a special case of the general problem of the cooperative behavior of interacting atoms (for example, during a first-order phase transition).

Ferromagnetism is largely a quantum phenomenon [15]. Nevertheless, even within the framework of the classical statistical approach, the theory considering order at close distances is certainly useful in illustrative and qualitative terms [15, 19].

L. S. Stilbans took into account the “magnetic order” at close distances in the Ising scheme [21] and theoretically explained the “remnants” of the heat capacity anomaly at temperatures above the Curie point. The abnormal heat capacity is due to the necessity of destroying the order at short distances, which is partially conserved above the Curie point.

This method was developed by S. V. Vonsovsky [22–24]. He theoretically showed the differences between the ferromagnetic and paramagnetic Curie points. The results of his work prove that the paramagnetic susceptibility near the Curie point is finite, and does not tend to infinity, as follows from the theory without considering short-range order.

Such a great interest in the simplified Ising model is explained by the fact that it provides solving the fundamental difficulties arising in the theoretical interpretation of second-order phase transitions.

Analysis of regions with short-range ferromagnetic order in austenite using a computational experiment.

In this section, we study the inhomogeneity of the austenite magnetic state without external exposure to a magnetic field.

To visualize the system instantaneous spin configuration at selected moments, the spins are represented by white and black squares. White squares are spins oriented in the positive direction of the z axis (for example, under the impact of exchange forces and (or) an applied external magnetic field). Black squares are spins oriented in the negative direction of the z axis (Fig. 3).

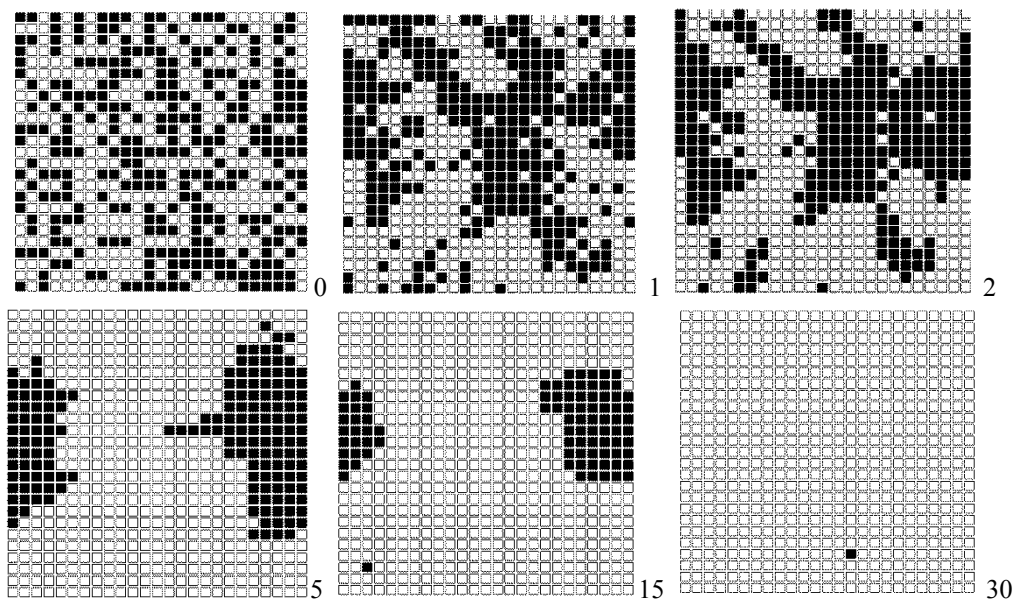


Fig. 3. System instantaneous configurations at selected moments ($T = 100$ K, $h = 0$)

Fig. 3 shows the system visualization at a temperature of 100 K (i.e., below the Curie point) without the action of a magnetic field at different moments. The following is an interpretation of these configurations.

- At time moment 0, the system is in the initial state, which is initiated using a random value generator (fully disordered state).
- At time 0, the system is in the initial state, which is initiated using a random value generator (fully disordered state).
- The transition to moment 1 means that each spin of the system ($N = 625$) was considered to make a decision on its revolution according to the conditions described above.
- By the third step, each spin was examined three times for a flip.
- Subsequent moments show that the system tends to a state with a ferromagnetic order.
- At the 30th step, a completely ordered state is recorded (with the exception of one spin). A similar picture (with small fluctuations of 1–3 spins) is observed at all subsequent moments. The total number of steps is $N_t = 2500$. Consequently, the system has come to a stable state (that is, the relaxation stage has been completed before the 30th step).

It should be noted that the described picture is characteristic of the current generation of the model with given conditions. When generating the model, a random number generator is used, therefore, the results of the recounting will differ in details, but qualitatively, the model always behaves in a similar way under the same initial conditions.

Consider the graphs of the instantaneous values of energy (Fig. 4 *a*) and magnetic moment (Fig. 4 *b*) of the system versus time.

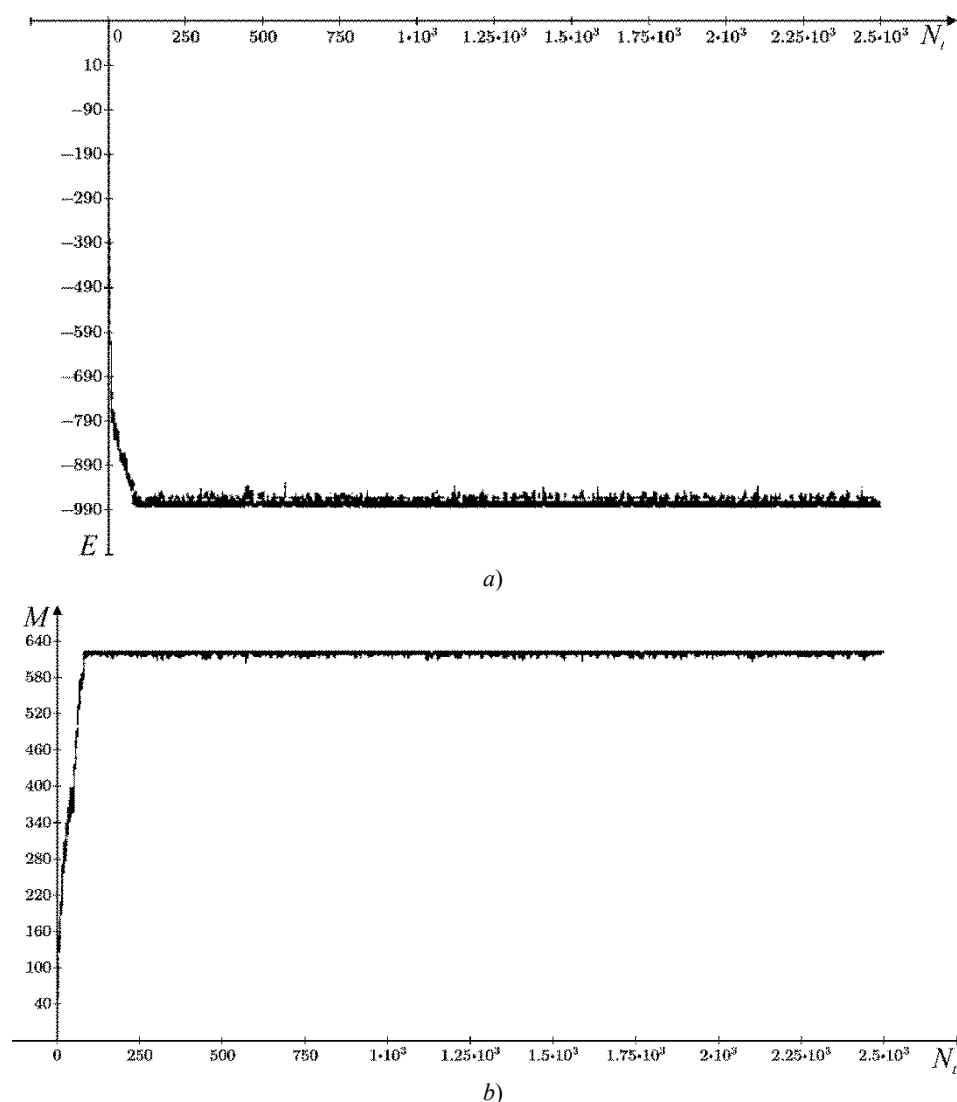


Fig. 4. Dependence of the instantaneous values of the system total energy (*a*) and magnetic moment (*b*) on time

Fig. 4 shows that the system quickly tends to an equilibrium state (relaxation process). After the transition of the system to the equilibrium state, only small fluctuations are noted. Upon reaching equilibrium for a given temperature, macro parameters (average energy, magnetization, magnetic susceptibility, specific heat) were statistically calculated from the system configurations. For this, the ratio of the relaxation time of the static system to the equilibrium state was estimated from the corresponding graphs. The initial system configurations were cut off for 400 steps (16% of the total calculation time), that, on the safe side, blocked the relaxation stage of the system, which did not exceed 150 steps (see Fig. 4).

When hardening U8 steel, the martensitic transformation starts at a temperature of ~ 500 K. It is interesting to study the model behavior near this temperature, because under quenching in a magnetic field, the field action initiating the phase transition is manifested here. Naturally, at this temperature, the paramagnetic state of austenite will be stable, as the model showed that. However, in the spin state of austenite, nanoscale regions with short-range order in the arrangement of spins are observed [9]; they play a significant role under the impact of an external magnetic field [8] (the

effect of the field is manifested in the influence on the size and stability of such regions, but they exist without an external field).

To obtain the most reliable statistical data on ferromagnetically ordered regions in austenite, a system was simulated with the maximum possible (according to the technical limitations of the RAM and processor speed) number ($N = 10000$) of spins at temperatures from 100 to 500 K. Other initial conditions remained the same.

Fig. 5 presents the results of measuring ordered regions in austenite. The size was determined by the number of atoms per horizontal and vertical sections of the ordered region: \bar{L} is average size, Max is maximum, Min is minimum, σ is root-mean-square deviation.

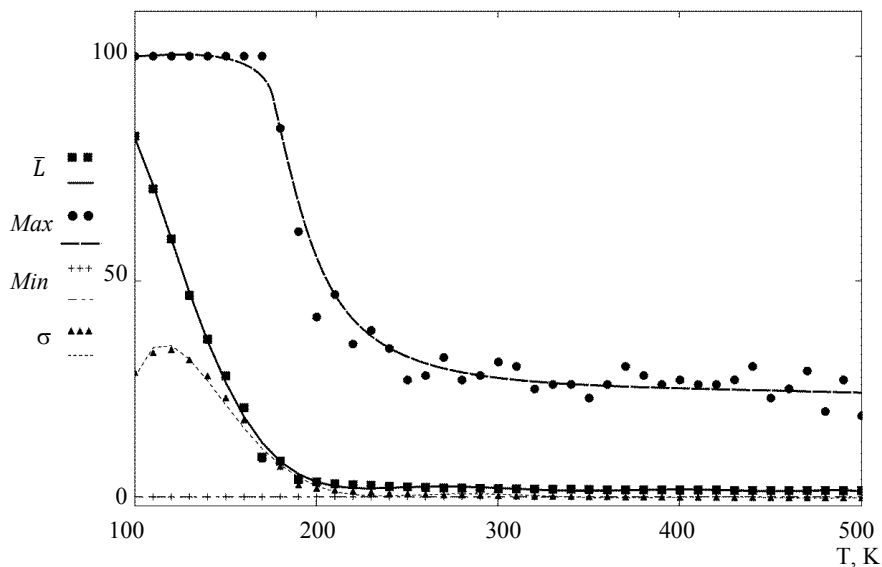


Fig. 5. Temperature dependence of area sizes with ferromagnetic order in austenite

According to the data obtained, fluctuations of the short-range magnetic order in U8 steel are preserved up to temperatures of about 500 K, when martensitic transformation starts under the steel quenching. In this case, the maximum sizes of such regions in austenite at a temperature of 500 K can reach 20 atoms in the cross section (~ 7.2 nm). The maximum size at temperatures in the region of the Curie point and below is limited by the model conditions and does not exceed 100 atoms (i.e., the maximum transverse size of the modeled region). The observed oscillations on the curve of the maximum cluster size are associated with the use of a random number generator in the model.

The Weiss theory considers only the order at long distances [19], which is determined by the difference in the number of spins oppositely directed throughout the domain, regardless of their detailed relative position. It turns out that the short-range order is simply equated to the long-range order, i.e., the numbers of the nearest neighbors of different orientations for any spin are assumed to be proportional to the total numbers of multidirectional spins in the domain. Thus, the local magnetization of the nearest neighbors at each spin is equal to the magnetization calculated over the entire crystal. A different picture is observed in a real crystal: parallel spins under the action of exchange forces tend to unite into separate “swarms” [9, 19] like gas atoms during its condensation or the formation of fluctuations in a non-ideal gas. As can be seen from Fig. 5, at low temperatures, these fluctuations are very large. At high temperatures, a more reasonable approximation does not consider the short range order. However, in this case, there are still fluctuations of parallel spins in small volumes caused by the exchange forces and leading to nonzero local magnetization in the absence of the resulting magnetic moment in the entire volume (i.e., in the absence of long-range order).

Thus, the model predicts the existence of regions with short-range magnetic order in the austenite of U8 steel before the martensitic transformation. In these areas, with a high degree of probability, martensite nuclei arise. Clusters with ferromagnetic ordering can overlap defects in the crystal lattice and instability regions of the crystal lattice [4] that occur before the phase transition. In this case, the probability of martensite nucleation is especially high.

Adding an external magnetic field to the austenite magnetic state model. The presence of an external magnetic field counteracts the temperature disordering of spins. Fig. 6 shows the dependences of the cluster parameters in

austenite with short-range order (the parameters are the same as in Fig. 5) on the external magnetic field strength for U8 steel at a temperature of 500 K.

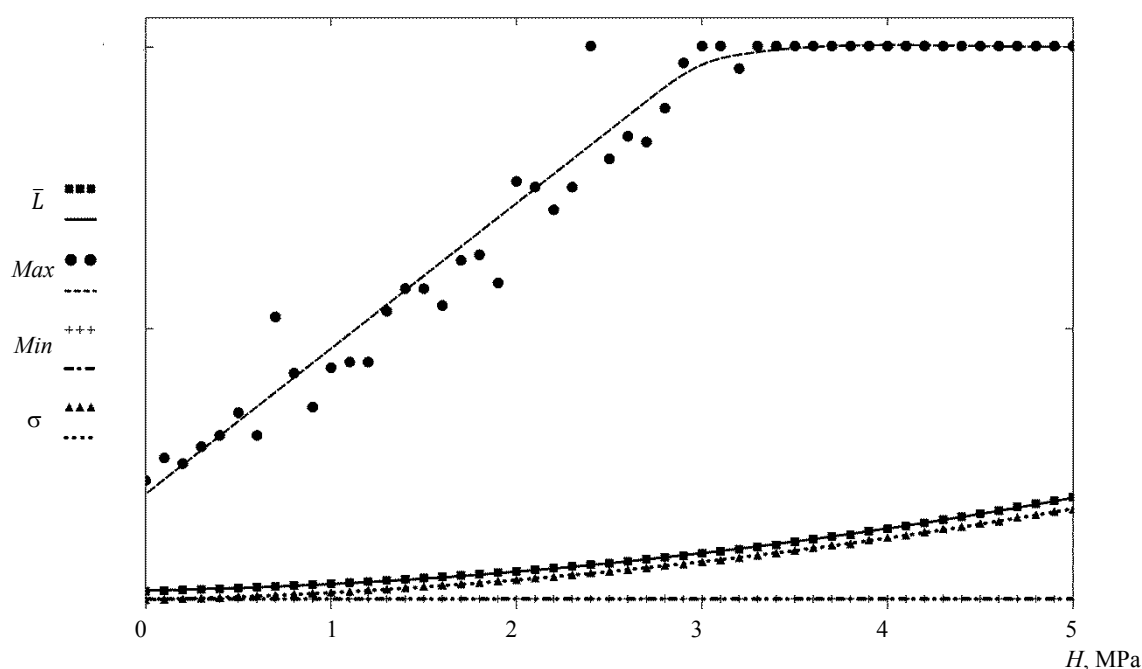


Fig. 6. Dependence of sizes of regions with ferromagnetic order in austenite on strength of external magnetic field at a temperature of 500 K

As can be seen from Fig. 6, with increasing magnetic field strength, cluster sizes grow up to the state of complete magnetic ordering at high magnetic field strength. Thus, under quenching in a magnetic field, regions with short-range order expand. Moreover, the probability of martensite nucleation is higher, and the number of nucleation sites is greater.

Discussion and Conclusions. A two-dimensional computer model of the spin state of austenite of U8 carbon steel is developed. The computational experiments with various parameters of the model have shown that there is a short-range order in the arrangement of spins above the Curie temperature. With an increase in the temperature of the system, the sizes of ordered regions decrease; however, even at the temperature of the onset of martensitic transformation (500 K), short-range fluctuations with a maximum size of ~ 7 nm are possible. When an external magnetic field is applied and its intensity is enhanced, the sizes of clusters with ferromagnetic ordering increase. Using the presented model in future research, it is supposed to study in more detail the impact of the magnetic field on the characteristics of the swarm of spins, their number, lifetime and interaction features.

References

1. Pustovoi VN, Dolgachev YuV. Tekhnologiya bezdeformatsionnoi zakalki v magnitnom pole tonkostennykh detalei kol'tsevoi formy [Unstrain tempering technology in magnet space of thin-walled ring items]. Vestnik of DSTU. 2011;11(7):1064–1071. (In Russ.)
2. Pustovoi VN, Brover AV, Magomedov MG, Dolgachev YuV. Sverkhplastichnost' stali v temperaturnom intervale Md-Mn kak stimul dlya «vnutrennei» magnitnoi [Super-ductility of steel in Md-Mn warm-up interval as stimulus for internal magnetic correction]. University News. North-Caucasian region. Technical Sciences Series. 2006;6:42–46. (In Russ.)
3. Pustovoi VN, Dolgachev YuV. Distortion-free heat treatment of thin rods in magnetic field. Materials Performance and Characterization. 2019;8(2):320–324. <https://doi.org/10.1520/MPC20170159>.
4. Pustovoi VN, Dolgachev YuV. Zarozhdenie martensita v usloviyakh sverkhplastichnosti austenita i vozdeistviya vneshnego magnitnogo poly [The emergence of martensite under superplasticity conditions and the impact of external magnetic field]. Izvestia VSTU. 2016;2(181):114–120. (In Russ.)

5. Zener C. Impact of Magnetism upon Metallurgy. JOM. 1955;7(5):619–630. <https://doi.org/10.1007/BF03377550>.
6. Voronchikhin LD, Romashev LN, Fakidov IG. Anomalous superparamagnetism of the γ phase of the Fe-Cr-Ni alloy. Soviet Physics-Solid State. 1975;16(9):1708–1711.
7. Romashev LN, Voronchikhin LD, Fakidov IG. Izmenenie magnitnykh svoystv stali vblizi martensitnoi tochki [Change in the magnetic properties of steel near the martensitic point]. The Physics of Metals and Metallography. 1973;36(2):291. (In Russ.)
8. Pustovoi VN, Dolgachev YuV. Ferromagnetically ordered clusters in austenite as the areas of martensite formation. Emerging Materials Research. 2017;6(2):249–253. <https://doi.org/10.1680/jemmr.17.00042>.
9. Spooner S, Averbach BL. Spin correlations in iron. Physical Review. 1966;142(2):291–299. <https://doi.org/10.1103/PhysRev.142.291>.
10. Bozorth RM. Magnetic Properties of Metals and Alloys. Cleveland: American Society for Metals; 1959. 349 p.
11. Ising E. Beitrag zur Theorie des Ferromagnetismus. Zeitschrift für Physik. 1925;31(1):253–258. <https://doi.org/10.1007/BF02980577>.
12. Landau LD, Lifshitz. EM. Statistical Physics. Vol. 5. Oxford: Elsevier; 2013. 544 p.
13. Hill TL. An Introduction to Statistical Thermodynamics. New York: Courier Corporation; 1986. 508 p.
14. Binder K. Monte Carlo Methods in Statistical Physics. Berlin: Springer Science & Business Media; 2012. 416 p.
15. Dyson FJ, Lieb EH, Simon B. Phase Transitions in Quantum Spin Systems with Isotropic and Nonisotropic Interactions. Journal of Statistical Physics. 1978;18(4):335–383. https://doi.org/10.1007/978-3-662-10018-9_12.
16. Creutz M. Microcanonical cluster Monte Carlo simulation. Physical Review Letters. 1992;69(7):1002–1005. <https://doi.org/10.1103/PhysRevLett.69.1002>.
17. Beichl I, Sullivan F. The metropolis algorithm. Computing in Science & Engineering. 2000;2(1):65–69. <https://doi.org/10.1109/5992.814660>.
18. Vonsovskii SV. Magnetizm [Magnetism]. Moscow: Nauka; 1971. 305 p. (In Russ.)
19. Porshnev SV. Komp'yuternoe modelirovanie fizicheskikh protsessov v pakete MATLAB [Computer simulation of physical processes in MATLAB]. Saint Petersburg: Lan'; 2011. 726 p. (In Russ.)
20. Pustovoi VN, Dolgachev YuV, Arefeva LP. Features of martensitic transformation in steel during quenching in a constant magnetic field. Materials Science Forum. 2019;946:304–308. <https://doi.org/10.4028/www.scientific.net/MSF.946.304>.
21. Stil'bans LS. Blizhnii i dal'nii poryadok v ferromagnitnykh telakh [Short and long range order in ferromagnetic bodies]. Journal of Experimental and Theoretical Physics. 1939;9:432. (In Russ.)
22. Vonsovskii SV. O ferromagnitnoi i paramagnitnoi tochkakh Kyuri ferromagnetikov [On ferromagnetic and paramagnetic Curie points of ferromagnets]. Doklady Akademii nauk SSSR. 1940;27(5):550–553. (In Russ.)
23. Vonsovskii SV. Ferromagnetizm kak problema uporyadocheniya [Ferromagnetism as a problem of ordering]. Izvestiya Akademii nauk SSSR. 1947;11(5):485–486 (Physics Series). (In Russ.)
24. Vonsovskii SV, . Shur YaS. Ferromagnetizm [Ferromagnetism]. Moscow; Leningrad: OGIZ; 1948. 816 p. (In Russ.)

Submitted 26.12.2019

Scheduled in the issue 19.02.2020

About the authors

Dolgachev, Yurii V., associate professor of the Physical and Applied Materials Science Department, Don State Technical University (1, Gagarin sq., Rostov-on-Don, 344000, RF), Cand.Sci. (Eng.), associate professor, ORCID: <https://orcid.org/0000-0002-8558-1136>, yuridol@mail.ru

Pustovoit, Viktor N., professor of the Physical and Applied Materials Science Department, Don State Technical University (1, Gagarin sq., Rostov-on-Don, 344000, RF), Dr.Sci. (Eng.), professor, ORCID: <https://orcid.org/0000-0001-6999-3520>, fipm-dstu@mail.ru

Filonenko, Irina O., student of the Physical and Applied Materials Science Department, Don State Technical University (1, Gagarin sq., Rostov-on-Don, 344000, RF), ORCID: <https://orcid.org/0000-0002-0572-5030>, 89896231497i@gmail.ru.

Ivankov, Ivan V., student of the Physical and Applied Materials Science Department, Don State Technical University (1, Gagarin sq., Rostov-on-Don, 344000, RF), ORCID: <https://orcid.org/0000-0001-6466-412X>, vanya.ivankov.99@mail.ru.

Claimed contributorship

Yu.V. Dolgachev: basic concept formulation, research objectives and tasks setting, computational analysis, text preparation, formulation of conclusions. V.N. Pustovoit: academic advising, research results analysis, the text revision, correction of the conclusions. I.O. Filonenko: implementation of the model algorithm in the programming environment, preparation of calculations. I.V. Ivankov: simulation modification and model adjustment in the programming environment, participation in the preparation of calculations.

All authors have read and approved the final manuscript.

MACHINE BUILDING AND MACHINE SCIENCE



UDC 534:62–13

<https://doi.org/10.23947/1992-5980-2020-20-1-61-67>

Determination of linear characteristics of rotor mounting groups under load

S. I. Lazarev, O. V. Lomakina, V. I. Galaev

Tambov State Technical University (Tambov, Russian Federation)



Introduction. The paper considers analytical studies on the “rotor – gapped-type support” dynamic system under process loading. The research objective is to obtain expressions for determining the equivalent stiffness characteristics of the system.

Materials and Methods. A rotor rotating in the elastic gapped-type supports is considered. A dynamic model that enables to consider the problem of determining the linear equivalent stiffness characteristics of mounting groups is proposed. To solve the problem, a system of differential equations is compiled, and a detailed analysis is performed.

Results. From the obtained dynamic equations of the system in question, we can calculate the static angular deviation of the rotor pins due to the action of the load. The proposed expressions for determining equivalent stiffness characteristics testify that it is possible to study the rotor dynamics as on the linear elastic supports with the above parameters. The obtained system of equations is analyzed, and all special cases of applying the first approximation formulas for equivalent stiffness of the rotor mounting groups are listed.

Discussion and Conclusions. The results obtained make it possible to study many dynamic processes on the basis of linear differential equations considering the nonlinear properties of the system. For shavers used in the production of leather materials, the determination of rotor vibrations in the horizontal plane provides the quality and accuracy of operations.

Keywords: mechanical engineering, rotor, dynamic rotor equipment, rotor balance, rotor mounting groups, linear equivalent stiffness parameters of rotor units, rotor operating modes.

For citation: S.I. Lazarev, O.V. Lomakina, V.I. Galaev. Determination of linear characteristics of rotor mounting groups under load. Vestnik of DSTU, 2020, vol. 20, no. 1, pp. 61–67. <https://doi.org/10.23947/1992-5980-2020-20-1-61-67>

Funding information: the research is done on theme no. 10.4798.2017/БЧ within the frame of the government task of RF Ministry of Education and Science in R&D



Introduction. Technological progress imposes new, higher requirements for the quality of engineering products. Mainly, it is about high reliability, durability of machines, their productivity and safety. All these parameters should be taken into account and calculated at the design stage.

From the point of view of production processes, the dynamic rotor equipment that provides the continuity of the process is of particular importance [1-3]. In [4], structural designs and the principle of operation of various rotary machines are presented; patent searches for each type are performed. In [5], the nature of the dependence of equivalent stiffness on the frequency of oscillations for a specific model is considered; the dependence of the critical frequencies on the equivalent stiffness of the supports is given. In [6], the authors consider in detail the issues of vibration control, vibro-adjustment work and prevention of increased vibration of rotor machines, and equilibrium of rotors. In addition, vibration sources are listed here and basic information from oscillation theory is provided. The problems of the dynamics of a rigid unbalanced rotor with four degrees of freedom are discussed in [7–9]. The study [10] is based on the assumption that bearing reactions are quasilinear forces with cubic nonlinearity. With this in mind, the effect of the radial clearance on the movement in space of a dynamically unbalanced rotor under the impact of internal friction forces is considered. In [11], the interrelation of transverse and torsional vibrations arising under the rotation of the centrifuge

rotor is shown. A linearized mathematical model of the rotor in elastic supports is developed due to the impact of transverse and torsional vibrations.

The literature review suggests that the study on the oscillatory process and the corresponding parameters of linear mechanical systems is of interest. In this paper, the rotor, in particular, its gapped-type supports, is considered. The study objective is to determine the values under load of linear equivalent stiffness parameters of the named mounting groups.

Materials and Methods. A dynamic model that provides for rotation in elastic gapped-type supports was used as a rotor (Fig. 1).

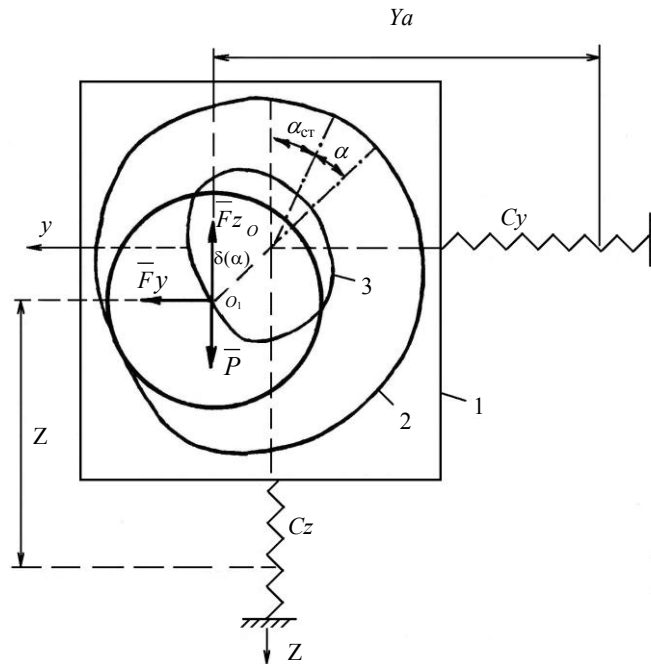


Fig. 1. Dynamic model of a rotor that rotates in elastic gapped-type supports

In Fig. 1, the following designations are adopted: 1 is rotor support; 2 is the contact boundary of the support with the rotor axle; 3 is the curve of relative motion of the rotor axle center; m is the rotor mass; $\beta(\alpha)$ is the radial clearance in the rotor bearings (represented by the angular displacement function of its journals from the vertical guides); C_y , C_z are the general stiffness of the casings of the mounting groups in the horizontal and vertical guides, respectively; y_{ct} , z_{ct} is the static shift of the center of rotor mass in the horizontal and vertical direction caused by deformations in the mounting groups; α is the dynamic tilt angle of the rotor journals; α_{ct} is the angle of inclination from the equilibrium position caused by the process load on the rotor; y_a , z_a are total dynamic displacements of the rotor mass center in the above directions; $f = F_z / F_y$ is the relationship of the vertical and horizontal components of the process load.

To determine the potential (Π) and kinetic (T) energies of the system under study, we use the following equalities:

$$\begin{aligned} \Pi = & \frac{1}{2} C_y \left[y_a + y_{cm} - \delta(\alpha + \alpha_{cm}) \sin(\alpha + \alpha_{cm}) + \delta(\alpha_{cm}) \sin \alpha_{cm} \right]^2 + \\ & + \frac{1}{2} C_z \left[z_a + z_{cm} - \delta(\alpha + \alpha_{cm}) \cos(\alpha + \alpha_{cm}) + \delta(\alpha_{cm}) \cos \alpha_{cm} \right]^2 - \\ & - mg \left[z_a + z_{cm} + \delta(\alpha_{cm}) \cos \alpha_{cm} \right]; \\ T = & \frac{1}{2} m (\dot{y}_a^2 + \dot{z}_a^2) + \frac{1}{2} A \omega^2. \end{aligned}$$

Here, A is polar moment of inertia, ω is the angular velocity of a rotating rotor.

It should be borne in mind that the acting forces are not potential. Moreover, the generalized forces to which the previously introduced coordinates y_a , z_a , α correspond, take the form:

$$Q_{y_a} = F_y, \quad Q_{z_a} = -F_z,$$

$$Q_\alpha = F_y \left\{ \left[\delta(\alpha + \alpha_{cm}) \cos(\alpha + \alpha_{cm}) + \delta'(\alpha + \alpha_{cm}) \sin(\alpha + \alpha_{cm}) \right] + \right. \\ \left. + f \left[\delta(\alpha + \alpha_{cm}) \sin(\alpha + \alpha_{cm}) - \delta'(\alpha + \alpha_{cm}) \cos(\alpha + \alpha_{cm}) \right] \right\}.$$

Here, $\delta'(\alpha + \alpha_{cm})$ is α angle derivative of radial clearance; $f = \frac{F_z}{F_y}$ is the relationship of vertical and horizontal components of the process load.

Under these conditions, equations expressing the dynamics of the system can be written as:

$$\begin{cases} m\ddot{y}_a + C_y \cdot y_a - C_y \delta(\alpha + \alpha_{cm}) \sin(\alpha + \alpha_{cm}) + C_y \delta(\alpha_{cm}) \sin \alpha_{cm} = 0, \\ m\ddot{z}_a + C_z \cdot z_a - C_z \delta(\alpha + \alpha_{cm}) \cos(\alpha + \alpha_{cm}) + C_z \delta(\alpha_{cm}) \cos \alpha_{cm} = 0, \\ mg \left[\delta(\alpha + \alpha_{cm}) \sin(\alpha + \alpha_{cm}) - \delta'(\alpha + \alpha_{cm}) \cos(\alpha + \alpha_{cm}) \right] - \\ - C_y \left[y_a - \delta(\alpha + \alpha_{cm}) \sin(\alpha + \alpha_{cm}) + \delta(\alpha_{cm}) \sin \alpha_{cm} \right] \times \\ \times \left[\delta'(\alpha + \alpha_{cm}) \sin(\alpha + \alpha_{cm}) + \delta(\alpha + \alpha_{cm}) \cos(\alpha + \alpha_{cm}) \right] + \\ + C_z \left[z_a - \delta(\alpha + \alpha_{cm}) \cos(\alpha + \alpha_{cm}) + \delta(\alpha_{cm}) \cos \alpha_{cm} \right] \times \\ \times \left[\delta(\alpha + \alpha_{cm}) \sin(\alpha + \alpha_{cm}) - \delta'(\alpha + \alpha_{cm}) \cos(\alpha + \alpha_{cm}) \right] = \\ = F_y \left\{ \left[\delta(\alpha + \alpha_{cm}) \cos(\alpha + \alpha_{cm}) + \delta'(\alpha + \alpha_{cm}) \sin(\alpha + \alpha_{cm}) \right] + \right. \\ \left. + f \left[\delta(\alpha + \alpha_{cm}) \sin(\alpha + \alpha_{cm}) - \delta'(\alpha + \alpha_{cm}) \cos(\alpha + \alpha_{cm}) \right] \right\}. \end{cases} \quad (1)$$

Having examined in more detail the third equation of the system (1), we determine the angle of inclination α_{cm} considering $\alpha = 0$. After transformations in the equations (1), we obtain a simpler system:

$$\begin{aligned} m\ddot{y}_a + C_{y_{\text{эКБ}}}^y \cdot y_a + C_{y_{\text{эКБ}}}^{yz} \cdot z_a &= 0, \\ m\ddot{z}_a + C_{z_{\text{эКБ}}}^z \cdot z_a + C_{z_{\text{эКБ}}}^{zy} \cdot y_a &= 0. \end{aligned} \quad (2)$$

An analysis of the equations (2) enables, in the first approximation of the values, to consider the elastic gapped-type support as a support with linear elastic characteristics (both in horizontal and vertical guides):

$$F_y = C_{y_{\text{эКБ}}}^y \cdot y_a + C_{y_{\text{эКБ}}}^{yz} \cdot z_a, \quad F_z = C_{z_{\text{эКБ}}}^z \cdot z_a + C_{z_{\text{эКБ}}}^{zy} \cdot y_a.$$

Here,

$$\begin{aligned} C_{y_{\text{эКБ}}}^y &= \frac{C_y \left[mg \cdot r + \cos^3 \alpha_{cm} (\theta + f \cdot z \cdot z^2 \cdot C_z) \right]}{\Delta}, \quad C_{y_{\text{эКБ}}}^{yz} = \frac{C_z \left[mg \cdot r + \cos^3 \alpha_{cm} (\theta + f \cdot z \cdot \theta^2 \cdot C_y) \right]}{\Delta}, \\ C_{z_{\text{эКБ}}}^z &= C_{z_{\text{эКБ}}}^{zy} = \frac{C_y C_z \cos^3 \alpha_{cm} \cdot \theta \cdot z (\theta + f \cdot z)}{\Delta}, \\ r &= \delta^2(\alpha_{cm}) + 2\delta'(\alpha_{cm})^2 - \delta(\alpha_{cm}) \cdot \delta''(\alpha_{cm}), \\ \theta &= \delta(\alpha_{cm}) + \delta'(\alpha_{cm}) \cdot \operatorname{tg} \alpha_{cm}, \quad z = \delta(\alpha_{cm}) \cdot \operatorname{tg} \alpha_{cm} - \delta'(\alpha_{cm}), \\ \Delta &= mg \cdot r + \cos^3 \alpha_{cm} (\theta + f \cdot z) \cdot (C_z \cdot z^2 + C_y \cdot \theta^2). \end{aligned} \quad (3)$$

Research Results. In the system (3), the quantities $C_{y_{\text{эКБ}}}^y$, $C_{z_{\text{эКБ}}}^z$, $C_{y_{\text{эКБ}}}^{yz}$ express the equivalent stiffness characteristics of the gapped-type support.

To obtain the dependences of the equivalent stiffness characteristics of a non-linear mechanical system, we use the expansion of trigonometric functions in the system (1) taking into account higher-order summands. To determine the required values, we indicate:

$$y_a = A_y \cdot \sin \omega_1 t, \quad z_a = B_z \cdot \cos \omega_1 t,$$

where B_z , A_y is the amplitude of the general oscillation of the rotor in the vertical and horizontal guides, respectively; ω_1 is the frequency of oscillations.

Thus,

$$\begin{aligned} C_{\text{эКБ}}^y &= \frac{\omega_1}{\pi A_y} \int_0^{\frac{2\pi}{\omega_1}} \Phi_y(y_a, z_a) \sin \omega_1 t dt, \\ C_{\text{эКБ}}^z &= \frac{\omega_1}{\pi B_z} \int_0^{\frac{2\pi}{\omega_1}} \Phi_z(y_a, z_a) \cos \omega_1 t dt. \end{aligned} \quad (4)$$

Here, $\Phi_y(y_a, z_a)$, $\Phi_z(y_a, z_a)$ are functions of y_a , z_a coordinates. These quantities can be determined through the system of differential equations (1).

Solving the system of equations (4) by integration methods, we represent the quantities in the form:

$$\begin{aligned} C_{\text{эКБ}}^y &= \frac{C_y (mgr + C_z \cos \alpha_{cm} \cdot b \cdot z^2)}{\Delta} + \frac{C_y^2 \cos \alpha_{cm} \cdot \psi \cdot \theta \cdot b^3 (C_y^2 \cdot \theta^2 \cdot A_y^2 + C_z^2 \cdot z^2 \cdot B_z^2)}{8\Delta^3}, \\ C_{\text{эКБ}}^z &= \frac{C_z (mgr + C_y \cos \alpha_{cm} \cdot b \cdot \theta^2)}{\Delta} + \frac{C_z^2 \cos \alpha_{cm} \cdot \psi \cdot z \cdot b^3 (C_y^2 \cdot \theta^2 \cdot A_y^2 + C_z^2 \cdot z^2 \cdot B_z^2)}{8\Delta^3}. \end{aligned} \quad (5)$$

Here,

$$\begin{aligned} b &= \cos^2 \alpha_{cm} (\theta + f \cdot z), \\ \psi &= \delta(\alpha_{cm}) + 3\delta'(\alpha_{cm}) \operatorname{tg} \alpha_{cm} - 3\delta''(\alpha_{cm}) - \delta'''(\alpha_{cm}) \operatorname{tg} \alpha_{cm}, \\ \xi &= \delta(\alpha_{cm}) \operatorname{tg} \alpha_{cm} - 3\delta'(\alpha_{cm}) - 3\delta''(\alpha_{cm}) \operatorname{tg} \alpha_{cm} + \delta'''(\alpha_{cm}). \end{aligned}$$

Analyzing (5), we can talk about the interdependence not only between the stiffness of the housings in the rotor bearings C_y , C_z , but also the amplitudes A_y , B_z of its general vibrations.

It must be emphasized that stiffness $C_{\text{эКБ}}^{yz}$ is expressed as the relationship of rotor movements in the horizontal and vertical planes. In the case $C_{\text{эКБ}}^{yz} = 0$ in the system (2), the equations will not be connected, which enables to consider all possible options. They are listed below.

— In the absence of changes in the radial clearance over time and $\alpha_{cm} = 0$, we have $C_{\text{эКБ}}^z = C_z$. This option is typical for idle rotor operation. Moreover, the radial displacement of the rotor with respect to the support in the vertical guides is a very small amount, although of a higher order than the displacement in the horizontal guides.

— If we accept $z = 0$, then $C_{\text{эКБ}}^z = C_z$. This situation is characteristic of the radial movement of the rotor relative to the support surrounded by a point through which the horizontal tangent passes to the trajectory of the relative movement of the journal center.

— When the value of the radial clearance in the bearings is zero, we have $C_{\text{эКБ}}^y = C_y$ and $C_{\text{эКБ}}^z = C_z$.

— If there are no changes in the radial clearance and $\alpha_{cm} = 90^\circ$, then $C_{\text{эКБ}}^y = C_y$. This is possible if the rotor operates at under the process load with a selected gap, i.e., in horizontal rails, the radial displacement assumes small values in comparison to the vertical direction.

— When $\theta = 0$, $C_{\text{эКБ}}^y = C_y$. In this case, the radial displacements of the rotor take place in the vicinity of the point through which the vertical tangent passes to the line of relative motion of the journal center.

— It is possible to accomplish the equality $\theta + f \cdot z = 0$. This is true in the case of a radial displacement of the rotor with respect to the support surrounded by such a point through which a normal is drawn which coincides with the line of action of the resulting forces F_r and F_b . In this case, $C_{\text{эКБ}}^y = C_y$ and $C_{\text{эКБ}}^z = C_z$.

Consider the characteristics of the rotor on elastic supports the rigidity of which is equal to $C_{\text{эКБ}}^y$, $C_{\text{эКБ}}^z$. Let us denote ε the eccentricity of the rotor, and ω its angular velocity. We represent the oscillation equations in the form of the system:

$$\begin{cases} m\ddot{y}_a + C_{\text{эКБ}}^y \cdot y_a = m \cdot \varepsilon \cdot \omega^2 \sin \omega t \\ m\ddot{z}_a + C_{\text{эКБ}}^z \cdot z_a = m \cdot \varepsilon \cdot \omega^2 \cos \omega t \end{cases} \quad (6)$$

Solving the (6), we write the expressions for the oscillation amplitudes:

$$A_y = \frac{m \cdot \varepsilon \cdot \omega^2}{C_{\text{yкв}}^y - m \cdot \omega^2}, \quad B_z = \frac{m \cdot \varepsilon \cdot \omega^2}{C_{\text{yкв}}^z - m \cdot \omega^2}. \quad (7)$$

Note that the summands $C_{\text{yкв}}^y$, $C_{\text{yкв}}^z$ in the denominators depend on the amplitudes A_y , B_z . We represent the graphically considered system (Fig. 2).

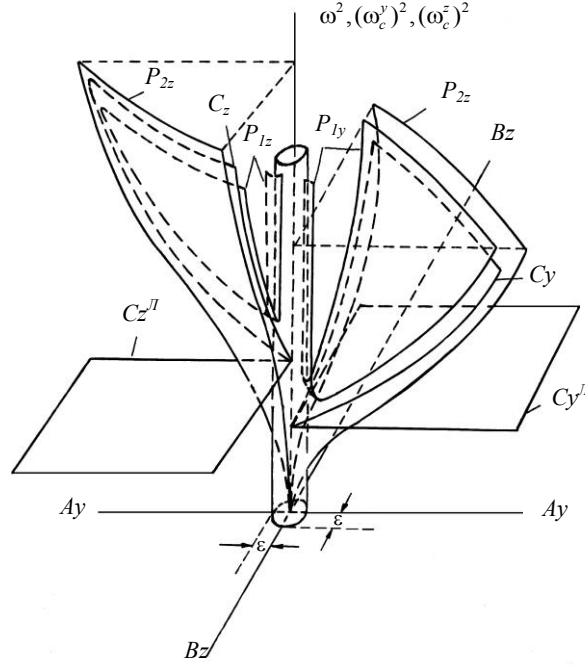


Fig. 2. Graphical representation of dynamic characteristics of absolute oscillations of the rotor in gapped-type supports

The surfaces P_{1y} , P_{2y} , P_{1z} , P_{2z} (resonant) and C_y , C_z (skeleton) are constructed under the assumption that the amplitudes A_y and B_z vary independently based on (7) and the equalities $C_{\text{yкв}}^y = m(\omega_c^y)^2$, $C_{\text{yкв}}^z = m(\omega_c^z)^2$.

The amplitudes of forced oscillations A_y , B_z correspond to the frequency of disturbing forces ω_0 . Given this fact, to obtain expressions of the indicated amplitudes, we first construct the plane $\omega^2 = \omega_0^2$.

At the intersection lines of the constructed plane with the surfaces P_{1y} , P_{2y} and P_{1z} , P_{2z} there will be points with identical coordinates. These points are the desired amplitudes of the rotor oscillations.

Planes C_y^{II} , C_z^{II} are the skeleton surfaces of a linear system. In this case, only the first summands are taken in the expressions for equivalent stiffness. They indicate that the frequencies of free vibrations of a linear system are independent of amplitudes.

Resonant surfaces represent rotor oscillations in horizontal guides, and skeleton surfaces – in vertical guides. They are built in various coordinate octants. The skeleton surfaces are elliptical paraboloids in shape. ω_c^y , ω_c^z represent the frequencies of free oscillations of the system in Fig. 2.

Discussion and Conclusions. Multiple points may be suitable for a single frequency. This means that several modes of oscillations including unstable ones are possible in the studied system. For the transition of a system from one stable mode of motion to another, some external impacts are necessary, which is characteristic of nonlinear systems.

As an example of the application of the dependences obtained, we can cite the problem on forced oscillations of the rotor due to its static imbalance.

Dependences presented in the paper (4) indicate that equivalent angular stiffness properties are interdependent not only through the stiffness characteristics C_y , C_z of the bodies, but also through the amplitudes A_y , B_z of general rotor oscillations.

As a result of the study on the linear characteristics of the mounting groups of the loaded rotor, the following results are obtained.

1. A dynamic model of a rotor rotating in elastic gapped-type supports is proposed. This model provides investigating the problem of determining the linear equivalent stiffness characteristics of mounting groups.
2. The system of equations is analyzed, and the possibilities of applying the formulas are listed. In particular, they can be used to determine rotor oscillations in the horizontal plane on shavers used to produce leather blanks.

References

1. Banaszek S. The modeling of defects in the rotor-trains of turbomachinery-simulation-based diagnostics. *Problems of Mechanical Engineering*. 2013;16(3):73–78.
2. Galaev VI. Vibroaktivnost' vzaimodeistviya sistemy neuravnovesennykh valov, vrashchayushchikhsya v uprugo-massovykh oporakh [Vibro-activity of interaction system of unbalanced shafts rolling in elastic-mass bearing]. *Transactions of TSTU*. 2004;10(3):747–754. (In Russ.)
3. Lomakina OV, Galaev VI. Dynamic linearization of stiffness characteristics of elastic bearings with radial clearance of loaded rotor. *Problems of Contemporary Science and Practice*. Vernadsky University. 2011;2(33):387–393.
4. Grinev DV. Konstruktivnye skhemy i printsipy raboty rotorno-lopastnykh mashin [Constructive schemes and principles of operation of the rotor-blade machines]. *Vestnik PskovSU (Economic and Technical Sciences)*. 2014;5:142–150. (In Russ.)
5. Biyalt MA, Plotnikova AA, Ur'ev EV. Raschetnoe issledovanie vibratsionnykh kharakteristik dinamicheskoi sistemy «Rotor - podshipniki - opory» [Design study on vibration characteristics of the “Rotor - bearings – supports” dynamic system]. *Young Scientist*. 2012;11:23–26. (In Russ.)
6. Gol'din AS. Vibratsiya rotornykh mashin [Rotary machine vibration]. Moscow: Mashinostroenie; 1999. 344 p. (In Russ.)
7. Timoshenko SP. Kolebaniya v inzhenernom dele [Fluctuations in engineering]. Moscow: Mashinostroenie; 1985. 40 p. (In Russ.)
8. Kel'zon AS, Tsimanskii YuP, Yakovlev VI. Dinamika rotorov v uprugikh oporakh [Dynamics of rotors in elastic supports]. Moscow: Nauka; 1982. 280 p. (In Russ.)
9. Kel'zon AS, Meller AS. Dinamika staticheskii neuravnovesennogo rotora v podshipnikovykh oporakh [Dynamics of statically unbalanced rotor in bearings]. *Doklady Akademii nauk SSSR*. 1991;318(1):69–72. (In Russ.)
10. Pasyukova IA. Ustanovivshiesya dvizheniya neuravnovesennogo rotora v podshipnikakh s radial'nym zazorom [Steady motion of unbalanced rotor in bearings with radial clearance]. *Vestnik of Saint Petersburg University*. 2005;3:87–95. (In Russ.)
11. Vul'fon II, Kolovskii MZ. Nelineinye zadachi dinamiki mashin [Nonlinear problems of machine dynamics]. Leningrad: Mashinostroenie; 1968. 284 p. (In Russ.)

Submitted 16.01.2020

Scheduled in the issue 27.02.2020

About the authors

Lazarev, Sergei I., Head of the Mechanics and Engineering Drawing Department, Tambov State Technical University (106, Sovetskaya St., Tambov, 392000, RF), Dr.Sci. (Eng.), professor, ORCID: <https://orcid.org/0000-0003-0746-5161>, sergey.lazarev.1962@mail.ru

Lomakina, Olga V., associate professor of the Mechanics and Engineering Drawing Department, Tambov State Technical University (106, Sovetskaya St., Tambov, 392000, RF), Cand.Sci. (Pedagogy), ORCID: <https://orcid.org/0000-0002-6908-6055>, lomakinaolga@mail.ru

Galaev, Valentin I., associate professor of the Mechanics and Engineering Drawing Department, Tambov State Technical University (106, Sovetskaya St., Tambov, 392000, RF), Cand.Sci. (Eng.), associate professor, ORCID: <https://orcid.org/0000-0002-6793-6693>, geometry@mail.nnn.tstu.ru

Claimed contributorship

S. I. Lazarev: basic concept formulation; research objectives, tasks, and methods. O. V. Lomakina: literature review, text preparation, results obtaining and formulation of conclusions. V. I. Galaev: analysis of the research results, the text revision.

All authors have read and approved the final manuscript.

MACHINE BUILDING AND MACHINE SCIENCE



UDC 620.20

<https://doi.org/10.23947/1992-5980-2020-20-1-68-78>

Statistical analysis of sizing features of dust generated under the mechanical metal-working

N. N. Azimova, E. N. Ladosha, S. N. Kholodova, D. S. Tsymbalov, O. V. Yatsenko

Don State Technical University (Rostov-on-Don, Russian Federation)



Introduction. The paper considers the mathematical analysis of the fractional composition of dust generated during the operation of the rail-cutting machine. It is established that the studied polydisperse material is well described by the one-parameter exponential distribution. At the same time, the lognormal particle size distribution, whose parameters are determined by mathematical programming methods, seems adequate for the purposes of calculating cyclones. The work objective was to develop mathematical methods for correct averaging of the size and mass parameters of dust under the solid metal machining.

Materials and Methods. We studied the possibility of approximating experimental data by Rosin – Rammler distributions (classical, generalized three-parameter $P(x, D, n, m)$, and simplified exponential $P(x)$, in which $n = 1$). The corresponding results were compared to each other and to the data of approximation of the lognormal and double lognormal functions. These results indicate close approximation quality using the following model distributions $P(x)$:

- five-parameter double lognormal;
- three-parameter type of Rosin-Rammler;
- two-parameter classical Rosin - Rammler;
- one-parameter exponential.

Results. The primary physical analysis of cutting waste was carried out by the laboratory measuring complex *Fritsch Analysette 22 Compact* which uses the *LALLS – low angle laser scattering* method. The built-in software provides output of measurement results in primary graphic and digital forms. It was found that the simplest exponential distribution is best suited for a detailed analysis of the dust particle-size distribution based on the experimental data. This distribution enables reproduction of all the integral indicators provided by the instrumental measuring complex along with the graphical data.

Discussion and Conclusions. The results obtained can be used to rationalize the local suction machine, and the mathematical models and algorithms can be used for the parametric analysis of any dust captured by cyclones.

Keywords: metal cutting, dust, size distribution, statistics, mathematical programming

For citation: N.N. Azimova, E.N. Ladosha, S.N. Kholodova, et al. Statistical analysis of sizing features of dust generated under the mechanical metal-working. Vestnik of DSTU, 2020, vol. 20, no. 1, pp. 68–78. <https://doi.org/10.23947/1992-5980-2020-20-1-68-78>



Funding information: The research is done on theme “Development of the basics for designing integrated systems and means of operator protection from exposure to hazardous and harmful production factors” no. 5,6968,2017/БЧ within the frame of the government task of the Ministry of Education and Science of the Russian Federation in R&D.

Introduction. Dust generated during machining (cutting, drilling, grinding, polishing, etc.) of hard metals and alloys can cause direct or indirect damage to human health and lead to environmental pollution. To eliminate these negative consequences, cyclones are widely used — devices of general and local air purification using aerodynamic capture of dust by inertia forces with its subsequent screening from the air stream into the accumulator [1]. The efficiency of cyclones is ensured by calculation, the purpose of which is to guarantee the capture of solid particles suspended in an air stream of a given category at minimal economic costs. Since particle capture is provided by competition between inertial and aerodynamic forces, the corresponding physical criteria form the basis for the calculation of cyclones [2]. The key components of these criteria are the dimensional and mass characteristics of dust particles. Due to the natural heterogeneity of industrial dust, these characteristics are of a statistical nature, which puts forward narrow requirements for the correctness of their averaging when calculating dust cleaning systems (cyclones). Thus, reliable scientific information on the dimensional and mass parameters of dust for various types of mechanical metalworking is a challenge since their practical application provides for a rational organization of dust collection through cyclones.

This study objective is to develop mathematical methods for the correct averaging of size and mass parameters of dust under the machining of hard metals. The results obtained were used to rationalize the local exhaust machine; and the mathematical models and algorithms developed by the authors are applicable without significant restrictions for the parametric analysis of any dust to be captured by cyclones.

The theoretical framework for the study. The dust particle is under the impact of gravity and inertial forces, which is proportional to the mass of the particle equal to $\rho \cdot x^3$, where ρ is the density of the forming material in $[\text{kg/m}^3]$; x is the characteristic particle size in $[\mu\text{m}]$. Therefore, knowledge of the dust inertial properties comes down to knowledge of its density and characteristic size. The magnitude of the aerodynamic force acting on such a particle from the flow side is proportional to the square of its characteristic size x^2 and does not depend on density. The ratio of these forces appearing in the cyclone efficiency criterion is, respectively, proportional to the complex $\rho \cdot x$. However, two important circumstances should be taken into account: firstly, dust particles differ significantly in size and, secondly, the shape of each dust particle is unique and far from the standards used (sphere, cube, etc.). These features put forward very narrow requirements for the procedure of double averaging of the characteristic size of a dust particle by its component size and shape. Obviously, the technique averaging the characteristic size of dust particles is targeted: in our case, it corresponds to the calculation of cyclone efficiency.

For the first time, J. Sauter studied systematically the parametric averaging of polydisperse media [3, 4]. The key results of his work are as follows:

1. For various purposes, specifically averaged medium particle sizes from an inhomogeneous population are important. Since the average size is a value expressed in fractions of a meter, the following method of dimensional averaging of an ensemble of particles with a distribution function $F(x)$ and, accordingly, a probability density $P(x) = dF(x)/dx$ is obvious:

$$\langle x \rangle_{ij} = \left[\int P(x) x^i dx / \int P(x) x^j dx \right]^{1/(i-j)} . \quad (1)$$

2. The formula (1) implies that all dust particles are characterized by a single size, i.e., they have the shape of a ball. Therefore, the value $\langle x \rangle_{ij}$ is called the Sauter diameter and is designated as D_{ij} (most often, the Sauter diameter is understood as D_{32}).

3. If the shape of the particles is substantially irregular and is characterized by two or two parameters, the shape factor is also introduced into consideration. The physical meaning and practical application of various Sauter diameters are given in Table 1, and important information about the shape coefficient is in [5].

Numerous studies on the dispersion of various media and materials allow us to state [6] that the solid particles obtained as a result of single crushing are distributed in size according to the two-parameter Rosin – Rammler law:

$$F(x, D, n) = 1 - e^{-(x/D)^n}, \quad P(x, D, n) = 1/D \cdot (x/D)^{n-1} \cdot e^{-(x/D)^n}, \quad (2)$$

where the value $\langle x \rangle = D \cdot G(1 + 1/n)$ characterizes the average particle size, and n is the degree of dimensional heterogeneity of the ensemble (the smaller n , the higher the polydispersity of the powder).

Under multiple grinding, the powders consist of particles whose sizes satisfy the two-parameter lognormal Gauss-Kolmogorov distribution [6]:

$$P(x, D, \sigma) = \frac{\lg e}{\sqrt{2\pi \cdot \lg \sigma} \cdot x} \cdot e^{-\frac{1}{2} \left(\frac{\lg x - \lg D}{\lg \sigma} \right)^2}. \quad (3)$$

In the distribution (3), the parameter $\lg D$ corresponds to the conditional average particle size, and the parameter $\lg \sigma$ corresponds to the spread in real particle sizes around the conditional average.

The principal advantage of the Gauss – Kolmogorov model is the convenience of recalculating the values of D_{ij} from the linear Hatch – Choute relations [7], which links them to the quantities D and σ . The form of these relations is such that at any two known quantities D_{nm} and D_{kl} , all other quantities can be calculated.

It is important to note that the powder analyzed by the authors (rail cutting waste) is not necessarily described by the classical models given here. Firstly, the cutting process contains elements of both uniqueness (each contact of the abrasive wheel with the rail material is unique) and multiplicity (such interactions are extremely repetitive). Secondly, the shape of metallic filings is far from spherical. Finally, along with metal filings, cutting waste contains particles of a chipping abrasive. The content of the latter, due to the characteristics of the process and the requirements for the tool, can vary significantly. Thus, the study on the distribution of exhaust dust by particle size seems to be a practically important and scientifically significant task.

Experimental data. The initial physical analysis of the cutting waste was carried out using the *Fritsch Analysette 22 Compact* laboratory measuring complex through the *LALLS — low angle laser scattering* method [8]. The embedded software implements measurement results in primary graphic and digital forms. The disadvantages of the software part of the complex are: lack of detailed information on the conversion algorithms of the measured quantities and on the output data nature, as well as the quantitative errors of the data displayed in the form of graphs. In particular, it may seem that the scale of the differential distribution function (probability density) is given on printouts with a several-fold error. A deeper examination allows us to conclude that in fact on this graph, the dependence of the quantity $P(x_k) dx_k$ on x_k is shown, and the partition of particles by size into groups of width dx_k is not uniform. In addition, the integral characteristics of the particle D_{ij} size distribution calculated by the program are not documented, which requires their verification for compliance with both the original graphic data and the classical models of Rosin – Rammler and Gauss – Kolmogorov.

The noted circumstances, when evaluating the results of the analysis output by the built-in program, determine the implementation of additional measures: normalization of the initial curve of the differential distribution function, as well as checking the concordance of the integrated indices D_{ij} of both this distribution function and the basic model distributions. The implementation of these tasks requires high-quality digitization of the graphical results of fractional composition provided by the *Fritsch Analysette 22 Compact*, and this requires the specialized software [9, 10] and the development of appropriate data verification algorithms.

Digitization technique and experimental data verification. To digitize the initial graphic data of the dispersion analysis obtained using the *Fritsch Analysette 22 Compact* instrument, the specialized *Grafula* program [11] was used. This information freeware provides for translating graphically represented dependences into a tabular form.

The digitization procedure is reduced to reading the graph, placing the axes of the Cartesian coordinates on it, setting the scale and drawing a sufficient number of markers on the line representing the dependence.

The result of automatic digitization refers to the position of the points input by the user and is formed into an *Excel*-compatible table. The error in the resulting digital data has several components:

- error in the schedule generation due to the features of the *Fritsch Analysette 22 Compact* complex;
- defects in printing or displaying as an electronic photograph (screenshot);
- inaccuracy in digitizing the graph through the *Grafula* program;
- impossibility of accurately marking the curve on the graph due to limitations both in the resolution of the system and in the psychomotor capabilities of a person.

The last of these errors, apparently, is the most significant. The noted circumstances require supplemental checks of the digitization results to eliminate critical errors and evaluate correctly the result error.

To verify the digitization results, this study was carried out in several stages. At first, as applied to data in a normal particle size representation relative to those presented on a logarithmic scale, and then the initial analysis results were compared graphically. In this case, both digitized series were renormalized in order to eliminate the systematic error and ensure that the condition important for the distribution function $F(x)$ is fulfilled: $F(\infty) = 1$. Subsequently, on the basis of each of the results, the uniform model distributions were constructed whose empirical parameters were determined by mathematical programming methods [12] and compared. The last test stage was comparison of the averaged indicators of the dust dimensional composition calculated from the constructed model distributions with the integral characteristics of the distributions that are issued by the *Fritsch Analysette 22 Compact* instrument software.

It turned out that the distortion of the distribution function $F(x)$ as a result of the inability to extract it from the instrument directly in the digital representation is 15% when digitizing the graph in a linear (particle size) scale and 8% when digitizing the graph in a logarithmic scale. Fig. 1, from which it follows that both restored distributions practically coincide starting with a diameter of 10 μm , gives an idea of the coordination of the data obtained in two ways. At the same time, one and a half dozen of the first points available for reading from a graph having a logarithmic size scale indicate the presence of a significant proportion of small, most dangerous for humans particles smaller than 10 microns. This circumstance is secondary since active air purification systems capture predominantly small particles.

The fact, that at $x \geq 10 \mu\text{m}$, the graphic distributions displayed by the *Fritsch Analysette 22 Compact* at different scales coincide, is confirmed by the following test. If we approximate both series of experimental data by the Rosin – Rammler curve and compare the obtained curves, we can quantitatively evaluate the effect of the digitization error on the final result.

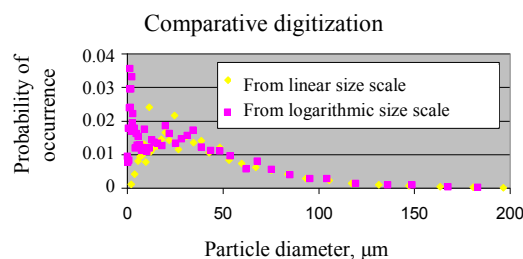


Fig. 1. Digitization results of dispersion analysis data of metal-abrasive dust

For approximation of the compared data presented in Fig. 1 by the model (2), the optimization problem related to mathematical programming was solved numerically [12]. The discrepancy between the actual and theoretical particle size distributions was minimized. If the discrepancy is determined by the Cartesian norm convenient for calculations, it is required to minimize the functional (Φ):

$$\Phi(x, D, n) = \sum_k [P(x_k, D, n) - P_k]^2 \rightarrow \min,$$

where k is the number of the nodal (tabular) point; P_k is the experimental probability density value; D and n are the described above parameters of the Rosin-Rammler model distribution.

Solving this problem through *Excel*, we obtain the following result. For the data obtained from a graph linear in x , the values of D and n are equal to 48.37 μm and 1.588 μm , respectively. Moreover, the curve approximating $P(x, D, n)$ is characterized by an average residual with experimental points 0.00274 and a correlation coefficient of 0.894. Similarly, solving the problem for 35 right points reconstructed from a logarithmic graph, we obtain the values of $D = 48.61 \mu\text{m}$, $n = 1.346$, residual — 0.00187, correlation coefficient — 0.934. The proximity of the parameters D and n for both tables, together with a small residual and a high correlation, indicate the approximate equivalence of the studied graphic images of the analyzed result. The correlation of the functions $P(x, D, n)$ with the calculated and above parameter values provides for the difference in the presentation of data in a formula form obtained from the compared graphic sources. Its value is 0.99.

Since the dust dimensional characteristics averaged on the basis of a certain realistic distribution are important, we calculate the set of indicators D_{ij} according to the Rosin-Rammler model initialized above for the values of the parameters D and n obtained in different ways. Then, we compare the results to each other and to the D_{ij} integral indicators recorded by the *Fritsch Analysette 22 Compact*.

The purpose of comparing the analyzed graphic distributions to the integral indicators D_{ij} recorded by the device is to find out exactly which distribution is shown on these graphs. The fact that on the screen of the *Fritsch Analysette 22 Compact*, the D_{43} value coincides with the arithmetic mean diameter in five decimal places, and the D_{32} value coincides with the geometric mean size just as accurately, suggests that not the parameter $P(x_k)$, but the differential x^3 -weighted distribution function is recorded:

$$dF(x_k) = P(x_k) x_k^3 dx_k. \quad (4)$$

This is a key circumstance in interpreting the dimensional analysis results of dust particles based on histograms printed by the device. We verify the proposed hypothesis through calculating the moments D_{ij} . The results of comparing the calculations when accepting or rejecting the hypothesis of the authors to the corresponding numerical data recorded by the *Fritsch Analysette 22 Compact* are given in Table 1.

Table 1

Comparison of Sauter's dust diameters based on approximations of digitized graphic data

Diameter, μm	Hypothesis (4) is not true		Hypothesis (4) is true		Instrument numeric data, μm
	$D = 48.4 \mu\text{m},$ $n = 1.588$	$D = 48.6 \mu\text{m},$ $n = 1.346$	$D = 48.4 \mu\text{m},$ $n = 1.588$	$D = 48.6 \mu\text{m},$ $n = 1.346$	
D_{43}	90.2	107.1	43.4	44.4	43.5
D_{42}	83.2	97.9	30.4	27.5	20.9
D_{41}	75.2	87.1	15.6	12.5	8.18
D_{40}	65.5	73.6	7.61	6.11	4.23
D_{32}	76.7	89.5	21.3	17.0	10.0
D_{31}	68.6	78.5	9.38	6.62	3.55
D_{30}	58.9	64.9	4.26	3.15	1.95
D_{21}	61.4	68.8	4.13	2.57	1.25
D_{20}	51.6	55.2	1.90	1.35	0.66
D_{10}	43.4	44.4	0.88	0.71	0.59

As can be seen from the table, the hypothesis on the essence of the data obtained using the *Fritsch Analysette 22 Compact* service program is correct. This conclusion is crucial when interpreting the dust dimensional analysis results.

Statistical analysis results of graphic data and their interpretation. To better describe the finely dispersed part of the dust, we use the graphical data (Fig. 1) in a logarithmic size scale and approximate them by a five-parameter distribution corresponding to the weighted sum of two lognormal distributions:

$$P(x, D_1, D_2, \sigma_1, \sigma_2, \alpha) = \frac{\lg e}{\sqrt{2\pi} \cdot x} \cdot \left[\frac{\alpha}{\sigma_1} + \frac{1-\alpha}{\sigma_2} \right] \left[\alpha \cdot e^{-\frac{1}{2} \left(\frac{\lg x - \lg D_1}{\lg \sigma_1} \right)^2} + (1-\alpha) \cdot e^{-\frac{1}{2} \left(\frac{\lg x - \lg D_2}{\lg \sigma_2} \right)^2} \right],$$

where D_1 and D_2 are the peak position; σ_1, σ_2 are the peak width, α is the fraction of particles in the first mode.

Solving the corresponding optimization problem using *Excel* tools yields the following result: $D_1 = 45.2 \mu\text{m}$, $D_2 = 7.0 \mu\text{m}$, $\sigma_1 = 1.97 \mu\text{m}$, $\sigma_2 = 2.1 \mu\text{m}$, $\alpha = 0.858$. The average discrepancy between the approximating function and the initial data is 31%, and the correlation coefficient is 0.977. This is a satisfactory agreement given the high error of the experimental values (Fig. 1). Note that this result refers to the x^3 -weighted true size distribution function of dust. It can be interpreted as follows: the bulk of the dust (about 85%) is made up of particles larger than $10 \mu\text{m}$; therefore, for practical air purification, this distribution can be replaced by a two-parameter lognormal (2) one with the following parameters: $D = D_1 = 45.2 \mu\text{m}$ and $\sigma_1 = \sigma_1 = 1.97 \mu\text{m}$. However, such a simplification will not allow a qualitative approximation of D_{ij} by $j < 3$, while the consideration of the fine fraction is significant for some applications, for example, for calculating all the used diameters D_{ij} and the moments of the distribution function $P(x)$. Below are the results of comparing the double lognormal and lognormal approximations of $P(x)$. Fig. 2 shows the experimental data approximation by a double lognormal distribution:

$$P(x) = 0.176 \cdot e^{-\frac{1}{2} \left(\frac{\lg x - 1.65}{0.416} \right)^2} + 0.563 \cdot e^{-\frac{1}{2} \left(\frac{\lg x - 0.898}{0.791} \right)^2}.$$

The mean-square ratio error is 0.31, and the correlation coefficient with experimental points is 0.977.

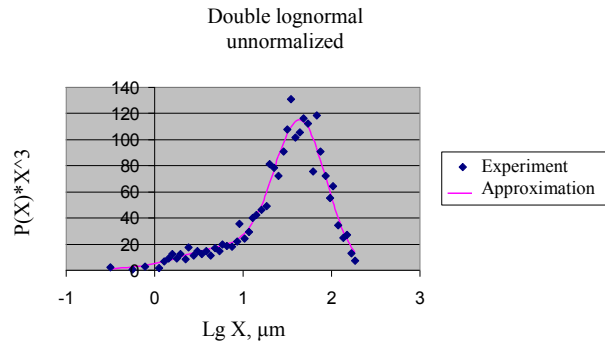


Fig. 2. Approximation of experimental data by double lognormal distribution

Fig. 3 shows the experimental data approximation by the lognormal distribution:

$$P(x) = 0.563 \cdot e^{-\frac{1}{2} \left(\frac{\lg x - 1.63}{0.435} \right)^2}.$$

The mean-square ratio error is 1.23, the correlation coefficient with experimental points is 0.970.

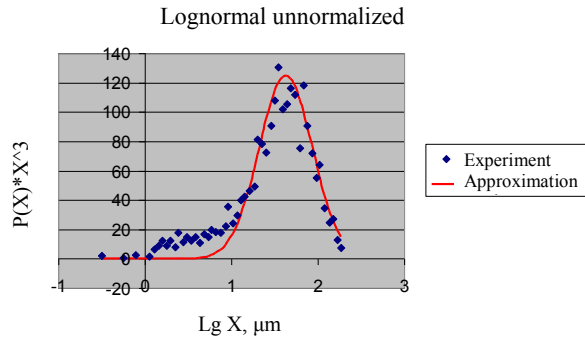


Fig. 3. Approximation of experimental data by lognormal distribution

The possibility of approximating experimental data by the Rosin-Rammler distributions was also studied:

- by classic generalized three-parameter:

$$P(x, D, n, m) = (x/D)^m \cdot e^{-(x/D)^n} / \int (x/D)^m \cdot e^{-(x/D)^n} dx;$$

- by simplified exponential:

$$P(x) = 1/D \cdot e^{-x/D}, n = 1.$$

Fig. 4 presents the experimental data approximation by the Rosin - Rammler distribution:

$$P(x) = 7.73 \cdot 10^{-3} \cdot x^{0.322} \cdot \exp[-(x/48.89)^{1.322}].$$

The mean-square ratio error is 0.47, and the correlation coefficient with experimental points is 0.972.

Fig. 5 shows the experimental data approximation by a three-parameter distribution of the Rosin-Rammler type:

$$P(x) = 6.66 \cdot 10^{-3} \cdot x^{0.4} \cdot \exp[-(x/66.18)^{1.235}].$$

The mean-square ratio error is 0.51, the correlation coefficient is 0.972.

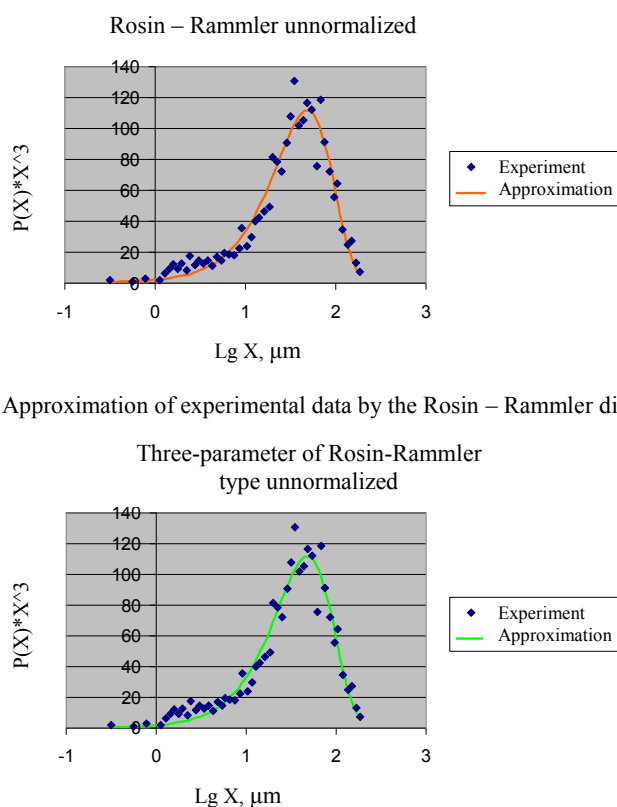


Fig. 4. Approximation of experimental data by the Rosin – Rammler distribution

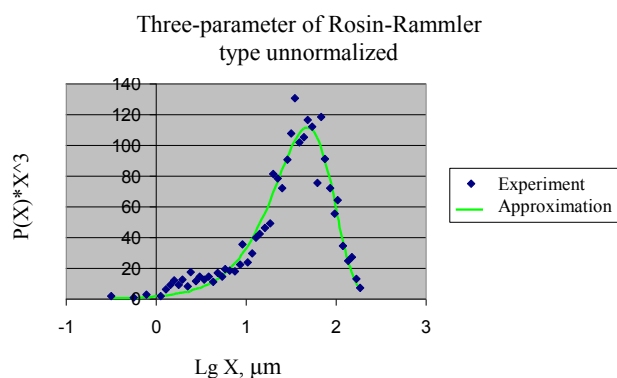


Fig. 5. Approximation of experimental data by three-parameter distribution of the Rosin-Rammler type

It follows from the analysis that for the problems other than cyclone calculations, it is convenient to approximate the experimental data of the authors by a one-parameter monotonically decreasing function:

$P(x) = 1/D \cdot e^{-x/D}$. Fig. 6 shows the approximation of experimental data by the exponential distribution $P(x) = 1/47.13 \cdot e^{-x/47.13}$. The mean-square ratio error is 0.42, the correlation coefficient with experimental points is 0.948.

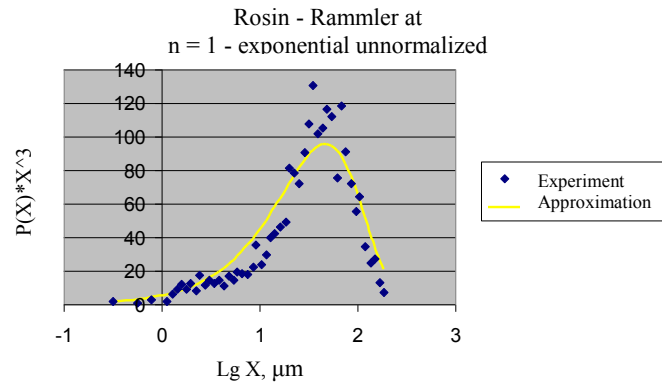


Fig. 6. Approximation of experimental data by exponential distribution

Table 2 shows the integrated indices of dust dispersion calculated on the basis of model distributions in comparison to the evaluated software of the *Fritsch Analysette 22 Compact*. Model distributions are initialized by graphic data.

Table 2

Integrated indices of dust dispersion

Parameter	Mathematical model used to evaluate					Actual value
	Lognormal	Double lognormal	Rosin - Rammler three-parameter	Rosin - Rammler	Exponential	
$D_{43}, \mu\text{m}$	51.7	44.8	44.7	45.2	43.6	43.5
$D_{42}, \mu\text{m}$	41.2	23.0	27.3	28.1	21.4	20.9
$D_{41}, \mu\text{m}$	32.0	9.45	12.2	12.9	8.61	8.18
$D_{40}, \mu\text{m}$	25.0	4.87	5.99	6.32	4.40	4.24
$D_{32}, \mu\text{m}$	32.8	11.8	16.6	17.5	10.3	10.0
$D_{31}, \mu\text{m}$	25.2	4.34	6.4	6.92	3.79	3.55
$D_{30}, \mu\text{m}$	19.6	2.32	3.07	3.28	2.03	1.95
$D_{21}, \mu\text{m}$	19.4	1.59	2.46	2.74	1.39	1.25
$D_{20}, \mu\text{m}$	15.1	1.03	1.32	1.42	0.904	0.858
$D_{10}, \mu\text{m}$	11.8	0.666	0.704	0.738	0.586	0.588
Mode, μm	52.1	45.2	48.9	48.4	43.9	43.4
MSR $\sigma, \mu\text{m}$	35.0	37.2	33.6	33.8	39.9	35.7
Asymmetry	1.49	1.17	1.19	1.20	1.41	1.25
Excess	2.28	1.49	1.46	1.50	1.66	1.66

The data in Fig. 4-6 and Table 2 provide for the comparison of the corresponding results to each other and to the approximation data of the lognormal and double lognormal functions. These results indicate a close approximation quality achieved using the five-parameter double lognormal, three-parameter Rosin-Rammler type, the two-parameter classical Rosin-Rammler type, and the one-parameter exponential model distributions $P(x)$. Meanwhile, the lognormal distribution does not correspond to the experimental data since it does not reflect the presence of a significant numerical fraction of very small particles in dust. At the same time, this distribution is best suited for the practical purpose of the study — optimization of the air purification system.

The approximation by one-parameter monotonically decreasing function $P(x) = 1/D \cdot e^{-x/D}$ demonstrates good agreement with the experiment for small-sized dust fractions, which, due to their representativeness, significantly affect the mean-square ratio approximation error.

Conclusion. The experimental data analysis performed by the authors regarding the size distribution of particles formed under a rail cutting reduces to the following:

1. The *Fritsch Analysette 22 Compact* is not optimal for studying the fractional composition of dust since it does not present measurement data in primary numerical form. The digitization of the graphs provided by this device is the major source of error in the interpretation of the relevant data.

2. For a detailed analysis of the dust particle size distribution based on the available experimental data (available from the authors), the simplest exponential particle size distribution $P(x) = 1/47.13 \cdot e^{-x/47.13}$ is best suited. Based on this distribution, all integrated indices provided by the instrumental measuring complex can be correctly reproduced, along with the graphical data.

3. The tasks of air purification require using a classic lognormal distribution:

$$P(x) = 0.563 \cdot e^{-\frac{1}{2} \left(\frac{\lg x - 1.63}{0.435} \right)^2},$$

whose parameters are calculated by the authors using mathematical programming methods. They made it possible to calculate the important for designing cyclones value $D_{32} = 32.8 \mu\text{m}$, which is three times higher than the numerical value produced by the *Fritsch Analysette 22 Compact*. This means that the application of the numerical values provided by the named device in the cyclone calculation will cause the inability to remove almost all large particles from the working area.

4. Due to the fact that the efficiency of the cyclone is affected not only by the value of D_{32} , but also by the density of the dispersed material consisting of steel and abrasive, a precise analysis is required to ensure the efficiency of air cleaning. Its subject is a separate study on the dispersion of metal and abrasive dust resulting from the operation of a rail-cutting machine.

References

1. Strauss W. *Promyshlennaya ochistka gazov: per. s angl.* [Industrial gas cleaning: transl. from English]. Moscow: Khimiya; 1981. 616 p. (In Russ.)
2. Ziganshin MG, Kolesnik AA, Posokhin VN. *Proektirovanie apparatov pylegazoochistki* [GTS design]. Moscow: Ehkopress - 3M; 1998. 505 p. (In Russ.)
3. Sauter J. Grössenbestimmung von Brennstoffteilchen. In: *Forschungsarbeiten auf dem Gebiete des Ingenieurwesens*. 1926. Heft 279.
4. Sauter J. Untersuchung der von Spritzvergasern gelieferten Zerstäubung. In: *Forschungsarbeiten auf dem Gebiete des Ingenieurwesens*. 1928. Heft 312.
5. Wadell H. Volume, Shape and Roundness of Quartz Particles. *J. Geology*. 1935;43(3):250-280.
6. Adushkin VV, Popel' SI, Shishaeva SI. Analiz melkodispersnoi fraktsii pri razrushenii gornykh porod vzryvom i obrazovanii skal'nykh opolznei [Analysis of the fine fraction under destruction of rocks by explosion and the formation of rock slips]. *Journal of Mining Institute*. 2007;171:32–38. (In Russ.)
7. Hatch J, Choate SP. Statistical description of the size properties of non-uniform particulate substances. *J. Franklin Inst.* 1929;207:369-387.
8. Kaye W, McDaniel JB. Low-Angle Laser Light Scattering – Rayleigh Factors and Depolarization Ratios. *Applied Optics*. 1974;13(8):1934-1937.

9. Bochkareva EA. Sravnitel'nyi analiz programm otsifrovki grafikov [Comparative analysis of the programs of digitizing graphs]. Modern Scientific Researches and Innovations. 2015;11. URL: <http://web.snauka.ru/issues/2015/11/60095> (accessed: 02.02.2020). (In Russ.)
10. Sharapova EhN, Dmitriev VL. Sistema otsifrovki graficheskikh dannykh [System of digitization of graphic data]. Software of Systems in the Industrial and Social Fields. 2011;1–2:166–171. (In Russ.)
11. Grafula — otsifrovka koordinat tochek otskanirovannykh grafikov dlya perenosa ikh v Excel: Matematicheskoe modelirovanie [Grafula - digitization of the coordinates of the points of scanned graphs for transferring them to Excel: Mathematical modeling]. URL : <https://mmodelling.blogspot.com/2012/07/excel.html> (accessed: 02.02.2020). (In Russ.)
12. Minoux M. Mathematical Programming: Theory and Algorithms. New York: John Wiley; 1986. 489 p.

Submitted 22.01.2020

Scheduled in the issue 02.03.2020

About the authors

Azimova, Natal'ya N., senior lecturer of the Life and Environment Protection Sciences Department, Don State Technical University (1, Gagarin sq., Rostov-on-Don, 344000, RF), ORCID: <http://orcid.org/0000-0002-9484-2430>, arkomaazimov@mail.ru

Ladosha, Evgenii N., Head of the Office of Digital Educational Technologies, Don State Technical University (1, Gagarin sq., Rostov-on-Don, 344000, RF), Cand.Sci. (Eng.), associate professor, ORCID: <http://orcid.org/0000-0001-7955-5073>, Ladoscha@mail.ru

Kholodova, Svetlana N., associate professor of the Life and Environment Protection Sciences Department, Don State Technical University (1, Gagarin sq., Rostov-on-Don, 344000, RF), Cand.Sci. (Eng.), associate professor, ORCID: <http://orcid.org/0000-0002-9690-715>, holls9@mail.ru

Tsymbalov, Denis S., senior lecturer of the Electrical Engineering and Electronics Department, Don State Technical University (1, Gagarin sq., Rostov-on-Don, 344000, RF), ORCID: <http://orcid.org/0000-0003-1409-1815>, Den.tsymbalov@mail.ru

Yatsenko, Oleg V., associate professor of the Applied Mathematics Department, Don State Technical University (1, Gagarin sq., Rostov-on-Don, 344000, RF), Cand.Sci. (Phys.-Math.), associate professor, ORCID: <http://orcid.org/0000-0003-2873-6944>, oleg_v_yatcenko@mail.ru

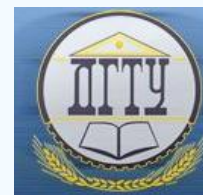
Claimed contributorship

N. N. Azimova: analysis of subject literature, selection of research objective, task setting, planning and organization of the collaboration; experimental studies on dust size distribution by the LALLS method, selection and analysis of model distributions; quantitative assessment of the validity of the models used, their adjustment, analysis of the methodology applicability for objects similar to those studied, as well as the possibility to improve it regarding reliability and versatility; wording of the paper (30%). E. N. Ladosha: data digitization, parametric identification of the models based on graphical experimental distributions using statistical methods and *Excel* spreadsheets (15 %). S. N. Kholodova: examination of the technical experiment results (primary data on the dispersed composition of dust)

and the models used for validity; comparison and analysis of dispersion models regarding qualitative and quantitative compliance with the experimental data; generation of proposals for the development of physical and mathematical analysis methods for high-precision identification of the dust size distribution (15 %). D. S. Tsymbalov: parametric identification of models based on integral indicators of experimental distributions using methods of mathematical programming (optimization) and the MathCAD package (15 %). O. V. Yatsenko: quantitative assessment of the models used validity, their adjustment, analysis of the methodology applicability for objects similar to those studied, the possibility to improve it regarding reliability and versatility; paper text follow-up (25 %).

All authors have read and approved the final manuscript.

MACHINE BUILDING AND MACHINE SCIENCE



UDC 62-192(075.8)

<https://doi.org/10.23947/1992-5980-2020-20-1-79-86>

Numerical modeling and experimental estimates of structural member fatigue characteristics

Yu. P. Man'shin, E. Yu. Man'shina

Don State Technical University (Rostov-on-Don, Russian Federation)



Introduction. In the algorithm for predicting the resource of machine parts, models of external actions, fracture resistance, and temporal development of a particular type of damage to these units interact. The applied issues of the resistance of machine parts to fatigue failure are considered. The scientific research and regulatory materials are adapted to determine the characteristics of endurance to the specifics of structures and materials of the construction-and-road machinery and agricultural machinery. The work objective is to use the analysis of existing methods to develop recommendations for the calculated determination of the endurance parameters of structural members of the agricultural machines.

Materials and Methods. The initial data were scientific studies on the fracture mechanics of the engineering materials and structures, as well as standards for endurance characterization methods. The need to test methods for determining fatigue characteristics to use them in the road construction machinery and agricultural machinery projects follows from the specifics of their designs, operation conditions and industry-specific range of materials. Based on the analysis of existing methods, it is required to develop recommendations for the calculation of the endurance parameters of structural parts of the agricultural machines. For this, the components of the load-bearing systems of the staged design were presented in the form of a set of plates of the corresponding thickness; and the concept of the critical radius of the stress raiser at the welding sites was also used. Numerical methods using mathematical models were applied. The calculation results were verified through comparing them to experimentally determined fatigue characteristics of the members of a combine harvester on a test bench.

Results. Radius critical values of the stress raisers for various types of welds are obtained. The tables of the calculated and experimental endurance limits of the combine bearing components are well correlated and can be used under designing.

Discussion and Conclusions. The theoretical foundations laid down in the study open up great opportunities for applications to the design of various machines. The considered fragment of adaptation of the theoretical approach to the agricultural engineering objects can be used in the design of load-bearing systems in the related fields of engineering.

Keywords: endurance range, fatigue fracture, fatigue crack, weld joint, computational and experimental methods.

For citation: Yu.P. Man'shin, E.Yu. Man'shina. Numerical modeling and experimental estimates of structural member fatigue characteristics. Vestnik of DSTU, 2020, vol. 20, no. 1, pp. 79–86. <https://doi.org/10.23947/1992-5980-2020-20-1-79-86>



Introduction. In the computational and computational-experimental methods for predicting the durability of the load-bearing units of ground-based mobile mass-produced vehicles (automobiles, tractors, road construction, irrigation and drainage, agricultural, military equipment, etc.), it is recommended to take the early formation of a fatigue crack of 0.2 – 0.5mm length under conditions of high-cycle fracture as the key reliability criterion¹. In this case, the initial information on the structural properties is the characteristic of the fatigue curve. Consider the possibility of developing methods for determining the fatigue characteristics of machine parts².

¹ Kogaev VP, Makhutov NA, Gusenkov AP. Raschety detalei mashin i konstruktssii na prochnost' i dolgovechnost': Spravochnik [Strength and durability design of machine parts and structures: Reference Guide]. Moscow: Mashinostroenie; 1985. 224 p.

² RP 206–86. Raschety i ispytaniya na prochnost'. Metody opredeleniya kharakteristik soprotivleniya ustalosti detalei mashin s uchedom rasseyaniya: Metodicheskie rekomendatsii [Calculations and strength tests. Methods for determining of fatigue resistance characteristics of machine parts considering scattering: Recommended practice] Moscow: VNIImash; 1986. 50 p..

Structural parts are represented by plates working in push-pull. The stress concentration is caused by a sharp change in the thickness of the plates with a certain radius of curvature ρ at the junctions, up to a sharp cut. The stress concentration associated with the formation of a weld on the plates under study is considered the subject of independent research and is taken into account as a result.

The correct parameter selection to fatigue damage of machine parts and load-bearing systems is the basis for calculating resources and predicting reliability [1]. Consider the methodology and the calculation results of the characteristics of the fatigue resistance of the elements (zones) of the loadbearing structure based on the model shown in Fig. 1.

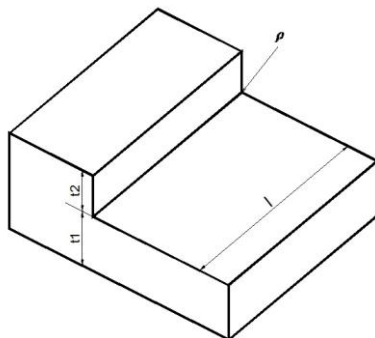


Fig. 1. Scheme for the calculated determination of fatigue characteristics

The model is a fragment of a welded joint of thick-walled units. It is typical of many self-propelled and trailed vehicles of land transport, for example, a frame system of self-propelled combines. The initial data for the calculation are given in Table 1.

Table 1

Initial data for determining fatigue characteristics of joint assemblies shown in Fig. 1

Option	1	2	3	4
Steel grade	09G2	09G2	20	20
Working conditions		corrosion		corrosion
$\bar{\sigma}_b$, MPa	460	460	420	420
$\bar{\sigma}_T$, MPa	300	300	250	250
$\bar{\sigma}_{-1}$, MPa	232	232	213	213
$V_{\sigma-1}$	0.069	0.069	0.062	0.062
$K_{F\sigma}$	0.85	0.55	0.85	0.58
K_V	0.50	0.50	0.50	0.50
K_A	0.95	0.95	0.95	0.95
$t_1 = t_2$, mm	10	10	4	4
ρ , mm	0.1–2	0.1–2	0.1–2	0.1–2
$\bar{\rho}$, mm	0.5	0.5	0.5	0.5
V_ρ	0.36	0.36	0.36	0.36
l , mm	200	200	80	80

The median endurance limit is calculated by the expression^{1,2}:

¹ Kogaev VP, Makhutov NA, Gusenkov AP. Op. cit. P. 112–224.

² GOST 25.504–82. Raschety i ispytaniya na prochnost'. Metody rascheta kharakteristik soprotivleniya ustalosti [GOST 25.504–82. Strength calculation and testing. Methods of fatigue strength behaviour calculation]. Available at: <http://docs.cntd.ru/document/1200012858> (accessed: 11.12.2019).

$$\bar{\sigma}_{-1g} = \frac{\bar{\sigma}_{-1}}{K},$$

where $\bar{\sigma}_{-1}$ is the median endurance limit determined on smooth laboratory samples of standard diameter $d_0 = 7.5$ mm; K is the endurance limit reduction coefficient:

$$K = \left(\frac{K_{\sigma}}{K_{d\sigma}} + \frac{1}{K_{F\sigma}} - 1 \right) \frac{1}{K_V K_A},$$

where $K_{\sigma} = \frac{\sigma_{-1d}}{\sigma_{-1g}}$ is the effective stress concentration factor; $K_{d\sigma}$ is the full-size influence coefficient; $K_{F\sigma}$ is the surface condition influence coefficient; K_V is the influence coefficient of surface softening from metallurgical welding processes; K_A is the anisotropy factor of material properties.

For the example considered, we will use the recommendations [2]. We accept $K_V = 0.5$, For normal operating conditions, we accept $K_{F\sigma} = 0.85$. During operation or storage of the machine with the ingress of freshwater, moisture and the formation of corrosion, we accept for steel 09G2 on GOST 5521-93 $K_{F\sigma} = 0.55$, for steel 20 on GOST 2591-2006 $K_{F\sigma} = 0.58$. The initial data for calculating the endurance of the samples and their variation coefficients $V_{\sigma-1}$ are given in Table 1.

To determine the characteristic relations of parameters, the technique¹ recommends the formula:

$$\frac{K_{\sigma}}{K_{d\sigma}} = \frac{\alpha_{\sigma}}{0.5\zeta},$$

where α_{σ} is a theoretical coefficient that determines the degree of increase in stress in the zone of their concentration, it is calculated as per the local stress-strain state using finite element models; ζ is a distribution parameter.

The similarity equation for fatigue failure is close in form to the Weibull distribution. For plate elements, it has the form²:

$$J = -2.3 \lg(1-p) = \frac{t_1 + t_2}{\bar{G}_1} \left(\frac{u}{z} \right)^{\beta} \frac{1}{(\beta+1)(\beta+2)} \cdot \frac{(\zeta-1)^{\beta+2}}{\zeta^2}, \quad (1)$$

where \bar{G}_1 is the gradient of the first principal stress, it is determined by the formula:

$$\bar{G}_1 = 23/\rho; \left(\frac{u}{z} \right)^{\beta} = 0.0152(\beta+1),$$

here, V_{σ} is sensitivity of metal to the stress factor:

$$V_{\sigma} = 0.2 - 0.0001\sigma_b;$$

$$\beta = \frac{1}{V_{\sigma}} - 0.64.$$

We obtain the median value of the parameter $\bar{\zeta}$ with the probability of destruction $P = 0.5$ from the solution to the similarity equation (1). For the parts in question, the values of $\bar{\zeta}$ are given in Table 2.

¹ RP 206-86. Op. cit. 1986. 50 p.

² RP 206-86. Op. cit. 1986. 50 p.

Table 2

Design parameters of the structural fatigue resistance (Fig. 1)

Option	1	2	3	4
ρ_{sp} , mm	0.5	0.5	0.5	0.5
$\bar{\alpha}_\sigma$	2.2	2.2	1.7	1.7
$V_{\alpha\sigma}$	0.19	0.19	0.22	0.22
$\bar{\zeta}$	2.12	2.12	2.51	2.51
V_σ	0.154	0.154	0.158	0.158
β	5.85	5.58	5.69	5.69
\bar{G}_1 , 1/mm	4.6	4.6	4.6	4.6
$K_\sigma / K_{d\sigma}$	2.07	2.07	1.35	1.35
K	4.74	6.09	3.22	4.57
θ	0.49	0.49	0.20	0.20
$V_{\sigma max}$	0.05	0.05	0.06	0.06
$V_{\sigma-1g}$	0.21	0.21	0.24	0.24
ΔK_{th} , MPa	9.53	9.53	9.53	9.53

The average stress gradient in the zone of radius ρ , which is the place of concentration, is determined for the condition:

$$\rho = (\rho_{sp}) \approx 0.5 - 0.0004(\sigma_b - 500).$$

For the steels under consideration, the critical value of the radius of curvature in the connection of parts $\rho_{sp} = 0.5$ mm was established. It corresponds to the formation of fatigue cracks not running further¹. By this criterion, the value α_σ was selected. Fig. 2 shows the dependences of the theoretical stress concentration coefficient on the radius of curvature for various geometric design parameters. The calculated median endurance limits for the parts under consideration are presented in Table 3.

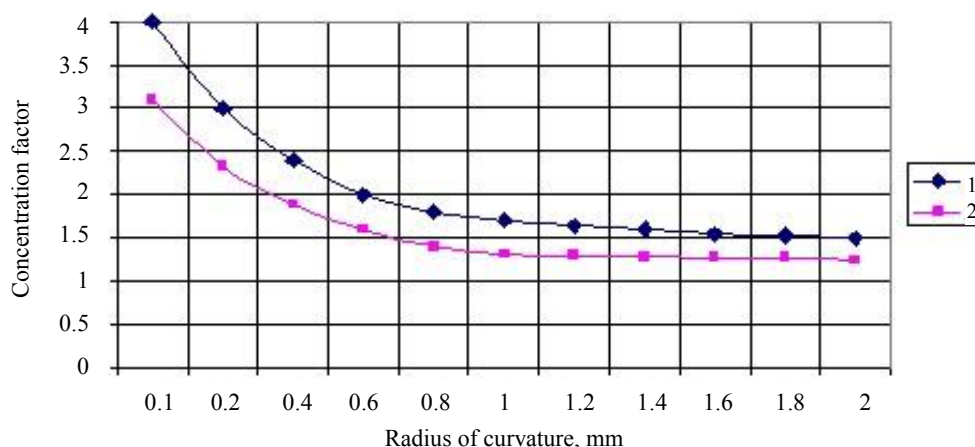


Fig. 2. Dependences of theoretical stress concentration coefficient on radius of curvature: 1 is $t_1 = t_2 = 10$ mm; 2 is $t_1 = t_2 = 4$ mm

¹ Kogaev VP, Makhutov NA, Gusenkov AP. Op. cit. P. 112-224.

Table 3

Design parameters to define joint assembly characteristics based on the initial data of Table 1 shown in Fig. 1

Option	1	2	3	4
$\bar{\sigma} - 1g$	49	38	66	46
$(\sigma - 1g)P = 0.05$, MPa	32	25	40	28
$(\sigma - 1g)P = 0.95$, MPa	66	51	92	64
m	4.54	3.52	6.36	4.48
$N_{\sigma}, 10^6 \text{ cycles}$	2.9	2.6	2.9	2.7
$\psi\sigma$	0.11	0.11	0.10	0.10
$\sigma - 1_{gkp}$, MPa	34	-	-	-

The variation coefficient of the fatigue limit is determined from the expression:

$$V_{\sigma-1g} = \sqrt{V_{\sigma_{\max}}^2 + V_{\sigma-1}^2 + V_{\alpha_{\sigma}}^2}, \quad (2)$$

where $V_{\sigma_{\max}}$ is the variation coefficient of maximum stresses in the concentration zone; $V_{\sigma-1}$ is the variation coefficient of the fatigue limit of the sample; $V_{\alpha_{\sigma}}$ is the variation coefficient of the theoretical coefficient in the concentration zone.

The variation coefficient $V_{\sigma-1}$ is set¹ and presented in Table 1 as source data. The variation coefficient $V_{\sigma_{\max}}$ is determined from the expression²:

$$V_{\sigma_{\max}} = \frac{0.1}{1 + \theta^{1/\sigma}},$$

where θ is the relative fatigue failure similarity criterion:

$$\theta = \frac{1}{88.3 \bar{G}_1}.$$

The design values of the parameters are given in Table. 2. The coefficient of variation $V_{\alpha_{\sigma}}$ is determined by the recommendations³:

$$V_{\alpha_{\sigma}} = \left| \frac{\partial \alpha_{\sigma}}{\partial \rho} \right|_{\rho=\bar{\rho}} \cdot \frac{\bar{\rho}}{\alpha_{\sigma}} V_{\rho}.$$

To find the derivative module, a linear approximation of the function $\alpha_{\sigma} = \varphi(\rho/t)$, is carried out, which is shown in Fig. 2 in the vicinity of the average value of the parameter $\bar{\rho}$. The calculation results are given in Table. 2. It also contains the results of calculating the variation coefficient of the fatigue limit from the expression (2).

We determine the values of the fatigue limit under the assumption of its normal distribution with a probability of destruction of 5% and 95% from the formula:

$$(\sigma_{-1g})_P = \bar{\sigma}_{-1g} (1 + Z_P V_{\sigma-1g}),$$

where Z_P is the fractile of the normal distribution. Table 3 shows the fatigue limit values with the indicated fracture probabilities.

Next, we present the dependences for calculating the fatigue curve parameters:

- indicator of the slope of the left branch of the fatigue curve⁴:

$$m = \left(5 + \frac{\sigma_b}{80} \right) / K_{\sigma};$$

- fatigue curve point abscissa:

$$N_{\sigma} = 10^5 \bar{\sigma}_{-1g}^{(0.997-0.003m)};$$

- coefficient of sensitivity to cycle asymmetry⁵:

$$\psi_{\sigma} = 0.02 + 2 \cdot 10^{-4} \sigma_b.$$

¹ Kogaev VP, Makhutov NA, Gusenkov AP. Op. cit. P. 112-224.

² RP 206-86. Op. cit. 1986. 50 p.

³ RP 206-86. Op. cit. 1986. 50 p.

⁴ RP 206-86. Op. cit. 1986. 50 p.

⁵ Kogaev VP, Makhutov NA, Gusenkov AP. Op. cit. P. 112-224.

The calculation results of these characteristics for the components under consideration are given in Table 3.

The studies have established¹, that in the zones of stress concentration, there are critical radii of curvature in the range of values $\rho_{kp} = 0.1\text{--}0.6$ mm [1]. At $\rho < \rho_{kp}$, there are other patterns of similarity of fatigue failure compared to the area $\rho > \rho_{kp}$. In this case, a crack-like ultimately sharp notch is considered, which is characteristic of the weld zones of the joinable units in various engineering industries [3, 4]. Two fatigue limits are recommended² to determine:

1. Fatigue limit σ_{-1g} at $\rho > \rho_{kp}$. It is determined by the criteria for the appearance of the first microscopic fatigue cracks and depends on the radius of curvature.
2. Fatigue limit of final fracture σ_{-1gkp} at $\rho < \rho_{kp}$. It does not depend on the radius of notch curvature and is determined from the formula:

$$\sigma_{-1gkp} = \frac{11,5\Delta K_{th}}{\sqrt{t + \rho_{kp}}},$$

where ΔK_{th} is the fatigue crack growth threshold; t is the step depth in the zone of the voltage concentrator.

The threshold for the development of fatigue cracks for mild steels, considering the asymmetry coefficient, can approximately be determined from the formula³:

$$\Delta K_{th} \approx 6,74\sqrt{1-R}. \quad (3)$$

The parameter ΔK_{th} for the units under consideration is indicated in Table 2 at $R = 1$. The values σ_{-1gkp} calculated from the expression (3) are given in Table 3.

To assess the appropriateness of calculating the fatigue of structural elements presented in the form of plates with different transition radii in the connection zones up to an ultimately sharp notch, bench tests of field samples were carried out. The test results are presented in Table 4.

Table 4

Experimental characteristics of fatigue resistance of harvesting machine metal structures

Weld zone	m			$(\sigma_{-1g}), \text{MPa}$			(σ_{-1g}) P = 0.05 MPa		(σ_{-1g}) P = 0.95 MPa		$V_{\sigma-1g}$	$N_{\sigma} \cdot 10^6$ cycles
	min	mean	max	min	mean	max	by mean	by min	by mean	by max		
flange and drive axle housing	3.2	3.7	4.3	31	37	43	4	4	70	81	0.54	3.7
gearbox bracket and drive axle housing	3.1	3.9	4.7	31	39	47	24	19	54	65	0.23	3.6
mounting plate and drive axle housing	3.5	4.1	4.8	33	38	43	21	18	55	62	0.27	3.9
frame racks	4.2	4.9	5.6	38	45	52	35	29	55	64	0.14	4.1

For bench testing, the highest accuracy group was selected with a relative error $0.1 \leq \varepsilon \leq 0.2$, confidence probability $\beta = 0.8$. The number of tested structures was in the range of 11-14 units.

¹ Kogaev VP, Makhutov NA, Gusenkov AP. Op. cit. P. 112-224.

² RP 206–86. Op. cit. 1986. 50 p.

³ RP 206–86. Op. cit. 1986. 50 p.

The data of Table 4 show large scatter of empirical estimates. Even if we exclude the weld zone of the flange and wheel axle beam from consideration, whose spread of values is caused by the instability of the process, in a given confidence interval, the value σ_{-1g} differs by 1.8–2.9 times.

Conclusion. A comparison of the calculated (Table 3) and experimental (Table 4) characteristics of fatigue resistance in the zones of welded joints shows their good compossibility. The confidence intervals of the experimental values overlap similar intervals of the calculated values for the areas of the wheel drive axle. The average values for normal operating conditions differ by 1.3 times, and coincide under corrosion. For frame metal structures, the calculated values under normal conditions differ 1.5 times, and under corrosion conditions, they practically coincide. Good agreement with real values is shown by values σ_{-1gxp} calculated by the threshold of development of fatigue cracks.

The materials presented provide for the conclusion that there is sufficient life reliability of the calculated characteristics of fatigue resistance based on the proposed method at the forecasting stage. The correct characteristics of fatigue resistance with a known or obtained from a field experiment distribution can serve as the foundation for calculating the design life with the required probability of failure-free operation resulting from the technical specifications for the corresponding machine [5].

Thus, through analyzing the existing methods, recommendations have been developed on the calculated determination of the endurance parameters of structural elements of agricultural machines. Under the engineering change of a project or a product prototype up to standard durability through structural and technological techniques, the characteristics of fatigue resistance are used in methods of approximate and functional resource estimates [6, 7].

References

1. Spichenkov VV, Shostenko AB. Sovremennye metody raschetnoi otsenki silovykh konstruksii [Modern methods of design assessment of power structures]. In: Development of design and research of processes of agricultural machines: RIATM coll. of papers. Rostov-on-Don; 1993. P. 69–75. (In Russ.)
2. Keshe G. Korroziya metallov. Fiziko-khimicheskie printsipy i aktual'nye problemy [Corrosion of metals. Physicochemical principles and current problems]. Moscow: Metallurgiya; 1984. 400 p. (In Russ.)
3. Efremov LV. Praktika inzhener'nogo analiza nadezhnosti sudovoi tekhniki [Practice of engineering analysis of ship equipment reliability]. Leningrad: Sudostroenie; 1980. 175 p. (In Russ.)
4. Lukinskii EI, Zaitsev EI. Prognozirovaniye nadezhnosti avtomobilei [Car reliability prediction]. Leningrad: Politehnika; 1991. 222 p. (In Russ.)
5. Man'shin YuP, Man'shina EYu. Voprosy nadezhnosti detalei pri proektirovanii mekhanicheskikh sistem [Problems of parts reliability in the design of mechanical system]. Vestnik MSTU (Series Machine Building). 2019;5:56–73. (In Russ.)
6. Man'shin YuP, Man'shina EYu. Priblizhennaya otsenka resursa detali, obespechivayushchaya ee trebuemyi resurs s zadannoi veroyatnost'yu bezotkaznoi raboty [Approximate assessment of part life, assuring its required life with specified probability of no-failure operation]. Vestnik Mashinostroeniya. 2017;12:20–24. (In Russ.)
7. Man'shin YuP, Man'shina EYu. Estimating the Life of a Machine Part. Russian Engineering Research. 2018;38(3):157-162.

Submitted 17.01.2020

Scheduled in the issue 28.02.2020

About the authors

Man'shin, Yurii P., associate professor of the Machine Design Principles Department, Don State Technical University (1, Gagarin sq., Rostov-on-Don, 344000, RF), Cand.Sci. (Eng.), associate professor, ORCID: <http://orcid.org/0000-0002-2246-2965>, manshin@mail.ru

Man'shina, Elena Yu., senior lecturer of the Machine Design Principles Department, Don State Technical University (1, Gagarin sq., Rostov-on-Don, 344000, RF), ORCID: <http://orcid.org/0000-0002-3027-1309> elemans@mail.ru

Claimed contributorship

E.Yu. Man'shina: formulation of the basic concept, objective and task of the study; computational analysis; text preparation; formulation of conclusions. Yu.P. Man'shin: academic advising, analysis of the research results, the text revision, correction of the conclusions.

All authors have read and approved the final manuscript.

MACHINE BUILDING AND MACHINE SCIENCE



UDC 621.785: 669.14.018.29

<https://doi.org/10.23947/1992-5980-2020-20-1-87-92>

Adaptation of structures of steel laser hardening zones to friction conditions

A. V. Brover

Don State Technical University (Rostov-on-Don, Russian Federation)



Introduction. The structural state of the surface layers of engineering products manufactured through laser processing under various irradiation modes is considered. Structures with the highest possible stability with respect to external action under friction conditions, or with the possibility of optimal adjustment and additional hardening during operation by the formation of secondary structures, were implemented. Under the operating conditions, under the impact of mechanical and thermal pulses, an express rearrangement of one structure to another occurs, which is stable at a higher level of load-speed conditions. Thus, the phenomenon of structural-energy adaptability is realized. The resulting adaptable structures most efficiently dissipate the energy introduced into the tribosystem, and minimize the wear of friction pairs.

Materials and Methods. We studied samples of P6M5 steel using the following equipment:

- Kvant-16 processing station with a power density of 100 MW/m² for pulsed laser irradiation of samples;
- Neophot-21 optical microscope for metal physical studies;
- DRON-0.5 diffractometer for phase composition identification.

Results. It is established that the material of the samples after laser treatment is able to efficiently dissipate the energy supplied during friction through its transformations at various structural levels. As a result, it becomes possible to control the surface strength and wear resistance of materials using the concept of structural adaptability of friction pairs, which extends their range of performance. Wear resistance of the irradiated steels is determined by both their initial hardness and the work-hardenability during friction. It is established that the thermal-strength loading of the steel surface irradiated layers during friction destabilizes austenite to the $\gamma \rightarrow \alpha$ transformation, i.e., it contributes to its transformation into deformation martensite.

Discussion and Conclusions. In relation to the specific loading conditions, it is required to regulate the amount and degree of stability of the residual austenite in laser-hardened steels and alloys, which provides the necessary operational properties.

Keywords: laser irradiation, machine building materials, wear resistance, structural adjustability, surface strength

For citation: A.V. Brover. Adaptation of structures of steel laser hardening zones to friction conditions. Vestnik of DSTU, 2020, vol. 20, no. 1, pp. 87–92. <https://doi.org/10.23947/1992-5980-2020-20-1-87-92>



Introduction. To increase the efficiency of hardening technologies including laser processing, it is necessary to determine the possibilities of targeted use of internal reserves of structural adaptability of products for various functional areas from steel and alloys under operating conditions [1–8]. It is required to analyze features of the structure-energy state of laser-irradiated materials in friction pairs and determine major directions for increasing the wear resistance of tribosystems.

Under laser processing, several ways of transforming the structure were used to goal-oriented changes in the properties of materials [9–12]:

- increasing the structure dispersion under local plastic deformation as a result of dynamic polygonization in austenite, the formation of microdomains (fragments) of high density dislocations inherited under accelerated cooling, and as a result of phase hardening during polymorphic transformation;
- formation of nanoscale extractions under the impact of plastic deformation under thermal exposure;
- development of deformation in irradiated zones of martensite under external temperature-force loading.

It should be taken into account that structural transformation, on the one hand, is a mechanism of strain hardening determined by an increase in the martensite volume, and, on the other hand, causes relaxation of microstresses and additional development of plastic deformation. These two factors act simultaneously and are competing [13–15]. In the case of the predominance of the first factor, high strength with satisfactory ductility is provided in steels. If the second factor dominates, the steel ductility increases significantly while maintaining a sufficient level of tensile strength.

With an optimal combination of factors, martensitic transformation under loading provides the best complex of mechanical properties of the material [16, 17].

Research Objective. Problems of designing adaptable alloy structures with specified operational characteristics using laser irradiation under optimal conditions were considered. The following ways were used to dissipate the energy pumped through laser processing and during the subsequent temperature-force tribological action:

- transformation of part of the energy into heat;
- dissipation due to the motion of defects in the crystal structure and plastic deformation;
- dissipation under structural-phase transformations at different scale levels.

The last structural factor is crucial for improving the operational properties of products if the structures formed under laser exposure are adaptable to operating conditions [18–19]. Adaptable martensitic-austenitic structures with a predetermined ratio of components that are purposefully formed under laser processing should efficiently dissipate energy in the friction zones due to internal transformations, especially when peak loads are reached. This is possible under laser irradiation under optimal conditions and is a prerequisite for increasing the reliability and durability of products.

The study objective was to obtain scientific knowledge on the possibility of implementation of structures in the laser processing zones of steels and alloys that adapt to temperature-force loading under friction and thereby increase the wear resistance of products.

Materials and Methods. Metal physical studies of samples from P6M5 instrument steel were carried out using a *Neophot-21* optical microscope, a DRON-0.5 diffractometer, and a PMT-3 durometer. Laser irradiation was carried out on a Kvant-16 pulsed-action facility with a radiation power density of 80–150 MW/m². Wear tests were carried out on the MI-1M installation according to the “disk — block” scheme at a load of 500 N with a linear sliding speed of 190 m/min. Samples in the form of disks went through a full cycle of volumetric heat treatment — they were quenched and triple-tempered. Some disks were irradiated along a side surface 10 mm wide. Inserts made of steel ShKh15 having hardness HB 130–180 served as counterfaces. Disk wear before and after laser irradiation was determined by weight loss through periodical weighing on an analytical balance with an accuracy of 10⁻⁴ g.

Research Results. Metallographic and durometric analyses of hardened samples have shown that after laser treatment, a hardened layer with a depth of 80–120 μm is formed on the surface. Fig. 1 shows the wear test results that demonstrate a distinct advantage of steels after surface laser treatment. Moreover, due to the running-in of friction pairs and structural changes on contacting surfaces with an increase in test time, the advantage increases by 13 times.

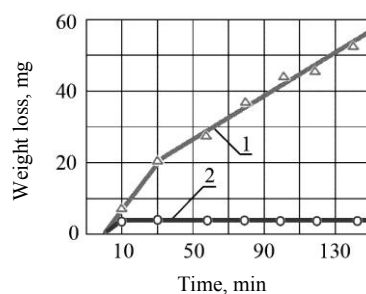


Fig. 1. Wear curves of samples from R6M5 steel after quenching at 1280°C and triple tempering (1), laser quenching (2)

Consider the features of structural and phase transformations realized in the surface layers of laser-hardened samples under friction and eventually causing an increase in the wear resistance of the material. X-ray diffraction studies of laser-irradiated samples of P6M5 steel were carried out before and after wear tests, for 15 minutes and 150 minutes. The results are presented in Fig. 2 in the form of fragments of X-ray patterns taken from the surfaces before and after friction.

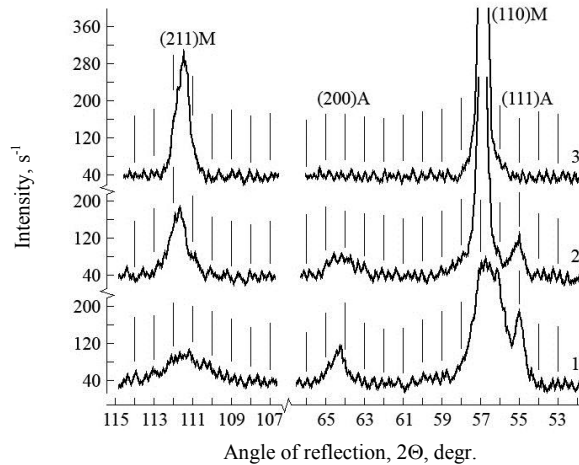


Fig. 2. Fragments of X-ray diagrams of R6M5 steel: 1 is after laser quenching; 2 is after laser quenching and wear tests for 15 min; 3 is after laser quenching and wear tests for 150 min.

Prior to wear tests, the surface layers of steel after laser hardening have a two-phase austenitic-martensitic structure (Fig. 2, curve 1). Moreover, the intensity of austenite reflections, and, consequently, its amount in the structure, decreases significantly with increasing the test time (Fig. 2, curves 2, 3). This is explained by the fact that the considered conditions of temperature-force loading destabilize austenite to martensitic transformation due to the precipitation of doped carbides from it. As a result of the γ -phase depletion by carbon, it acquires the ability to transform into martensite deformations with the properties similar to cooling martensite. This provides for technological and structural plasticity of the steel surface layers (micro TRIP effect).

It should be noted that martensite obtained through laser hardening, under the effect of temperatures and forces in the friction zones, also transforms due to strain hardening during wear (Fig. 2, curves 2, 3). Confirmation is the increase in the width of the martensite reflections in X-ray diffraction patterns caused by an increase in the density of dislocations and the refinement of the blocks of its fine structure. As a result, the hardness and performance of laser-irradiated steel is further enhanced. Thus, under friction, the structure of the irradiated surface layers adapts to the loading conditions in the friction pair, which leads to an increase in the hardness and wear resistance of steels after laser treatment.

Through changing the irradiation regime, a different amount of martensite and austenite was achieved in laser-hardened zones, and a connection between the development of phase transformations in the process of self-organization of structures and the properties of steels was established. The results of metal physical studies have shown that laser processing of P6M5 steel should be carried out with a power density in the range of 80–120 MW/m². In this case, the maximum possible hardening of steel is achieved at the level of 10–11.5 GPa, which causes an increase in the wear resistance of irradiated surfaces. An additional factor in increasing the wear resistance of steel under friction without lubrication is the preservation of insoluble carbides of tungsten, vanadium, chromium up to 30% in the laser processing zones.

It is established that under the action of high temperatures and pressures in the contact zones of the laser-irradiated metal, additional precipitation of carbides of the strengthening action occurs [20, 21]. This is facilitated by the high density of dislocations in steels both immediately after laser processing and additionally arising during friction.

Fig. 3 *a* shows the microstructure of irradiated P6M5 steel after the wear tests. A reference line is plotted; along it, a histogram of the surface profile height distribution, shown in Fig. 3 *b*, was determined. The line crosses the dispersed precipitated carbides. From the histogram, it follows that carbides have sizes in the range of 2–10 nm.

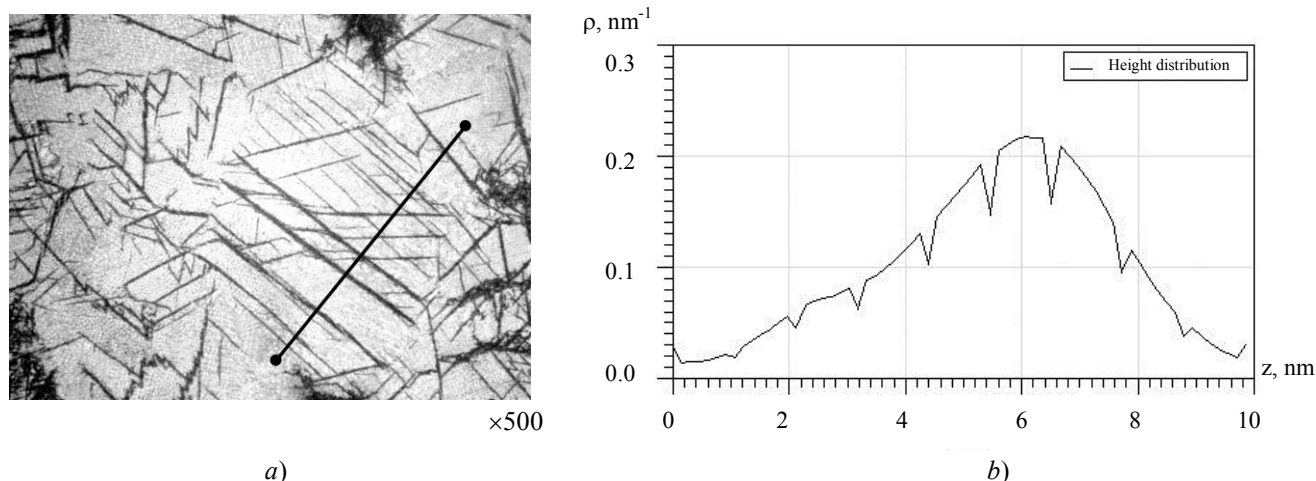


Fig. 3. Structure of laser-quenched R6M5 steel: *a*) optical microscopy results; *b*) histogram of surface profile height distribution

The precipitation of the dispersed carbide phase oriented along the sliding lines as a result of friction tests is noteworthy. The texture of dispersed precipitates thus formed causes a decrease in friction losses under the maintenance of products for various functional areas after laser treatment.

Discussion and Conclusions. We note the features of two-phase austenitic-martensitic zones of irradiated steels for different types of wear. The results considered in this paper were obtained under friction without lubrication. Under the abrasive wear, non-uniform structures of laser hardening have lower wear resistance compared to fully martensitic structures, which is explained by intensive wear of the austenitic structural component. Under the conditions of adhesive wear, as well as during the lubricated friction, two-phase structures of laser hardening zones are characterized by high wear resistance. In this case, the martensite sections play the role of a strong frame, and the wear-out austenite sections form microcavities on the working surface that hold the lubricant and improve the friction conditions.

Thus, to increase the wear resistance, it is required to design a structure adaptable to operating conditions with a certain ratio of the volumes of martensite, austenite and carbides by selecting the optimal laser processing mode. There are promising options for laser modification of the surface layers of steels with carbides or nitrides of doping elements, or laser quenching and subsequent tempering, the temperature of which depends on the steel grade.

Conclusions:

1. The possibilities of the purposeful use of internal reserves of structural adaptability of steels and alloys after laser surface treatment to improve their wear resistance under friction are determined.
2. The analysis of structural-phase transformations in the laser-irradiated zones of steels under temperature-force loading of friction pairs has been performed. It is shown that the transformation of residual laser hardened austenite into strain martensite, strain hardening of martensite obtained by laser heat treatment, and the multiple precipitations of dispersed reinforcing carbides in the irradiated zones of steels, contribute to increasing the wear resistance of materials.
3. Through changing the modes of laser treatment of steels, it is possible to form adaptable martensitic-austenitic structures in the irradiated zones with a given ratio of components that efficiently dissipate energy in the friction zones due to structural transformations at different levels.

References

1. Ginberg AM, Ivanov AF. Iznosostoikie i antifriktsionnye pokrytiya [Wear-resistant and anti-friction coatings]. Moscow: Mashinostroenie; 1982. 42 p. (In Russ.)
2. Kravchenko GN, Alekseev VV. Vliyanie plasticheskogo deformirovaniya drob'yu i tsiklicheskogo nagruzheniya na svoistva poverkhnostnogo sloya stali 30KHGSN2A [The plastic deformation effect on the surface layer

properties of steel 30KhGSN2A by shot and cyclic loading]. *Metal Science and Heat Treatment*. 1986;9:23–25. (In Russ.)

3. Grigor'yants AG, Safonov AN. *Metody poverkhnostnoi lazernoi obrabotki* [Surface laser methods]. Moscow: Vysshaya shkola; 1987. 191 p. (In Russ.)

4. McClintock F, Argon A. *Deformatsiya i razrushenie materialov* [Deformation and fracture of the materials]. Moscow: Mir; 1970. 443 p. (In Russ.)

5. Panin VE, Likhachev VA, Grinyaev YuV. *Strukturnye urovni deformatsii tverdykh tel* [Structural levels of deformation of solids]. Novosibirsk: Nauka; 1985. 226 p. (In Russ.)

6. Lyubarskii LM, Palatnik LS. *Metallofizika treniya* [Metallophysics of friction]. Moscow: Metallurgiya; 1976. 175 p. (In Russ.)

7. Rybakova LM, Kuksenova LI. *Metallovedenie v nauke o trenii i iznashivani* [Metal Science in the Science of Friction and Wear]. *Metal Science and Heat Treatment*. 1985;5:16–23. (In Russ.)

8. Marchenko EA. *O prirode razrusheniya poverkhnosti metallov pri trenii* [On the nature of metal surface deterioration under friction]. Moscow: Nauka; 1979. 17 p. (In Russ.)

9. Gorbach VG, Sidoruk IV, Izmailov EA. *Martensitno-austenitnye stali kak ehffektivnyi instrumental'nyi i konstruksionnyi material* [Martensitic-austenitic steels as an effective tool and structural material]. *Metal Science and Heat Treatment*. 1988;8:9–12. (In Russ.)

10. Brover AV. *Stpuktupnye osobennosti pptsessa povepkhnostnogo uppochneniya stali kontsentpipovanny-mi potokami ehnergii* [Structural features of the surface hardening process of steel by concentrated energy flows]. *Metallovedenie*. 2005;9:18–23. (In Russ.)

11. Brover AV. *Kompleks mekhanizmov uprochneniya metallicheskich materialov pri impul'snoi lazernoi obrabotke* [Set of mechanisms for hardening metal materials under pulsed laser processing]. *Perspektivnye materialy*. 2008;1:63–69. (In Russ.)

12. Brover AV. *Ehffekty strukturno-ehnergeticheskoi prisposablivaemosti poverkhnostno termouprochnennoi stali pri trenii* [Effects of structural-power adaptation of surface thermal strengthened steel at friction]. *Strengthening Technologies and Coatings*. 2006;5:43–47. (In Russ.)

13. Tushinskii LI. *Teoriya i tekhnologiya uprochneniya metallicheskich splavov* [Theory and technology of metal alloy hardening]. Novosibirsk: Nauka; 1990. 305 p. (In Russ.)

14. Serebryakov VG, Ehstrin EhI. *Vliyanie deformatsii na mekhanicheskie svoistva dvukhfaznoi austenitno-martensitnoi stali* [The deformation impact on the mechanical properties of two-phase austenitic-martensitic steel]. *The Physics of Metals and Metallography*. 1992;2:130–133. (In Russ.)

15. Malinov LS, Cheilyakh AP. *Vliyanie metastabil'nogo ostatochnogo austenita na mekhanicheskie svoistva stali Kh12M* [The effect of metastable residual austenite on the mechanical properties of X12M steel]. *Metal Science and Heat Treatment*. 1988;8:12–15. (In Russ.)

16. Bernshtein ML, Kaputkina LM, Prokoshkin SD. *Struktura i substruktura austenita, obrazuyushchegosya pri nagreve zakalennykh i termomekhanicheski uprochnennykh staley* [The structure and substructure of austenite formed during heating of hardened and TMT steels]. *The Physics of Metals and Metallography*. 1982;54(6):150–157. (In Russ.)

17. Bushe VV, Kopyt'ko VV. *Sovmestimost' trushchikhsvy poverkhnostei* [Friction Compatibility]. Moscow: Nauka; 1981. 127 p. (In Russ.)

18. Belyi AV, Karpenko GD, Myshkin NK. *Struktura i metody formirovaniya iznosostoikikh poverkhnostnykh sloev* [Structure and methods of forming wear-resistant surface layers]. Moscow: Mashinostroenie; 1991. 207 p. (In Russ.)

19. Bekrenev AN, Bezuglov AYU. *Samoorganizatsiya metallichesko*i sistemy pri ee nekvazistatsionarnoi relaksatsii [A metallic system self-alignment during nonquasi-equilibrium relaxation]. *Fizika i khimiya obrabotki materialov*. 1995;2:122–127. (In Russ.)

20. Portnoi KI, Babich BN. Dispersnouprouchnennye materialy [Dispersion-strengthened materials]. Moscow: Metallurgiya; 1974. 199 p. (In Russ.)

21. Popov VM, Farber VM, Bronfin BM. Vliyanie deformatsii na vydelenie karbida $M_{23}S_6$ v austenitnoi stali [The deformation effect on the precipitation of $M_{23}C_6$ carbide in austenitic steel]. The Physics of Metals and Metallography. 1974;38(2):337–343. (In Russ.)

Submitted 13.01.2020

Scheduled in the issue 21.02.2020

About the author

Brover, Andrei V., associate professor of the Physical and Applied Materials Science Department, Don State Technical University (1, Gagarin sq., Rostov-on-Don, 344000, RF), Cand.Sci. (Eng.), associate professor, ORCID: <https://orcid.org/0000-0002-3999-3703>, brover@mail.ru

The author has read and approved the final manuscript.

INFORMATION TECHNOLOGY, COMPUTER SCIENCE, AND MANAGEMENT



UDC 621.893

<https://doi.org/10.23947/1992-5980-2020-20-1-93-99>

Automatic license-plate recognition

A. V. Poltavskii¹, T. G. Yurushkina², M. V. Yurushkin³

^{1,3} Southern Federal University (Rostov-on-Don, Russian Federation)

² Don State Technical University (Rostov-on-Don, Russian Federation)



Introduction. The problem of automatic license plate recognition is considered. Its solution has many potential applications from safety to traffic control. The work objective was to develop an intelligent recognition system based on the application of deep learning algorithms, such as convolution neural networks that consider automotive standards for license plates in various countries and continents, and are tolerant to camera locations and quality of input images, as well as to changing lighting, weather conditions, and license plate deformations.

Materials and Methods. An integrated approach for the problem solution based on the application of convolution neural network composition is proposed. An experimental analysis of neural network models trained to meet the requirements of the universal license plate recognition task was conducted. Based on it, models that showed the best ratio of quality and speed were selected. Quality of the system is provided through the optimization of various models with different modifications. In particular, convolution neural networks were trained using images from several datasets. In addition, to obtain the best results, the models used were pre-trained on a specially generated synthetic dataset.

Results. The paper presents numerical experiments, the results of which imply the superiority of the developed algorithm over the commercial OpenALPR package on public datasets. In particular, on the 2017-IWT4S-HDR_LP-dataset, license plate recognition accuracy was 94 percent, and on the Application-Oriented License Plate dataset, 86 percent.

Discussion and Conclusions. The resulting algorithm can be used to automatically detect and recognize license plates. The experiments show that the algorithm quality meets or exceeds quality of the commercial OpenALPR package. The developed algorithm quality can be improved through increasing the training dataset, which does not require the participation of the developer.

Keywords: object detection and recognition, convolution neural networks, data generation and augmentation, license plate recognition

For citation: A.V. Poltavskii, T.G. Yurushkina, M.V. Yurushkin. Automatic license-plate recognition. Vestnik of DSTU, 2020, vol. 20, no. 1, pp. 93–99. <https://doi.org/10.23947/1992-5980-2020-20-1-93-99>



Introduction. Automatic License Plate Recognition (ALPR) systems are used for automatic speed control, identification of stolen vehicles, access control of vehicles in private premises and toll collection¹ [1,2,3]. However, most existing algorithms^{2, 3} work only for a specific license plate template or with complex image capture systems and are demanding on lighting conditions and types of vehicles [4,5,6].

Due to the rapid development of deep learning and its applications in the field of computer vision [7], it became possible to create an ALPR system capable of recognizing numerous license plate patterns in an arbitrary environment^{4,5,1}

¹ Lotufo RA, Morgan AD, Johnson AS. Automatic number-plate recognition. IEEE Colloquium on Image Analysis for Transport Applications. Feb, 1990. P. 1–6.

² Du S, et al. Automatic license plate recognition (ALPR): A state-of-the-art review. IEEE Transactions on Circuits and Systems for Video Technology. 2013;23(2):311–325.

³ Gou C., et al. Vehicle license plate recognition based on extremal regions and restricted Boltzmann machines. IEEE Transactions on Intelligent Transportation Systems. 2016;17(4):1096–1107.

⁴ Hsu G., Chen J., Chung Y. Application-oriented license plate recognition. IEEE Trans. Veh. Technol. 2013;62(2):552–561.

⁵ Li H., Shen C. Reading car license plates using deep convolutional neural networks and LSTMs. 2016. arXiv preprint arXiv:1601.05610.

[8]. The fundamental obstacles in recognizing license plates are specific shooting conditions — the presence of rain, snow or poor lighting. The recognition task becomes more difficult if the license plate has an uncommon area and aspect ratio, background color, shape, number of lines, font size, distance between characters, etc.

The study objective was to develop a license plate recognition system that supports various regional license plate standards, and does not depend on the conditions of video recording of cars, such as dirt on the numbers, weather conditions, etc.

Materials and Methods

Automatic system of detection and recognition of license plates. In the framework of this section, we give a description of the software implementation of the system of detecting a vehicle in the photograph, identifying the license plate in it, and its recognition.

The proposed system consists of a composition of several neural network models. The idea of the composition is that the result of the previous model is fed to the input of the next one, and the whole analysis process is divided into stages. Schematically, the principle of the system is shown in Fig. 1:



Fig. 1. Three-step approach for license plate detection and recognition

The first stage of the algorithm is to detect a vehicle. To solve this problem, we used the SSD Resnet² model, trained on a COCO (Common Objects in Context)³ dataset. The result of this model is fragments of the input image which include vehicles. At the second stage, the obtained fragments are fed to the input of the developed model for detecting car numbers, which returns image fragments that include only car numbers. At the final stage, the characters that make up the car number are recognized and glued together. A detailed description of the developed models used in the second and third stages of the algorithm is given in the respective sections of the paper.

The selected approach has the following advantages:

- objects that can be perceived as a license plate are cut off: signs in showcases, windows or fences;
- it becomes possible to establish a relationship between the number and the corresponding vehicle providing for the system expansion in the direction of recognition of other characteristics, such as the type, make and model of the vehicle, color and direction of movement, tracking in the video stream;
- system modularity consisting of independent models specializing in solving a specific problem at a high level is maintained.

License plate detection model. The initial data set for training the model was 1700 images of Indian cars taken at a certain angle. The model trained on this set was not variable for different conditions; therefore, the pseudo-labeling⁴

¹ Yuan Y., et al. A robust and efficient approach to license plate detection. IEEE Transactions on Image Processing. 2017;26(3):1102–1114.

²Tensorflow detection model zoo. Available at: http://download.tensorflow.org/models/object_detection/ssd_resnet50_v1_fpn_shared_box_predictor_640x640_coco14_sync_2018_07_03.tar.gz (accessed: 03.11.2019).

³ COCO — Common Objects in Context. Available at: <http://cocodataset.org/#home> (accessed: 03.11.2019).

⁴ Pseudo-Labeling and Confirmation Bias in Deep Semi-Supervised Learning / E. Arazo [et al.]. 2019. 8 Aug. // arXiv preprint arXiv:1908.02983.

method was applied for unlabeled data sets (images with vehicles). Thus, the initial data set for training was increased to 400 thousand images. The size of the validation dataset is 5% of the training dataset. Images were randomly selected and checked for correct marking of license plate coordinates.

To assess the quality of the model, IoU (Intersection over Union), mAP (mean Average Precision) and AR (Average Recall)¹ metrics were used:

'DetectionBoxes_Precision/mAP': class accuracy averaged over IoU threshold values in the range from 0.5 to 0.95 in 0.05 increments;

'DetectionBoxes_Precision / mAP @.50IOU': average accuracy of classes by IoU value equal to 0.5;

'DetectionBoxes_Precision/mAP (small)': average accuracy of classes for small objects (area <32² pixels);

'DetectionBoxes_Precision/mAP (medium)': average accuracy of classes for objects (32² pixels < area <96² pixels);

'DetectionBoxes_Precision/mAP (large)': average class accuracy for large objects (96² pixels < area < 10000² pixels).

Table 1

mAP result on validation data

Task	Model	mAP	mAP@.50IOU	mAP@.75IOU	mAP (small)	mAP (medium)	mAP (large)
License plate detection	SSD MobileNet v1 FPN	0.8292	0.9843	0.9739	0.7199	0.8197	0.8544

The resulting model is resistant to the size of the input image (Table 1), detects license plates at an angle, as well as with an uncommon aspect ratio.

Vehicle plate numbers recognition model. The problem of license plate recognition is reduced to the task of detecting objects of 36 classes: 26 letters of the uppercase Latin alphabet and 10 digits.

The initial data set for training the model was 1700 images of Indian cars. Validation took place at 10% of the initial set consisting mainly of hard-to-read images marked up manually.

For lack of a sufficient number of labeled data sets that meet the requirements of training the numbers recognition model, it was decided to generate a synthetic data set. Such transformations as rotation, blurring and darkening, as well as various sizes and colorings of the license plate, font styles, and the distance between characters were used as augmentations (Fig. 2).



Fig. 2. Samples from generated datasets

¹ mAP (mean Average Precision) for Object Detection. Available at: https://medium.com/@jonathan_hui/map-mean-average-precision-for-object-detection-45c121a31173 (accessed: 30.10.2019).

The model was trained on a synthetic dataset including 300 thousand images. To increase the accuracy and amount of real data for training the model, the pseudo-labeling technique was used, which increased the set of real data to 250 thousand. Recognition accuracy on the validation dataset has increased by 15% reaching the mark of 63% (Fig. 4). This growth is due to the presence in real images of artifacts that are not available under generation.

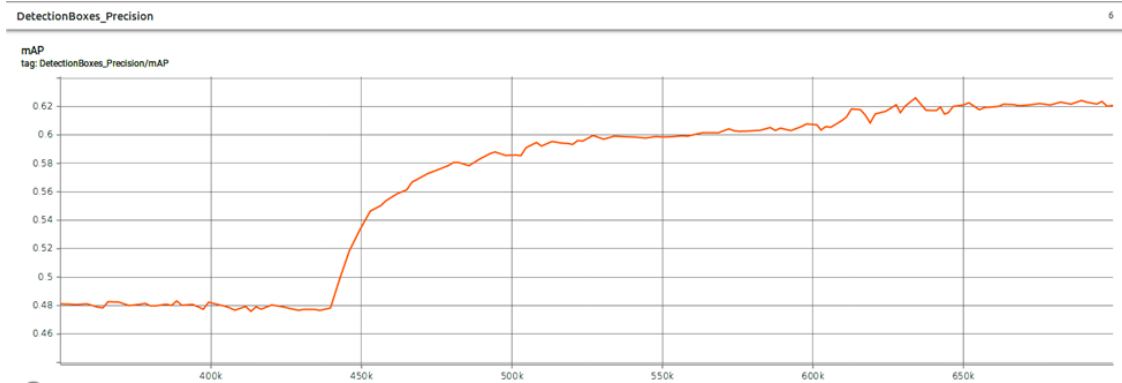


Fig. 3. mAP results of the model before and after adding real datasets

Table 2

Comparison of mAP models on validation data

Task	Model	mAP	mAP@,50IOU	mAP@,75IOU	mAP (small)	mAP (medium)	mAP (large)
License plate recognition	Faster R-CNN Resnet-101	0.4783	0.9372	0.3578	0.4689	0.5251	0.5543
		0.6332	0.9503	0.7228	0.6009	0.6397	0.7051
	Faster R-CNN Inception v2	0.5567	0.9534	0.6113	0.5569	0.6094	0.6493
		0.5784	0.9652	0.6184	0.5583	0.6157	0.6676

Research Results

In the resulting combination of neural network models, each of the classifiers was independently trained using images from several datasets including license plates of countries from all continents and methods of increasing these sets to achieve stability under various conditions^{1,2}.

IoU metrics were used to evaluate license plate detection results. For the task of recognizing license plate characters, the image in which all the characters in the license plate were correctly recognized was considered correctly marked out. An odd, missing or incorrectly recognized symbol was considered an error on the whole license plate.

The results were compared to the latest cloud version of the commercial OpenALPR³ package and the 2016 study⁴ mentioned above. The testing was performed on the 2017-IWT4S-HDR_LP-dataset (Table 3) provided in the study⁵ and the

¹ Pseudo-Labeling and Confirmation Bias in Deep Semi-Supervised Learning.

² Nowruz FE, et al. How much real data do we actually need: Analyzing object detection performance using synthetic and real data. 2019. arXiv preprint arXiv:1907.07061.

³ OpenALPR Cloud API. Available at: <https://api.openalpr.com/v2/> (accessed: 02.11.2019).

⁴ Li H., Shen C. Op. cit.

⁵ Hsu G., Chen J., Chung Y. Op. cit.

Application-Oriented License Plate (AOLP) (Table 4) provided in the study¹, which includes 2049 images with Taiwanese license plates. They were divided into three subsets with different levels of complexity and shooting conditions: Access Control (AC), Law Enforcement (LE) and Road Patrol (RP).

Table 3

Numerical experiment on public 2017-IWT4S-HDR_LP-dataset

Metrics	Ours	OpenALPR
Number of correct license plate recognitions	619 / 653	377 / 653
Percent of correct license plate recognitions	94.79	57.73

Table 4

Numerical experiment on public dataset

Metrics	Applied solutions	AC Subset (%)	LE Subset (%)	RP Subset (%)
IoU plate detection	ours	95.58	93.97	94.29
	OpenALPR	91.80	86.89	90.84
	[12] 1st approach(with CNN I)	93.53	89.83	86.58
	[12] 1st approach(with CNN II)	93.25	90.62	86.74
	[12] 1st approach(with CNN I & II)	93.97	92.87	87.73
	[12] 2nd approach(with global features only)	90.50	91.15	83.98
	[12] 2nd approach(with both local and global features)	94.85	94.19	88.38
Number of correctly recognized license plates:	ours	88.75	83.94	85.40
	OpenALPR	86.04	77.98	85.71

¹ Hsu G., Chen J., Chung Y. Op. cit.

Discussion and Conclusions. Models were built to detect and recognize vehicle license plates. According to the numerical experiments, the model for detecting numbers turned out to be more accurate than the solutions obtained in 2016 and 2019^{1, 2} on the dataset published in 2013³. The license plate recognition model turned out to be more accurate than the decision of 2019⁴ on the dataset obtained in 2017 [8]. To increase the accuracy of the models, methods of generating synthetic data and pseudo-labeling were used. The resulting system has appeared resistant to the size of the input image and the environmental properties.

References

1. Bernstein D, Kanaan AY. Automatic vehicle identification: technologies and functionalities. *Journal of Intelligent Transportation System*. 1993;1(2):191-204.
2. Kanayama K, et al. Development of vehicle-license number recognition system using real-time image processing and its application to travel-time measurement. In: *IEEE Vehicular Technology Conference*, May, 1991. P. 798–804.
3. Kessentini Y, Besbes MD, Ammar S, et al. A two-stage deep neural network for multi-norm license plate detection and recognition. *Expert Systems with Applications*. 2019;136:159–170.
4. Tian J, Wang R, Wang G, et al. A two-stage character segmentation method for Chinese license plate. *Computers & Electrical Engineering*. 2015;46:539–553.
5. Dong M, et al. A CNN-based approach for automatic license plate recognition in the wild. In: *British Machine Vision Conference (BMVC)*, 2017. P. 1–12.
6. LeCun Y, Bengio Y, Hinton G. Deep learning. *Nature*. 2015;521(7553):436–444.
7. Španhel J, et al. Holistic recognition of low quality license plates by CNN using track annotated data. In: *14th IEEE International Conference on Advanced Video and Signal Based Surveillance (AVSS)*, 2017. P. 1–6.

Submitted 16.01.2020

Scheduled in the issue 05.03.2020

About the authors

Poltavskii, Artem V., student of the Algebra and Discrete Mathematics Department, Vorovich Institute for Mathematics, Mechanics, and Computer Science (8a, Milchakova St., Rostov-on-Don, 344058, RF),

ORCID: <https://orcid.org/0000-0003-3937-1143>, poltavsky@sfedu.ru

Yurushkina, Tatyana G., lecturer of the Natural Sciences Department, Don State Technical University (1, Gagarin sq., Rostov-on-Don, 344000, RF), ORCID: <https://orcid.org/0000-0001-8413-8506>, t.yurushkina@gmail.com

¹ Li H., Shen C. Op. cit.

² OpenALPR Cloud API.

³ Hsu G., Chen J., Chung Y. Op. cit.

⁴ OpenALPR Cloud API.

Yurushkin, Mikhail V., senior lecturer of the Algebra and Discrete Mathematics Department, Vorovich Institute for Mathematics, Mechanics, and Computer Science (8a, Milchakova St., Rostov-on-Don, 344058, RF), Cand.Sci. (Phys.-Math.), ORCID: <https://orcid.org/0000-0003-2477-0459>, m.yurushkin@gmail.com

Claimed contributorship

A.A. Poltavskii: research, calculations, text preparation, formulation of conclusions, analysis of the results.
T.G. Yurushkina: computational analysis, text preparation, formulation of conclusions, analysis of the results.
M.V. Yurushkin: formulation of the basic concept, objectives and tasks, academic advising, the text revision, correction of the conclusions, research.

All authors have read and approved the final manuscript.

INFORMATION TECHNOLOGY, COMPUTER SCIENCE, AND MANAGEMENT



UDC 004.891.2

<https://doi.org/10.23947/1992-5980-2020-20-1-100-105>

Modeling an analytics system for industrial safety monitoring based on expert assessments

O. A. Zakharova¹, A. V. Selikhina², T. G. Vezirov³

^{1,2}Don State Technical University (Rostov-on-Don, Russian Federation)

³Dagestan State University of National Economy (Makhachkala, Russian Federation)



Introduction. A mathematical model of the industrial safety monitoring system in mechanical engineering is investigated. The work objective was to create a mathematical model based on expert assessments of workplace safety parameters with a calculated and experimental justification of its applicability to the “STRAZH” expert security monitoring system.

Materials and Methods. The classification of expert systems for engineering enterprises is proposed. The stages of creating expert systems are considered. A methodology for assessing the consistency of experts as a basis for models of expert systems in the field of mechanical facilities safety is presented.

Results. The basic safety parameters of the workplace are identified. A matrix of expert evaluation of parameters based on the opinion of leading experts in the field of engineering is created. The results of modeling the expert system “STRAZH” with the calculated and empirical support of the mathematical model validity are presented. The advantages of implementing expert systems to increase the level of personnel safety are proved.

Discussion and Conclusions. The results obtained have a high degree of expert coordination and can be used in the development of expert safety monitoring systems for engineering enterprises.

Keywords: modeling, expert systems, knowledge base, expert assessment, mechanical engineering, safety parameters, concordance.

For citation: O.A. Zakharova, A.V. Selikhina, T.G. Vezirov. Modeling an analytics system for industrial safety monitoring based on expert assessments. Vestnik of DSTU, 2020, vol. 20, no. 1, pp. 100–105. <https://doi.org/10.23947/1992-5980-2020-20-1-100-105>



Introduction. Difficult-to-formalize processes complicate full automation of engineering production. Smart manufacturing, smart enterprise and similar structures are implemented only on the basis of analysis information systems (AIS) using the components of artificial intelligence. At present, a uniform, classical definition of smart manufacturing is not presented in the technical and specialized literature. However, experts agree that “smart manufacturing”, “smart enterprise”, “smart factory” refers primarily to a widespread use of information technologies, computing devices, sensors and distributed networks to implement a highly efficient production process and provide its participants with maximum safety [1].

A modern approach to the development of intelligent AIS for smart manufacturing involves a widespread use of new methods for representing knowledge and programmed empirical algorithms for their processing [2].

First of all, among the AIS used in mechanical engineering, we single out two most promising classes.

1. Management information systems (MIS) are designed for monitoring and management of difficult-to-formalize process facilities. Core components in the MIS structure include:

- module for collection and processing databulk (big data) according to certain algorithms;
- module for the expert assessment formation [3].

2. Expert systems (ES) are designed for the collection, processing and analysis of formalized experience of experts in a specific field of engineering. Core components in the structure of ES include:

- module for the accumulation of expert knowledge in a specific field of engineering;
- module for the formation of alternative control scenarios under specific conditions based on the empirical experience of experts [4].

AIS of both classes are complex software systems created to replicate empirical experience and algorithms developed on its basis to increase the efficiency of engineering industries.

The knowledge base is the central system component that is formed in the process of ES modeling, designing and operating. The main difference between ES and other information systems involves the solution to a clearly limited range of problems in a specific area [5]. Unlike traditional machine solutions, ES use not a procedural analysis, but the processing of deductive reasoning. Similar systems can find a solution to poorly defined and unstructured problems [6].

Materials and Methods

ES in Mechanical Engineering. In the modern world, the accumulated, processed and analyzed knowledge is used for monitoring, preventing and forecasting emergencies that is the result of empirical studies of several generations of experts. In this regard, ES are essential in the modeling and prediction of dangerous events.

MIS and ES are designed in two stages:

- designing a module for the accumulation and structuring of knowledge in a specific field;
- designing a module for developing recommendations and making a control decision based on specific facts and parameters for monitoring the state of an object.

The use of ES in the field of labor protection at engineering enterprises is due to the need to reproduce the knowledge of experienced experts. This is one of the conceptual stages in the development of digital production. From the user point of view, ES are of interest at this time for a number of reasons:

- they can solve various practical problems and in terms of results are not inferior to expert people;
- they are focused on solving a wide range of tasks in nonformalized areas;
- they do not require special programming skills, and working with them is available for a wide audience of qualified users [7].

In mechanical engineering, ES help to make decisions, manage facilities, identify emergencies and failures, and design production. Fig. 1 shows the basic classes of problems solved by ES in mechanical engineering [8].

EXPERT SYSTEMS IN MECHANICAL						
Quality diagnosis - assembly, installation of machines - industrial equipment - productive capacity of the enterprise	Decision support - under planning repair work - in operational planning	Planning - production volumes - design tasks	Control and management - manufacturing process - electrical equipment	Monitoring - processing - product quality - equipment - emergency situations	Forecasting - non-conforming events at hazardous facilities - equipment performance	Training - ES work with process equipment

Fig. 1. Basic classes of problems solved by expert systems in engineering

In the practice of machine-building industries for TV-7 machines equipped with a function for controlling the accuracy of product processing, ES of the “Archimedes 2008” type are used. Under processing, the base circles in the cross and longitudinal sections and geometric parameters are calculated using the “Archimedes 2008” system to identify possible deviations. At the same time, problems with deviation of the longitudinal section profile, deviation from roundness, ovality, are identified, errors of sizing, waviness, etc., are determined [9].

The experience of using ES in mechanical engineering made it possible to identify the main advantages of their implementation:

- an increase in the quality of decisions made,
- improving the quality of manufactured products,
- increase in productivity,
- advanced training of employees.

It should be noted that it is advisable to use ES to solve complex problems in engineering production [10].

The key concept of labor protection in mechanical engineering is “workplace”. This is the place where an employee should be located or where he needs to arrive in connection with his job. It is directly or indirectly controlled by the employer. Workplace safety is regulated by the Occupational Safety Standards System SSBT (GOST 12). It should be noted that ES do not provide for full control of safety at the workplace.

To increase the reliability of control decisions, a generalized expert assessment should be introduced into the workplace safety model. The key point in conducting an expert assessment is the selection of competent specialists with experience in the claimed field and capable of an adequate assessment of the technological situation [11].

Research objective is to develop a mathematical model and conduct a calculation and experimental justification of its applicability for ES security monitoring “STRAZH” (“System for the exact calculation of vital activity algorithms”), based on the analysis of the subject area and expert assessments.

Initial data. Based on the analysis of literary sources and the opinion of practitioners, 11 basic parameters of workplace safety were identified.

1. Equipment (functional content).
2. Compliance of the equipment with the anthropometric characteristics of an employee.
3. The availability of personal and collective protective equipment, as well as fire extinguishing equipment.
4. Access to the workplace and the ability to quickly evacuate.
5. Serviceability of production equipment.
6. Performing production operations in accordance with the requirements of technological documentation.
7. Monitoring of distributed hazardous and harmful factors.
8. Keeping the established order and organization, high production, technological and labor discipline.
9. Qualification of the employee.
10. Timely training and retraining of the employee.
11. Regular monitoring.

The totality of data on the key parameters of the workplace safety provides you for such a characteristic of the work process as labor intensity. This integrated characteristic of the labor process shows the load on the nervous system, sensory organs, and considers the emotional component. Labor intensity is normalized by types of loads: intellectual, sensory, emotional, monotonous, and operational.

Development of mathematical model of the ES “STRAZH”. When developing the mathematical model of the ES “STRAZH”, 21 experts evaluated the safety parameters of the workplace on a scale from 1 to 12 points. The survey was conducted using questionnaires. Based on its results, a consolidated matrix for assessing workplace safety parameters has been created (Fig. 2).

PARAMETERS	EXPERTS																				
	1	2	3	4	5	6	7	8	9	10	11	12	13	14	15	16	17	18	19	20	21
Production equipment serviceability	11	10	11	11	12	11	12	10	11	8	11	10	10	11	12	11	10	11	10	11	7
Access to workplace and ability to quickly evacuate	10	11	12	10	9	10	7	9	7	5	10	11	12	10	10	7	12	10	11	8	10
Availability of personal protective equipment and fire extinguishing	9	9	9	8	10	9	9	11	9	9	12	9	8	9	9	10	9	9	9	9	11
Compliance of equipment to human anthropometry	5	6	5	7	5	5	6	5	5	2	5	5	6	4	6	5	6	5	7	5	3
Monitoring of distributed hazardous and harmful factors	12	12	10	12	11	12	11	12	12	12	9	12	11	12	11	12	11	12	12	12	9
Employee qualifications	2	2	2	2	4	2	2	3	2	10	2	2	2	2	3	2	2	2	2	2	6
Workplace equipment	6	5	6	6	6	6	5	6	6	6	6	6	5	6	5	6	3	6	6	6	5
Performance of production operations due to requirements	4	4	4	4	2	3	4	4	4	4	4	4	4	5	4	4	5	4	4	4	8
Employee training and retraining	7	7	8	5	7	8	10	7	10	7	7	7	7	7	7	9	8	7	5	7	4
Keeping order and discipline	3	3	3	3	3	4	3	2	3	3	3	3	3	3	2	3	4	3	3	3	12
Monitoring regularity	8	8	7	9	8	7	8	8	8	11	8	8	9	8	8	8	7	8	8	10	2

Fig. 2. Workplace safety rating matrix

A key outcome of the peer review methodology is Kendall's concordance coefficient, which measures the consistency of the expert group:

$$W = \frac{12 \cdot S}{m^2 \cdot (n^3 - n)}, \quad (1)$$

where W is the concordance coefficient, m is the number of experts, n is the number of parameters, S is the sum of squared deviations of the rank sums obtained by each parameter from the average rank sum of ranks.

The sum of squared rank deviations S is calculated from the formula:

$$S = \sum_{i=1}^n D_i^2 = \sum_{i=1}^n (d_i - \bar{d})^2, \quad (2)$$

where D_i is the rank deviation, i is the serial number of the parameter, d_i is the parameter rank, \bar{d} is the arithmetic mean of the parameter rank.

The concordance coefficient varies in the range from 0 to 1: 0 corresponds to the complete inconsistency of experts, 1 corresponds to complete coordination. If the concordance coefficient is equal to zero, it is necessary to check the initial data and (or) analyze the membership of experts in order to replace them (partly or completely). If the coefficient value exceeds 0.4–0.5, the quality of the assessment is considered satisfactory, if it reaches 0.7–0.8 — high.

Thus, when calculating the concordance coefficient according to the formulas (1) and (2), we obtain the following parameter values:

$$S = \sum_{i=1}^n (d_i - \bar{d})^2 = 5476 + 2916 + \dots + 361 = 39142,$$

$$W = \frac{12 \cdot S}{m^2 \cdot (n^3 - n)} = \frac{12 \cdot 39142}{21^2 \cdot (11^3 - 11)} = 0.806.$$

Using Pearson's "chi-square" criterion [12], the null hypothesis $h_0: W = 0$ (expert opinions do not agree with each other), at an alternative $h_1: W \neq 0$ (expert opinions are consistent with each other) is tested.

We introduce expert estimates, rank sums d_i , rank sum deviations D_i from the average \bar{d} and D_i^2 in the design Table 1.

Table 1

The concordance coefficient calculation

Parameters	Experts																					$d_i = \sum_{j=1}^m R_{ij}$	D_i	D_i^2
	1	2	3	4	5	6	7	8	9	10	11	12	13	14	15	16	17	18	19	20	21			
1	11	10	11	11	12	11	12	10	11	8	11	10	10	11	12	11	10	11	10	11	7	221	74	5476
2	10	11	12	10	9	10	7	9	7	5	10	11	12	10	10	7	12	10	11	8	10	201	54	2916
3	9	9	9	8	10	9	9	11	9	9	12	9	8	9	9	10	9	9	9	9	11	196	49	2401
4	5	6	5	7	5	5	6	5	5	2	5	5	6	4	6	5	6	5	7	5	3	108	−39	1521
5	12	12	10	12	11	12	11	12	12	12	9	12	11	12	11	12	11	12	12	12	9	239	92	8464
6	2	2	2	2	4	2	2	3	2	10	2	2	2	2	3	2	2	2	2	2	6	58	−89	7921
7	6	5	6	6	6	6	5	6	6	6	6	6	5	6	5	6	3	6	6	6	5	118	−29	841
8	4	4	4	4	2	3	4	4	4	4	4	4	4	5	4	4	5	4	4	4	8	87	−60	3600
9	7	7	8	5	7	8	10	7	10	7	7	7	7	7	7	9	8	7	5	7	4	151	4	16
10	3	3	3	3	3	4	3	2	3	3	3	3	3	3	2	3	4	3	3	3	12	72	−75	5625
11	8	8	7	9	8	7	8	8	8	11	8	8	9	8	8	8	7	8	8	10	2	166	19	361
																						1617		39142

The average rank sum of all parameters is $\bar{d} = \frac{\sum_{j=1}^m R_{ij}}{n} = \frac{1617}{11} = 147$.

We use the expression $\bar{d} = \frac{1}{2} \cdot m \cdot (n+1) = \frac{1}{2} \cdot 21 \cdot (11+1) = 147$, as a control of calculations.

To test the null hypothesis using Pearson's "chi-square" criterion, we calculate the empirical value $\chi^2 = m \cdot (n-1) \cdot W = 21 \cdot 10 \cdot 0.806 = 169.4$, which is compared to the critical values of "chi-square" for the number of degrees of freedom $n-1=10$.

The empirical value $\chi^2 = 169.4$ falls into the critical region $\chi^2 > \chi_{0.01}^2(n-1)$ ($169.4 > 23.2$), which allows us to reject the null hypothesis. The concordance coefficient differs significantly from zero; therefore, there is a fairly close consistency of expert opinions regarding the estimated parameters.

Research Results. An ES is developed in three stages: modeling, design, construction [13]. At the modeling stage, an analysis of the subject area to identify the most significant links and relationships between objects is carried out; the totality of input and output parameters, the degree of their input on the processes under study are determined. To build a mathematical model of the ES "STRAZH", the safety parameters of workplaces of the machine-building industries were identified. When assessing safety parameters, it became necessary to select empiric experts who were the most competent in the organization of the mechanical engineering processes, since there are no methods to guarantee single-value safety assessments. The experts selected were occupational safety engineers from leading enterprises of mechanical engineering in the Rostov Region, as well as leading lecturers from the Engineering Technology Department, Don State Technical University.

Discussion and Conclusions. According to the study, the concordance coefficient reached 0.806. This indicates a high consistency of expert opinions. It is verified by Pearson's criterion and is a prerequisite for the development of a high-precision ES model.

In modern science, a significant place is occupied by the problem of decision support using ES. The introduction of such systems in mechanical engineering will enable:

- to reduce the time on solving complex security issues;
- to reduce the likelihood of producing spurious solution;
- to raise the level of labor safety.

The study of this issue in the context of modern innovative production is of current interest.

References

1. Cook D, Das S. Smart Environments. Technologies, protocols and applications. Hoboken: Wiley-Interscience; 2005. P. 3.
2. Semenov IO, Serebryakova TA. Aktual'nost' ehkspertnykh sistem i ikh znachenie v ehkonomie [Expert systems relevance and their importance in the economy]. Studencheskii forum. 2018;3(24). URL: <https://nauchforum.ru/journal/stud/24/31118> (accessed: 07.05.2019). (In Russ.)
3. Rutkovskii L. Metody i tekhnologii iskusstvennogo intellekta [Artificial intelligence methods and technologies]. Moscow: Goryachaya liniya — Telekom; 2010. — 520 p. (In Russ.)
4. Waterman D. Rukovodstvo po ehkspertnym sistemam [A guide to expert systems]. Moscow: Mir; 1989. 388 p. (In Russ.)
5. Giarratano J, Riley G. Expert Systems — Principles and Programming. 4th ed. San Francisco: Course Technology; 2004. 302 p.
6. Shaptala VG, Shul'zhenko VN, Radoutskii VYu, Shaptala VV. Matematicheskoe modelirovanie pozharnoi bezopasnosti vysshikh uchebnykh za-vedenii [Mathematical modeling of fire safety in higher education]. Bulletin of BSTU (named after V.G. Shukhov). 2008;4:63–65. (In Russ.)
7. Popov EhV. Sistemy obshcheniya i ehkspertnye sistemy [Communication systems and expert systems]. Moscow: Radio i svyaz'; 1990. 464 p. (In Russ.)
8. Mokanu AA, Stramtsova ES, Pushina RA. Primenenie ehkspertnykh sistem v mashinostroenii [Application of expert systems in mechanical engineering]. In: Scientific community of students of the XXI century. Engineering: Proc. LXV Int. Stud. Sci.-Pract. Conf. URL: [https://sibac.info/archive/technic/5\(64\).pdf](https://sibac.info/archive/technic/5(64).pdf) (accessed: 13.05.2019). (In Russ.)
9. Sapozhnikov AYU, Krivosheev IA. Primenenie ehkspertnykh sistem v protsesse proektirovaniya aviatsionnykh GTD [Application of expert systems in the design of aircraft gas turbine engines]. Young Scientist. 2017;12:90–97. URL <https://moluch.ru/archive/12/972/> (accessed: 12.05.2019). (In Russ.)

10. Cross TB. Knowledge Engineering 2016 The Uses of Artificial Intelligence in Business. Boulder: TECHtionary Corporation; 2016. 236 p.
11. Litvak BG. Ehkspertnaya informatsiya: metody polucheniya i analiza [Expert information: methods for obtaining and analyzing]. 2nd ed. Moscow: Issledovatel'skii tsentr problem kachestva podgotovki spetsialistov; 2009. 223 p. (In Russ.)
12. Kharchenko MA. Korrelyatsionnyi analiz [Correlation analysis]. Voronezh: VGU; 2008. 30 p. (In Russ.)
13. Solonshchikov PN. Integral'naya otsenka tyazhesti truda, kak odin iz metodov prognozirovaniya neschastnykh sluchaev na predpriyatii [Workload integral assessment as one of the methods for predicting accidents at the enterprise]. Advanced Science. 2017;2:35. (In Russ.)

Submitted 14.01.2020

Scheduled in the issue 06.03.2020

About the authors

Zakharova, Ol'ga A., associate professor of the IT Department, Deputy Head of the Office of Digital Educational Technologies, Don State Technical University (1, Gagarin sq., Rostov-on-Don, 344000, RF), Cand.Sci. (Pedagogy), associate professor, ORCID: <https://orcid.org/0000-0001-6240-3268>, Oz64@mail.ru

Selikhina, Aleksandra V., graduate student of the Theoretical and Applied Mechanics Department, Don State Technical University (1, Gagarin sq., Rostov-on-Don, 344000, RF), ORCID: <https://orcid.org/0000-0002-6486-7792>, Selikhina90@mail.ru.

Vezirov, Timur G., professor of the Department of Information Technologies and Information Security, Dagestan State University of National Economy, (5, ul. Dzhambul'dina Ataeva, Makhachkala, 367008, RF), Dr.Sci. (Pedagogy), professor, ORCID: <https://orcid.org/0000-0003-4592-8462>, timur.60@mail.ru

Claimed contributorship

O.A. Zakharova: the problem formulation, research methodology, results representation — 40%. A.V. Selikhina: object domain research, research practice, processing of the results — 40%. T. G. Vezirov: selection and justification of safety parameters — 20%.

All authors have read and approved the final manuscript.

INFORMATION TECHNOLOGY, COMPUTER SCIENCE, AND MANAGEMENT



UDC 621.75.04 / UDC 621.91.04 / 004.9

<https://doi.org/10.23947/1992-5980-2020-20-1-106-111>

Distinction between concepts of “structural-functional-parametric model” and “parametric model” of information knowledge objects

E. N. Kolybenko

Don State Technical University (Rostov-on-Don, Russian Federation)



Introduction. Fundamentally important problems of the structure mapping and transformation, functions and parameters of various properties in the systems of information knowledge objects organization, as well as functionally different parameters in the management processes of transformations of material objects, are considered. For this purpose, structural-functional-parametric models and parametric models are respectively used. The distinction between these concepts is relevant and practically significant. The scientific novelty of the presented work involves studying methods and information tools used to determine functionally different technological schemes for the interaction of objects at the stages of design and pre-processing engineering.

Materials and Methods. The concept of a “structural-functional-parametric model” is associated with the definition of the structure of the basic knowledge objects of the subject area. In this case, the “linking base” is the methods and corresponding means of system engineering in the infological modeling technology that are used to solve practical problems. The concept of a “parametric model” is associated with the solution to practical problems of the process control. Nature of these tasks is functionally different (technical, physical, chemical, biological). It should also be clarified that, in this case, we are talking about converting the parameters of various properties of real objects by methods and means of system engineering (almost a mathematical apparatus).

Results. A “structural-functional-parametric model” and a “parametric model” are general theoretical concepts that have invariant properties necessary for solving practical problems of the subject knowledge area. Considering the organization system and management processes in this way, note that it is required to maintain data and logical connections between them under static and dynamic settings.

Discussion and Conclusions. To solve practical problems in the subject knowledge area according to the technology of information logical modeling, certain methods, tools, algorithms, and operations are used. The most complete mapping and transformation of information objects is possible only in structural-functional-parametric models and databases of their solutions. The application of structural-functional-parametric models is the most important condition for a successful transition to a high-level deterministic automation of information technology for solving practical problems of the subject area. As an example of such a problem, we can cite the machining production design engineering.

Keywords: production design engineering, cutting, system analysis, information technology, decision modeling, system technique.

For citation: E. N. Kolybenko. Distinction between concepts of “structural-functional-parametric model” and “parametric model” of information knowledge objects. Vestnik of DSTU, 2020, vol. 20, no. 1, pp. 106–111. <https://doi.org/10.23947/1992-5980-2020-20-1-106-111>



Introduction. The development of systems engineering allows us to distinguish between the concepts of “parametric model” and “structural-functional-parametric model” taking into account the properties of the concepts of “mathematical modeling” and “logical modeling”, as well as the functions of their knowledge [1, 2]. Systems engineering technology for determining the structural-functional-parametric model is based on the formalization of domain knowledge. Formalized concepts are first built into the structure of the basic knowledge objects, and then into the structure of basic knowledge objects of a higher level of the subject area. At this, the semantic and syntactic properties of the concepts [3] should be as strict as possible. In this case, the author’s updated interpretation of existing and new concepts is fundamentally important. By actualization, we mean activation, initialization of meaning by transferring from a static (outdated) state to a dynamic (updated) state while preserving all the necessary links and relationships within the system

and with the external environment. This approach to the formalization of knowledge of the subject area provides for its transfer to a higher level of organization.

We introduce the updated concept of “system principles”. These are information logical statements of the approach to solving the problems of researching manufacturing systems and processes of functionally different purposes. These principles are verified by the multiple practice of their use in the setting environment (static – for systems and dynamic – for processes).

Materials and Methods. We formulate system principles.

1. Information structural-functional-parametric and parametric models are investigated. The distinction is based on two system principles:

- unity and generality,
- difference.

Let us compare the structural-functional-parametric models of information objects and the parametric models of real objects.

Their unity and generality are manifested in the functions of destination under the computer processing of information: display, transformation, storage, transmission.

The difference is manifested in the methods and means of solving practical problems of the subject domain defined in the considered models.

Technologies for determining structural-functional-parametric models are implemented by methods and systems engineering tools: systems theory, systems analysis of decision making, set theory, and graph theory.

Set theory uses graphic means: formalized notation of concepts, logical operators for making statements by imposing links between formalized concepts.

Graph theory specifies overlays, intersections, and associations of links between functionally unified elements of the object structure according to the semantic and syntactic properties of the formalized concepts used. To this end, structure graphs and Venn diagrams are used.

To determine the algorithms in the technology of modeling systems for organizing information objects, conceptual notions are used: mapping, transformation, structure, set, etc.

In the practice of solving problems, systems engineering technologies are widespread. They are used in the processing of information on computers and servers (that is, in computer systems), as well as in the management of functionally different organization systems.

In [4], systems engineering technology is presented as system technique technology. This significantly narrows the scope of its application. The paper [5] can be recommended for information on the methodology of systems engineering in information technology for identifying large, sophisticated powerful systems in solving practical problems.

Technologies of system techniques are implemented by various mathematical methods and means. With their help, parametric models, based on the mapping and transformation of the parameters of various properties of real objects, are determined. In the parametric models, processes of controlling the transformation of real objects within the corresponding domain organization systems are mathematically modeled.

The authors of [6] investigate the solution to problems of the practice of manufacturing preparation of machining production. Here is an example of significant difficulties that arise under the implementation of this task by modern means of the mathematical apparatus on an insufficiently formalized reference basis of knowledge.

In [7], the practice of successful implementation of the systems engineering technology in functionally different management is described. In [8–13], various approaches to systems engineering technology for solving problems of controlling the mathematical apparatus are considered. The papers [14–15] providing for determining the state of the manufacturing preparation knowledge, are directly related to solving the problems of its practice.

The purpose-oriented properties of the “structural-functional-parametric model” concept and the knowledge functions following from its formulation. In the further presentation of the material, we use the updated concepts introduced in [1]:

- structure,

- main structure elements (integration, disintegration),
- design quality of the main elements (integration, disintegration) in the structure of objects {components} of the DPP stage and the structure of objects {initial blanks} of the PPE (TO) stage,
- basic object of knowledge,
- information “slave” (main) transformation object (TO).

The concept of “structure” will be considered in various aspects on the example of manufacturing preparation of machining production.

We introduce the formalized notation of concepts:

- DPP is the stage of designing preparation of production,
- PME (TO) is the stage of preproduction machining engineering,
- { ... } is multitude.

1. Consider the well-known judgment: “Everyone sees the material, the content is found only by someone who has something in common with it, and the form remains a mystery for most ... The form needs to be digested as well as the material, but it is much more difficult to digest”¹.

Between the elements of knowledge in the triad of cognition, the sequence of their link (material \Rightarrow content \Rightarrow form), since the content can change depending on the perception of the material, and for the same content the form of its display can change.

In most cases, knowledge is developed through transforming their display form, which determines the level of achievement of their depth and changes accordingly. A necessary condition for the transition from the knowledge content to the form of their display is the achievement of a certain level of combining concepts into a system.

2. A single environment of one level of the structural elements of the “slave” transformation object, in a general case, interacts (is interfaced) with a group of structural elements of the “leading” object. This interaction is provided by the imposition of functionally different relationships along the “reference” interface points from the side of the “leading” object structure to the structure elements of the coordinate systems of the “slave” object. It is on this coordination that structural-functional-parametric models are based.

3. The connection of the “slave” and “leading” objects of interaction enables to introduce the following concepts to define the concept of “structure” of basic knowledge objects:

- composition of the structural elements,
- type of working (functional) connection,
- communication overlay method,
- functions of working relationships,
- parameters of the properties of structural elements and the relationships between them.

4. The connection of objects is based on the system principle formulated in [16]: “The boundaries of their connection carry the greatest information about sets”. The structural elements of each of the interaction objects, determined by the boundaries of their connection, are functionally new. In this case, the tasks on determining the position of the elements in the coordinate system of the “slave” object are solved. This connection of objects is used to determine the structure of the basic knowledge objects of any subject area.

5. The existence of the structure of the base knowledge objects is provided only by those initial (previously defined) and obtained new concepts that can be defined as formalized (symbolic properties of concepts [3]), as well as unified analogues of structural elements and the relationships between them, to be embedded in the structure.

6. The main first and second base knowledge objects of the first type of the PME (TO) stage are specified in the corresponding two process charts for the interaction of “slave” objects according to the working functions performed by them (basing, geometric shaping of the form element).

7. The main base knowledge object of the fourth type of DPP stage is determined by the type of the main first base knowledge object of the first type of PME (TO) stage in the corresponding process chart of the interaction of ob-

¹ Gete IV. *Ob iskusstve* [On art]. Moscow; 1975. 623 p.

jects. In the structure of objects {components, assembly units} of the DPP stage, it is possible to identify three more “slave” objects according to the work functions performed by them (basing, guides, torque transmission, division and fixing) [17].

8. The scientific novelty of the presented paper involves studying methods and information tools used to determine functionally different process charts for the interaction of objects of the PME (TO) and DPP stages.

9. The information technology for the automated solution to the PME (TO) tasks assumes that the most important condition is met — the definition of two “slave” transformation objects as components in the structure of the {initial blanks, blanks} of the PME (TO) stage and in the general case of four “slave” transformation objects as an integral part in the structure of objects {components, assembly units} of the DPP stage.

10. The model information of the main base knowledge objects of PME (TO) is distributed in two parts: invariant and typical object-oriented parametric ones. They are logically unified and cannot be considered separately.

The invariant parts of the information model structure of the main base knowledge objects at the PME (TO) stage are designed to solve the problems of optimizing material and labor resources in the main and auxiliary technological operations. Typical object-oriented parametric parts of these main base knowledge objects serve as the basis for determining the base knowledge objects of a higher level of the subject area of the PME (TO).

11. Each of the two parts in the structure of information models of the main base knowledge objects is determined by the form of display (graphic in two-dimensional space, the corresponding analytical in three-dimensional space). This provides the conditions for the automated conversion of the form of their display from one view to the corresponding another and vice versa.

12. The information content and form of the base knowledge object can be determined due to its structural-functional-parametric information model for displaying and transforming the algorithm into technology for solving practical problems of the subject knowledge area from input to output under computer processing. Such information is perfect.

13. The main base knowledge objects (of the fourth type of the DPP stage, of the first and second types of the of the PME (TO) stage) form a systemic fundamental for the hierarchical structure of the knowledge base of the PME (TO) stage according to the seven levels of classification of its base objects of various types. Base knowledge objects of all types are defined in the contours of the coupling circuit of their structure elements according to the superimposition functions (relations, links) of the structure elements in the totality of logically and information-related coordinate systems. The fundamental of the knowledge base structure of the PME (TO) stage is made up of elementary and composite superimposed simple and complex functionally different {elements of geometric shape}. These {shape elements} are used primarily to determine the elements in the structure of the group of objects of interaction of functionally different flowcharts, and secondly – to determine elements in the structure of the main base knowledge objects of the first and second types of the PME (TO) stage, as well as of the fourth type of the DPP stage. The first first-type base knowledge object of the stage is {basing flowcharts} on their possible set for fulfilling the functions of basing production objects and cutting tools into machining attachments, as well as the devices — into the corresponding working bodies of the cutting machine. The second first-type base knowledge object is {basing flowcharts of the shape elements into working machines and geometric formation shape elements by cutting on working machines} on their possible set. The second-type base knowledge object is {working machines} as an information and logical connection of the first first-type base knowledge object in a general case with a limited necessary set of the second first-type base knowledge objects. The third-type base knowledge object is {working machine systems} as an information and logical connection of the fourth-type base knowledge object of the DPP stage in a general case with a limited necessary set of logically and information-related second-type base knowledge objects of the PME (TO) stage. The fourth-type base knowledge object of the DPP stage is {basing flowcharts} on their possible set for fulfilling the basing functions for parts and assemblies into design products. The fifth-type base knowledge object of the DPP stage is {design products}.

Research Results. In the paper presented, structural-functional-parametric models of functionally different types are used to determine the hierarchical structure of the knowledge base of the PME (TO) stage at seven levels. The

structure of the hierarchical knowledge base of the PME (TO) is determined from the results of extensive practice of cooperation with metalworking enterprises. This is the most complete structure of the composition of the elements and relationships between them. It has invariant properties with respect to a possible set of subject knowledge areas for its distribution, for example, pressure, welding, computer processing of information, management.

Discussion and Conclusions. The hierarchical structure of the knowledge base of the PME (TO) subject area is grounded on:

- structural-functional-parametric models of the main base knowledge objects of various types;
- databases formed on a possible set of model solutions.

Base knowledge objects of all types are distributed among the levels of the knowledge base structure. These objects are connected through an organic unity of the design quality parameters of the main elements (integration, disintegration) of their structure [1], which makes their separate consideration impossible.

The solution to practical problems in the invariant parts of the structure of information models for the main base knowledge objects provides for an adequate calculation of the material and human resources needed to optimize the design and organization of the CKD production.

The solution to practical problems in typical object-oriented parametric parts of the structure for information models of base knowledge objects of all types provides for the design quality of the basic elements (integration, disintegration) of the structure of “slave” transformation objects.

References

1. Kolybenko EN. Razgranichenie ponyatii matematicheskogo i logicheskogo modelirovaniya [Distinction between the concepts of mathematical and logical modeling]. Vestnik of DSTU. 2019;19(3):262–267. <https://doi.org/10.23947/1992-5980-2019-19-3-262-267> (In Russ.)
2. Kolybenko EN, Mordovtsev AA. Funktsional'no razlichnye aspekty tekhnologii sistemnoi inzhenerii v poznanii bazy znaniy predmetnoi oblasti v primere tekhnologicheskoi podgotovki mekhanooabratyvyushchego proizvodstva [Functionally different aspects of system engineering technology in cognition of domain knowledge base in the example of machining process engineering] In: XXIII International Scientific-Practical Conference “System analysis in design and management”. Saint Petersburg: SPbGTU Publ. House. 2019;3:281–293. (In Russ.)
3. Ustenko AS. Osnovy matematicheskogo modelirovaniya i algoritimizatsii protsessov funktsionirovaniya slozhnykh sistem [Fundamentals of mathematical modeling and algorithmization of complex system operation processes]. Moscow: BINOM, 2000. 235 p. (In Russ.)
4. Good HH, Machol RE. Sistemotekhnika. Vvedenie v proektirovanie bol'shikh sistem [System Engineering. Introduction to the design of large systems]. Moscow: Sovetskoe radio, 1962. 383 p. (In Russ.)
5. Hall AD. A methodology for systems engineering. New York: Van Nostrand, 1962. 478 p.
6. Mitin SG, Bochkarev PYu. Proektirovanie operatsii so slozhnoi strukturoi v mnogonomenklaturnykh mekhanooabratyvyushchikh sistemakh [Designing operations with complex structure in generic machining systems]. Saratov: Saratov State Technical University, 2016. 108 p. (In Russ.)
7. Ikujiro Nonaka, Hirotaka Takeuchi. Kompaniya — sozdatel' znaniya. Zarozhdenie i razvitie innovatsii v yaponskikh firmakh [Knowledge-Creating Company. The origin and development of innovation in Japanese firms]. Moscow: Olimp-Biznes, 2011. 384 p. (In Russ.)
8. Volkova VN, Kozlov VN, eds. Modelirovanie sistem [System modelling]. Saint Petersburg: SPbGTU Publ. House, 2012. 440 p. (In Russ.)
9. Malikov RF. Osnovy razrabotki komp'yuternykh modelei slozhnykh sistem [Fundamentals of the development of computer models of complex systems]. Ufa: Izd-vo BGPU, 2012. 256 p. (In Russ.)
10. Devyatkov VV. Metodologiya i tekhnologiya imitatsionnykh issledovaniy slozhnykh sistem: sovremennoe sostoyanie i perspektivy razvitiya [Methodology and technology of simulation studies of complex systems: current status and development potential]. Moscow: Vuzovskii uchebnik: INFRA-M, 2013. 448 p. (In Russ.)
11. Chikurov NG. Modelirovanie sistem [System modeling]. Moscow: RIOR: INFRA-M, 2013. 398 p. (In Russ.)

12. Ghallab M, Nau D, Traverso P. Automated Planning and Acting. Cambridge: Cambridge University Press, 2016. 354 p. DOI:10.1017/CBO9781139583923
13. Caillaud E, Rose B, Goepp V. Research methodology for systems engineering: some recommendations. IFAC-Papers OnLine. 2016;49(12):1567–1572. URL: <https://reader.elsevier.com/reader/sd/pii/S2405896316310850?token=081F668FA42CD690B2813FD064DE507C747C207F28E3BA31745AA02DB655CF7CEC0059E433B5D4427AC71CE085842B4F> (accessed 20.01.2020).
14. Bez"yazychnyi VF, Suslov AG. Osnovnye ponyatiya i polozheniya v tekhnologii mashinostroeniya [Basic concepts and regulations in engineering techniques]. Science Intensive Technologies in Mechanical Engineering. 2018;2(80):3–9. (In Russ.)
15. Kondakov AI, Vasil'ev AS. Sistemnoe modelirovanie vzaimodeistvii v tekhnologicheskikh sredakh [System modeling of interactions in process media]. Proceedings of Higher Educational Institutions. Machine Building. 1998;4:92. (In Russ.)
16. Turner D. Veroyatnost', statistika i issledovanie operatsii [Probability, Statistics and Operations Research]. Moscow: Statistika, 1976. 431 p. (In Russ.)
17. Rakovich AG. Osnovy avtomatizatsii proektirovaniya tekhnologicheskikh prispособlenii [Fundamentals of automation of designing machining attachments]. Minsk: Nauka i tekhnika, 1985. 285 p. (In Russ.)

Submitted 13.01.2020

Scheduled in the issue 02.03.2020

About the author:

Kolybenko, Evgenii N., Leading Research Scholar, Don State Technical University (1, Gagarin sq., Rostov-on-Don, 344000, RF), Cand.Sci. (Eng.), ORCID: <https://orcid.org/0000-0003-1851-3885>, e.n.kolybenko@mail.ru

The author has read and approved the final manuscript

The issue is prepared by:

Inna V. Boyko, Marina P. Smirnova (English version)

Passed for printing 26.03.2020,
imprint date 26.03.2020.

Format 60×84/8. C.p.sh. 22.6

Font «Times New Roman»

Circulation 1000 cop.

Order no. 26/03

Free price.

Founder's, publisher's and printery address:

Gagarin Sq. 1, Rostov-on-Don, 344000, Russia.

Phone: +7 (863) 2-738-372

E-mail: vestnik@donstu.ru

<http://vestnik.donstu.ru/>